Published for SISSA by Springer

Received: December 8, 2025
Revised: January 28, 2026
Accepted: February 26, 2026
Published: April 23, 2026

Supersymmetric AdS solitons, Coulomb branch flows and twisted compactifications

Dimitrios Chatzis[a], **Madison Hammond**[a], **Georgios Itsios**[b], **Carlos Nunez**[a] and **Dimitrios Zoakos**[c]

[a] *Centre for Quantum Fields and Gravity, Department of Physics, Swansea University, Swansea SA2 8PP, U.K.*
[b] *Institut für Physik, Humboldt-Universität zu Berlin, IRIS Gebäude, Zum Großen Windkanal 2, 12489 Berlin, Germany*
[c] *Department of Physics, University of Patras, 26504 Patras, Greece*

E-mail: dchatzis@proton.me, m.hammond.2412736@swansea.ac.uk, georgios.itsios@physik.hu-berlin.de, c.nunez@swansea.ac.uk, dzoakos@upatras.gr

Abstract: This work, which accompanies [1], is about constructing smooth solutions in type II and eleven dimensional supergravity which describe supersymmetry preserving RG flows from four-dimensional SCFTs in the UV to three-dimensional SQFTs in the IR, through holography. We show that all the different UV fixed points flow to theories which confine external quarks and have a mass gap. We proceed by presenting extended calculations of a plethora of observables and analyse the dual field theories in great detail. This includes a boundary analysis and application of holographic renormalization methods in the simplest case of the type IIB solution. Many of the observables computed here have a universal behaviour: they factorize into two parts, one of which includes information about the UV SCFTs, and the other describing the dynamics of the RG flow, which is the same regardless of the UV fixed point.

Keywords: AdS-CFT Correspondence, Confinement, Gauge-Gravity Correspondence

ArXiv ePrint: 2511.18128

https://doi.org/10.1007/JHEP04(2026)184

JHEP04(2026)184

Contents

1 Introduction and organization of the paper **2**

2 5d gauged supergravity **4**
- 2.1 The supersymmetric AdS soliton 4
- 2.2 Singularity study 5

3 New deformed supergravity backgrounds **8**
- 3.1 Type IIB background 8
- 3.2 Embedding in Romans' SU(2) × U(1) 5d gauged supergravity 10
- 3.3 Eleven dimensional supergravity backgrounds 10
- 3.4 Type IIA backgrounds 13

4 Observables of the dual field theories **19**
- 4.1 Wilson loop 20
- 4.2 't Hooft loop 32
- 4.3 Entanglement entropy 36
- 4.4 Flow central charge 39
- 4.5 D7 brane embeddings in the Anabalon-Ross deformed $AdS_5 \times \mathbb{S}^5$ solution 42

5 Holographic renormalization **44**
- 5.1 Anabalon-Ross solution 44
- 5.2 Anabalon-Nastase-Oyarzo 46

6 The stability analysis of the classical solution for the Wilson loops **47**
- 6.1 The classical solution 47
- 6.2 Expansion of the action and equations of motion for the fluctuations 49
- 6.3 Transformation to a Schrödinger potential 50
- 6.4 Solving for the fluctuations 53

7 Penrose limits of the Anabalon-Ross deformed $AdS_5 \times \mathbb{S}^5$ solution **55**
- 7.1 Motion along (t, ϕ, φ_1) 57
- 7.2 Motion along (t, ϕ, φ_2) 59
- 7.3 Motion along (t, ϕ, φ_3) 60

8 Conclusions and discussion **62**

A Polyakov loop embedding **64**

B Gauge coupling **65**

C Details of the computations **67**

JHEP04(2026)184

1 Introduction and organization of the paper

In the ongoing quest to deepen our understanding of the strongly coupled dynamics of QFTs, particularly those that exhibit features akin to real-world QCD_4, the gauge/gravity duality has proven to be one of the most powerful theoretical tools since its introduction by Maldacena in [2]. The duality provides a means of studying non-perturbative aspects of gauge theories through a classical gravitational description, enabling the investigation of phenomena such as confinement and phase structure, chiral symmetry breaking, the computation of form factors, and the spectra of mesons, hadrons, and glueballs, among many others. The gravitational systems that holographically capture these features arise as extensions of the original duality between type II string theory on $\mathrm{AdS}_5 \times \mathbb{S}^5$ and $\mathcal{N} = 4$ SYM on $\mathbb{R}^{1,3}$ [3–6].

Over the years, a substantial body of work has been devoted to extending and generalizing the original duality, thereby broadening our understanding of strongly coupled gauge dynamics reminiscent of those encountered in QCD_4. One class of such developments involves solutions with branes wrapped on internal cycles [7–10], while another considers D-brane configurations at the tip of deformed Calabi-Yau singularities [3, 6, 11]. These constructions have been remarkably successful in reproducing several desirable features, including the ability to describe a broad range of $\mathcal{N} = 1, 2$ four-dimensional quiver gauge theories with bifundamental matter, as well as systems with reduced or broken supersymmetry [6, 7, 12–15].

Nevertheless, the conventional approaches to constructing backgrounds dual to confining QFTs often face challenges related to their UV behaviour. In the dual field theories of these models, the number of degrees of freedom tends to grow without bound as one approaches the UV, corresponding to an infinite sequence of Seiberg dualities [6]. This behaviour complicates the application of holographic renormalization techniques developed in subsequent works [16–18], making it technically demanding to extract precise information about operators and their correlation functions. Recently, this issue has been addressed in [19], where the introduction of orientifold planes was shown to regulate the UV dynamics, leading to the emergence of a fixed point that effectively terminates the duality cascade with a finite number of degrees of freedom.

An alternative approach to constructing confining holographic backgrounds is provided by the so-called AdS soliton, obtained via a double Wick rotation of gravity solutions such as the Schwarzschild-AdS black hole. This setup has been extensively used to model systems dual to pure QCD_3 with additional massive Kaluza-Klein excitations [20, 21]. The AdS soliton constitutes a smooth solution of the supergravity equations of motion, characterized by a cigar-like geometry in the infrared, $\mathrm{d}s^2 \sim \mathrm{d}r^2 + r^2\mathrm{d}\phi^2$ ($\phi \sim \phi + L_\phi$), that caps off smoothly at a finite value of the radial coordinate $r = r_\star$ for an appropriate choice of L_ϕ. A defining feature of such geometries is that the spacetime ending at $r = r_\star > 0$ introduces a mass gap in the dual field theory, which corresponds to $\mathcal{N} = 4$ SYM compactified on $\mathbb{R}^{1,2} \times \mathbb{S}^1_\phi$. Depending on the boundary conditions imposed on the fermions, globally well-defined spinors can be periodic or antiperiodic along $\mathbb{S}^1_\phi$, with the latter case breaking supersymmetry.

To preserve a fraction of supersymmetry, one may employ a *topological twist*, achieved by mixing a global symmetry with a spacetime symmetry. Concretely, this amounts to modifying the covariant derivative so that the antiperiodic contribution of the spin connection is cancelled, allowing spinors to remain periodic and form supersymmetric multiplets in three dimensions.

JHEP04(2026)184

In practice, this is realized by introducing a Wilson line in the geometry — equivalently, a constant background gauge field $\mathcal{A} = \mathcal{A}_\phi \mathrm{d}\phi$ with nonzero holonomy (see [22, 23] for a clear review of the mechanism). In a recent advance, Anabalon and Ross [24] constructed a new AdS soliton solution derived from a charged black hole background that is 1/2 BPS. This solution implements the twisted compactification described above and has proven to be an excellent seed for generating higher-dimensional uplifts yielding gapped and confining systems with AdS_5 factors in type II string theory and M-theory [25–32]. More recently, another supersymmetric AdS soliton was presented in [33], generalizing the construction of [24] by including a non-trivial scalar profile, an additional gauge field, and an extra free parameter. This broader solution has been interpreted as describing Coulomb branch deformations of $\mathcal{N} = 4$ SYM, in the sense of [34, 35].

The present work complements and extends the results of [1], where new infinite families of string-theory backgrounds were constructed by uplifting the AdS soliton of [33] to type II supergravity and M-theory. These geometries provide holographic duals to Coulomb branch deformations of various SCFT_4s compactified on a circle, which flow in the IR to three-dimensional gapped QFTs preserving four real supercharges. The resulting solutions include a type IIB background (already discussed in [33]), an infinite family of M-theory backgrounds, and a corresponding family of type IIA backgrounds. Despite originating from distinct CFTs in the UV, these systems exhibit strikingly similar non-perturbative dynamics in the IR, reflecting universal features of supersymmetric confinement and dimensional reduction. The present paper provides a more detailed analysis of these systems, including new computations that elucidate the properties of the dual field theories. In particular, additionally to the content of [1], we start by providing a more thorough presentation of the construction of the backgrounds, using the five-dimensional gauged supergravity solution. We then further probe the confining features of the IR effective dual theories by considering more involved F1 embeddings for the Wilson loop, as well as studying the behaviour of 't Hooft loops and the entanglement entropy on a strip. We also included a study of a D7-brane embedding and of the Penrose limit of the solution, providing alternative probes of the confining properties. Moreover, we include a boundary analysis for the type IIB uplift that matches our previous analysis for the VEVs dual to the operators turned on by the deformation. Finally, as stated in [1], we perform a stability analysis on the fluctuations of the Wilson loop configuration used in the type IIB calculation (what in this work is dubbed "embedding I") in section 4.1.

The paper is organized as follows: sections 2 and 3 review the supergravity solutions of [1], with the latter also including a discussion of Page charge quantization. Section 4 contains detailed computations of various field-theory observables exhibiting *universality*. A discussion on the embedding of a D7-brane probe in the deformed $\mathrm{AdS}_5 \times \mathbb{S}^5$ solution of [24], is also presented. In section 5, we perform a boundary analysis and apply holographic renormalization to identify the vacuum expectation values (VEVs) of the operators responsible for deforming the UV CFTs. Finally, sections 6 and 7 are devoted to the stability analysis of the Wilson loop configurations in the type IIB background and to a study of Penrose limits in the deformed $\mathrm{AdS}_5 \times \mathbb{S}^5$ solution of [24].

JHEP04(2026)184

2 5d gauged supergravity

In this section we study the 5d soliton solution which will act as the "seed solution" for our string backgrounds. We will be uplifting it to get solutions in Type IIA, Type IIB and M-theory (11d supergravity). We first present the solution and its bosonic action, and then study important features like smoothness, which will be carried-up to the higher dimensional uplifts.

2.1 The supersymmetric AdS soliton

We start by presenting the five-dimensional gauged supergravity soliton solution found in [33], which one can obtain in a truncation of the compactification of type-IIB supergravity on the five-sphere. This is a generalization of the solution found in [24], which contains an extra charge parameter as well as a scalar profile.

The bosonic sector of the 5d theory, containing a metric, three abelian gauge fields A_i and two scalars Φ_1, Φ_2, can be written in the following way:

$$\begin{aligned}
\mathrm{S} &= \frac{1}{2\kappa}\int \mathrm{d}^5x\sqrt{-g}\Big[R - \frac{1}{2}(\partial\Phi_1)^2 - \frac{1}{2}(\partial\Phi_2)^2 - \frac{1}{4}\sum_{i=1}^{3} X_i^{-2}F^i_{\mu\nu}F^{i\,\mu\nu} \\
&\quad + \frac{1}{4}\epsilon^{\mu\nu\rho\sigma\lambda}A^1_\mu F^2_{\nu\rho}F^3_{\sigma\lambda} + \frac{4}{L^2}\sum_{i=1}^{3} X_i^{-1}\Big], \\
F^i &= \mathrm{d}A^i, \qquad X_i = e^{-\frac{1}{2}\vec{a}_i\cdot\vec{\Phi}}, \qquad \vec{\Phi} = (\Phi_1, \Phi_2), \\
\vec{a}_1 &= \left(\frac{2}{\sqrt{6}}, \sqrt{2}\right), \quad \vec{a}_2 = \left(\frac{2}{\sqrt{6}}, -\sqrt{2}\right), \quad \vec{a}_3 = \left(-\frac{4}{\sqrt{6}}, 0\right).
\end{aligned} \tag{2.1}$$

Here κ is related to Newton's constant in 5d as $\kappa^2 = 8\pi G_5$ and the coupling of the gauged supergravity has been set to $g = L^{-1}$. The equations of motion for this theory are the Bianchi identities and Maxwell equations for the field strengths, Einstein's equations for the metric as well as the equations of motion for the two scalar fields. They read:

$$\mathrm{d}\left(\sqrt{-g}X_i^{-2}F^i\right) = 0, \quad \mathrm{d}\star\left(\sqrt{-g}X_i^{-2}F^i\right) = 0, \tag{2.2}$$

$$\begin{aligned}
G_{\mu\nu} &= \frac{1}{2}T^\Phi_{\mu\nu} + \sum_{i=1}^{3}\frac{1}{2X_i^2}T^i_{\mu\nu}, \quad T^i_{\mu\nu} = F^i_{\mu\rho}F^{i\,\rho}_\nu - \frac{1}{4}g_{\mu\nu}F^i_{\rho\sigma}F^{i\,\rho\sigma}, \\
T^\Phi_{\mu\nu} &= \partial_\mu\Phi_1\partial_\nu\Phi_1 + \partial_\mu\Phi_2\partial_\nu\Phi_2 - g_{\mu\nu}\left[\frac{1}{2}(\partial\Phi_1)^2 + \frac{1}{2}(\partial\Phi_2)^2 - \frac{4}{L^2}\sum_{i=1}^{3}X_i^{-1}\right],
\end{aligned} \tag{2.3}$$

$$\begin{aligned}
\Box\Phi_1 &= \sum_{i=1}^{3}\left[-\frac{1}{2}X_i^{-3}\left(\frac{\partial X_i}{\partial\Phi_1}\right)F^i_{\mu\nu}F^{i\,\mu\nu} + \frac{4}{L^2}X_i^{-2}\left(\frac{\partial X_i}{\partial\Phi_1}\right)\right], \\
\Box\Phi_2 &= \sum_{i=1}^{3}\left[-\frac{1}{2}X_i^{-3}\left(\frac{\partial X_i}{\partial\Phi_2}\right)F^i_{\mu\nu}F^{i\,\mu\nu} + \frac{4}{L^2}X_i^{-2}\left(\frac{\partial X_i}{\partial\Phi_2}\right)\right].
\end{aligned} \tag{2.4}$$

Where we defined $\Box\Phi = \frac{1}{\sqrt{-g}}\partial_\mu\left(\sqrt{-g}\partial^\mu\Phi\right)$. We now consider a consistent truncation of (2.1), in the sense that the solution we present below can be embedded in the above system:

$$\begin{aligned}
\mathrm{d}s_5^2 &= \frac{r^2\lambda^2(r)}{L^2}\left(-\mathrm{d}t^2 + \mathrm{d}z^2 + \mathrm{d}w^2 + L^2F(r)\mathrm{d}\phi^2\right) + \frac{\mathrm{d}r^2}{r^2\lambda^4(r)F(r)}, \\
\Phi_1 \equiv \Phi &= \sqrt{\frac{2}{3}}\ln\lambda^{-6}(r), \qquad \Phi_2 = 0,
\end{aligned}$$

$$A^1 = A^2 = q_1\left[\lambda^6(r) - \lambda^6(r_\star)\right] L\,\mathrm{d}\phi, \quad A^3 = q_2\left[\frac{1}{\lambda^6(r)} - \frac{1}{\lambda^6(r_\star)}\right] L\,\mathrm{d}\phi, \tag{2.5}$$
$$F(r) = \frac{1}{L^2} - \frac{\varepsilon\ell^2 L^2}{r^4}\left(q_1^2 - \frac{q_2^2}{\lambda^6(r)}\right), \quad \lambda^6(r) = \frac{r^2+\varepsilon\ell^2}{r^2}.$$

The warp function $F(r)$ has a largest root which we denote as $r_\star$ and is responsible for ending the space at the finite point $r = r_\star$, ℓ is a parameter, while according to [33] $\varepsilon = \pm 1$ distinguishes between two non-diffeomorphic branches of the supergravity solution. The truncated action from (2.1) reads:

$$\mathrm{S} = \frac{1}{2\kappa}\int d^5x\sqrt{-g}\left[R - \frac{1}{2}(\partial\Phi)^2 + \frac{4}{L^2}\left(\frac{2}{X} + X^2\right) - \frac{1}{2X^2}F^1_{\mu\nu}F^{1\,\mu\nu} - \frac{1}{4}X^4F^3_{\mu\nu}F^{3\,\mu\nu}\right],$$
$$X = e^{-\Phi/\sqrt{6}}. \tag{2.6}$$

Let us also note that this metric asymptotes to that of AdS_5 as $r \to \infty$, since $F(r) \to L^{-2}$ and $\lambda(r) \to 1$. One can think of the above solution as a double analytic continuation of electrically charged black hole solutions in $\mathrm{U}(1)^3$ truncated 5d supergravity found in [36]. One can also make use of the ansatz presented in the same work and uplift (2.5) to a solution of the equations of motion of type IIB supergravity, that is Ricci flat.[1] This solution was also included in [33] and we study it in section 3.1.

2.2 Singularity study

Before continuing to embeddings of this solution in other supergravities and string backgrounds, let us study more closely the singularity structure in 5d. The contents of this subsection will hold for all the uplifted solutions that we will present in section 3. From here onwards, we will only consider the supersymmetric case for which we set[2] $|q_1| = |q_2| = Q$ and four real supercharges are preserved. This is a choice, as the various expressions will be valid even for q_1, q_2 not satisfying this condition, and the limit $Q \to 0$ corresponds to $q_1 \to 0, q_2 \to 0$. We also choose to work with the dimensionless variable $\xi = \frac{r}{r_\star} \geq 1$ and the parameter $\hat{\nu} = \varepsilon\frac{\ell^2}{r_\star^2}$, in terms of which the gauge fields and functions take the form:

$$A^1 = A^2 = Q\hat{\nu}L\left(1 - \frac{1}{\xi^2}\right)\mathrm{d}\phi, \qquad A^3 = \frac{Q\hat{\nu}L(\xi^2-1)}{(1+\hat{\nu})(\xi^2+\hat{\nu})}\mathrm{d}\phi,$$
$$\lambda^6(\xi) = \frac{\xi^2+\hat{\nu}}{\xi^2}, \qquad F(\xi) = \frac{(\xi^2-1)\left[\xi^4 + (1+\hat{\nu})\xi^2 + 1 + \hat{\nu}\right]}{L^2\xi^4(\hat{\nu}+\xi^2)}, \tag{2.7}$$

where the condition $F(r_\star) = 0$ was used to eliminate Q from the last expression.[3] First we fix the periodicity of the cigar-like coordinate ϕ in order to avoid conical singularities. The

[1] The dilaton of this solution is zero and therefore its equation of motion yields $R = 0$.

[2] According to the Killing spinor analysis performed in [33], in the 5d solution the supersymmetric point happens when $q_1 = -q_2$, while when the solution is uplifted to the 10d string background of section 3.1 the relation $q_1 = q_2$ also provides supersymmetric preservation. We abuse this detail by writing $Q = |q_1| = |q_2|$ in the 5d solution as well.

[3] F can be brought to the following form in the r variable, isolating the root $r_\star$ from the fourth order polynomial:

$$F(r) = (r^2 - r_\star^2)\left[\frac{r^4 + (r_\star^2+\varepsilon\ell^2)r^2 + r_\star^2(r_\star^2+\varepsilon\ell^2)}{L^2r^4(r^2+\varepsilon\ell^2)}\right].$$

JHEP04(2026)184

expansions of the various quantities near the end of the space $\xi = 1$ yield:[4]

$$\begin{aligned} \lambda(\xi) &\approx (1+\hat{\nu})^{1/6} + \mathcal{O}(\xi-1), \qquad & F(\xi) &\approx \frac{2(2\hat{\nu}+3)(\xi-1)}{L^2(1+\hat{\nu})} + \mathcal{O}((\xi-1)^2), \\ A_{1\phi} &\approx 2Q\hat{\nu}(\xi-1) + \mathcal{O}((\xi-1)^2), \qquad & A_{3\phi} &\approx \frac{(6+4\hat{\nu})}{(1+\hat{\nu})^2}(\xi-1) + \mathcal{O}((\xi-1)^2). \end{aligned} \tag{2.8}$$

Then the metric of the subspace spanned by the angle ϕ and the radial coordinate takes the form:

$$\mathrm{d}s^2_{r,\phi} \approx \frac{L^2}{(4\hat{\nu}+6)(\xi-1)}\mathrm{d}\xi^2 + \frac{r_\star^2(\xi-1)(4\hat{\nu}+6)}{L^2(1+\hat{\nu})}\mathrm{d}\phi^2 = \mathrm{d}\rho^2 + \frac{r_\star^2(4\hat{\nu}+6)^2}{4L^4(1+\hat{\nu})}\,\rho^2\,\mathrm{d}\phi^2, \tag{2.9}$$

where in the last step we defined the coordinate $\rho = 2L\sqrt{\frac{\xi-1}{4\hat{\nu}+6}}$. If we now redefine the angle to be

$$\phi = \frac{2L^2\sqrt{1+\hat{\nu}}}{r_\star(4\hat{\nu}+6)}\hat{\phi}, \tag{2.10}$$

the metric is free of conical singularities, as it describes a flat space in cylindrical coordinates $(\rho, \hat{\phi})$ with $\rho \geq 0, \quad \hat{\phi} \in [0, 2\pi)$. The latter range of values forces the original cigar coordinate to range as:

$$\phi \in [0, L_\phi), \quad \text{with } L_\phi = \frac{4\pi L^2\sqrt{1+\hat{\nu}}}{r_\star(4\hat{\nu}+6)}. \tag{2.11}$$

We comment that even though requiring a singularity-free metric is not a feature directly related the confining properties of the dual field theory, it can be the case that a conical singularity in the IR may spoil confinement. This is because even if a singular background does lead to an area law for the Wilson loop, small perturbations of the coordinates will not be necessarily well behaved, as their masses are weighted by components of $R_{\mu\nu\rho\sigma}$ [37] which can be divergent. Overall, it is preferred to have a smooth IR geometry in order to gain a better control over the string corrections, as having a singularity would lead to ambiguous descriptions of the dual QFT.

Let us now focus on studying the root structure of the sixth order polynomial F responsible for capping off the space, which can be rewritten as:

$$F(\xi) = \frac{(\xi^2-1)\,(\xi^2-\xi_+^2)\,(\xi^2-\xi_-^2)}{L^2\xi^4(\hat{\nu}+\xi^2)} \quad \text{with} \quad \xi_\pm^2 = \frac{-(1+\hat{\nu}) \pm \sqrt{(\hat{\nu}+1)(\hat{\nu}-3)}}{2}. \tag{2.12}$$

We should first determine the range of possible values for the parameter $\hat{\nu}$ to figure if real values for the roots $\xi_\pm$ can occur. For this, we can directly solve for the equation $F(r_\star) = 0$ with the form of F appearing in (2.5) to acquire an expression in terms of the charge Q and the parameters:

$$\begin{aligned} r_\star &= \frac{1}{\sqrt{6}}\sqrt{2^{2/3}\ell^{4/3}\Lambda + 2\ell^2\varepsilon\left(-1 + \frac{2^{1/3}\ell^{2/3}\varepsilon}{\Lambda}\right)}, \\ \Lambda &:= \left[-2\varepsilon\ell^2 + 3Q\left(9L^4Q + L^2\sqrt{81L^4Q^2 - 12\ell^2\varepsilon}\right)\right]^{1/3}. \end{aligned} \tag{2.13}$$

[4]Here we denote as $A_{i\phi}$ the components of each 1-form A^i.

JHEP04(2026)184

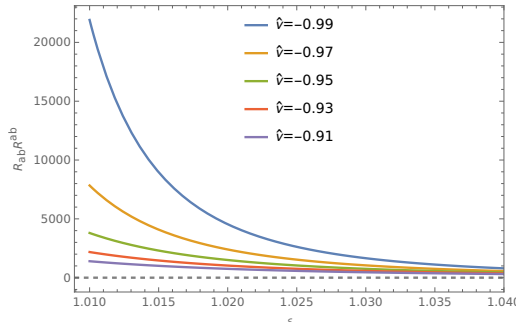

(a) Contraction of the Ricci tensor with itself as a function of the dimensionless radial coordinate ξ, for various values of $\hat{\nu} \approx -1$.

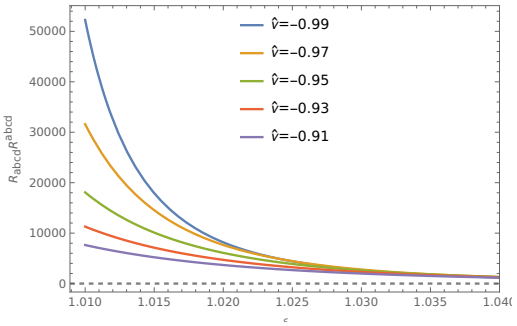

(b) Contraction of the Riemann tensor with itself as a function of the dimensionless radial coordinate ξ, for various values of $\hat{\nu} \approx -1$.

Figure 1. Invariants of the 5d geometry (2.5) for values of the parameter $\hat{\nu}$ close to -1. Approximately below the value -0.95 they start growing rapidly.

We notice by taking the limit $Q \to 0$ in (2.13) we get $r_\star \to 0$ for $\varepsilon = +1$ and $r_\star \to \ell$ for $\varepsilon \to -1$. In fact, substituting (2.13) in the definition of $\hat{\nu}$ reveals that in the $\varepsilon = +1$ branch $\hat{\nu}$ is manifestly positive, while in the branch where $\varepsilon = -1$ it is bounded from below by the value $\hat{\nu} = -1$ for all values of ℓ, L and Q. Using all of the above we deduce the following:

For $\hat{\nu} > -1$ there are no real values for $\xi_\pm$ and therefore the only root of F is $\xi = 1$, or $r = r_\star$, where the space terminates smoothly.

However when $\hat{\nu} = -1$, which can only be reached when $Q = 0$, in which case $\varepsilon = -1$ and $r_\star = \ell$, we have $\xi_+ = \xi_- = 0$ and therefore F takes the constant value L^{-2}. Moreover, the scalar field Φ diverges at this point, since $\lambda(r) \to 0$, while the metric component along ϕ vanishes.

We make the claim that at the later value of the parameter $\hat{\nu} = -1$ and at the point $\xi = 1$, the solution is singular (in both Einstein and string frames). To safely deduce this, we plot two invariants of the geometry ($R_{ab}R^{ab}$ and $R_{abcd}R^{abcd}$). These are depicted in figure 1. What we find is that indeed, their expressions diverge when $\hat{\nu} = -1$ & $\xi = 1$ which is a confirmation of the metric being singular at this point. Notice however that if we restrict ourselves to study solutions with $\hat{\nu} > -1$, but still explore the values close to $\hat{\nu} = -1$, the invariants grow extremely large as $\hat{\nu} \to -1^+$ but the metric is *smooth*. When the soliton is uplifted to Type IIB — see section 3.1, the point $\hat{\nu} = -1$ can be thought of as the Coulomb branch singularity in the 10d solution of [34]. In fact, many of the gravity systems participating in the holographic modelling of confinement include such naked singularities, see [4, 38, 39], which often have 5d origins. The presence of such singularities makes the analysis of observables not trustable. We wish to emphasize that in our case, we have a *smooth geometry* but there is still a region of very large curvatures for specific value of the parameters ($\hat{\nu} \approx -1^+$), at which the supergravity approximation is afflicted by higher curvature corrections that are as important as the leading term. For our purposes, this means that there are some states in the IR spectrum of the dual QFT that are not captured by the supergravity approximation.

JHEP04(2026)184

3 New deformed supergravity backgrounds

Having made many of our arguments in the 5d gauged supergravity system, we now present the three types of uplifts of (2.5) to string theory and eleven dimensional supergravity, in order to apply holography. The first is the solution in type IIB presented in [33], while the rest are new infinite families of solutions of 11d supergravity and type IIA supergravity respectively, introduced in [1].

3.1 Type IIB background

In this section we review the ten-dimensional supergravity background constructed in section 5 of [33]. This is an uplift to type IIB of the 5d solution we presented earlier, which amounts to further deforming the background of a distribution of D3 branes found in [34] (in particular the cases of $n = 2$ ($\varepsilon = +1$) and $n = 4$ ($\varepsilon = -1$) found in table 1 of section 2 of [34]). These geometries describe a Coulomb branch deformation of $\mathcal{N} = 4$ SYM by a nonzero VEV of an operator of dimension $\Delta = 2$ proportional to $\varepsilon\ell^2/L^2$ (already presented in [34]) as well as a VEV of an operator of dimension $\Delta = 3$. The metric takes the form:

$$\begin{aligned} \mathrm{d}s^2 = \frac{\zeta(r,\theta)}{L^2}\left[r^2(-\mathrm{d}t^2+\mathrm{d}w^2+\mathrm{d}z^2+L^2F(r)\mathrm{d}\phi^2)+\frac{L^2\mathrm{d}r^2}{F(r)r^2\lambda^6(r)}+L^4\mathrm{d}\theta^2\right] \\ +\frac{L^2}{\zeta(r,\theta)}\left[\cos^2\theta\mathrm{d}\psi^2+\cos^2\theta\sin^2\psi\mathrm{D}\phi_1^2+\cos^2\theta\cos^2\psi\mathrm{D}\phi_2^2+\lambda^6(r)\sin^2\theta\mathrm{D}\phi_3^2\right], \end{aligned} \tag{3.1}$$

where $\mathrm{D}\phi_i = \mathrm{d}\phi_i + \frac{A^i}{L}$, the function ζ is defined to be:

$$\zeta(r,\theta) = \sqrt{1+\varepsilon\frac{\ell^2}{r^2}\cos^2\theta}, \tag{3.2}$$

while λ and F are defined in (2.5). The range of values for the angles parametrizing the deformed $\mathbb{S}^5$ are: $\theta, \psi \in [0, \frac{\pi}{2}]$, $\phi_i \in [0, 2\pi)$. The solution also contains an self-dual RR five-form:

$$F_5 = (1+\star)G_5\,, \tag{3.3}$$

where

$$\begin{aligned} G_5 = {}& \frac{2r^3}{L^4}(1+\zeta^2)\mathrm{d}t\wedge\mathrm{d}w\wedge\mathrm{d}z\wedge\mathrm{d}\phi\wedge\mathrm{d}r-\frac{\varepsilon\ell^2r^2F}{L^2}\sin(2\theta)\mathrm{d}t\wedge\mathrm{d}w\wedge\mathrm{d}z\wedge\mathrm{d}\phi\wedge\mathrm{d}\theta \\ & -\frac{r^3A'_{1\phi}}{2L}\cos^2\theta\,\sin(2\psi)\mathrm{d}t\wedge\mathrm{d}w\wedge\mathrm{d}z\wedge\mathrm{d}(\phi_1-\phi_2)\wedge\mathrm{d}\psi \\ & -\frac{r^3}{2L}\sin(2\theta)\mathrm{d}t\wedge\mathrm{d}w\wedge\mathrm{d}z\wedge\mathrm{d}\theta\wedge\Big(A'_{1\phi}(\sin^2\psi\,\mathrm{d}\phi_1+\cos^2\psi\,\mathrm{d}\phi_2) \\ & -\lambda^{12}A'_{3\phi}\,\mathrm{d}\phi_3+\frac{1}{L}(A_{1\phi}A'_{1\phi}-\lambda^{12}A_{3\phi}A'_{3\phi})\mathrm{d}\phi\Big)\,. \end{aligned} \tag{3.4}$$

JHEP04(2026)184

Equivalently, we can express things in terms of a frame, in the mostly plus metric convention:

$$
\begin{aligned}
&e^0 = \frac{\sqrt{\zeta}}{L}\, r\, \mathrm{d}t\,, && e^1 = \frac{\sqrt{\zeta}}{L}\, r\, \mathrm{d}w\,, && e^2 = \frac{\sqrt{\zeta}}{L}\, r\, \mathrm{d}z\,, \quad e^3 = \sqrt{\zeta\, F}\, r\, \mathrm{d}\phi\,,\\
&e^4 = \sqrt{\frac{\zeta}{F}}\frac{\mathrm{d}r}{\lambda^3 r}\,, && e^5 = L\sqrt{\zeta}\, \mathrm{d}\theta\,, && e^6 = L\frac{\cos\theta}{\sqrt{\zeta}}\, \mathrm{d}\psi\,,\\
&e^7 = L\frac{\cos\theta\, \sin\psi}{\sqrt{\zeta}}\left(\mathrm{d}\phi_1 + \frac{A_1}{L}\right), && e^8 = L\frac{\cos\theta\, \cos\psi}{\sqrt{\zeta}}\left(\mathrm{d}\phi_2 + \frac{A_2}{L}\right), &&\\
&e^9 = L\frac{\lambda^3 \sin\theta}{\sqrt{\zeta}}\left(\mathrm{d}\phi_3 + \frac{A_3}{L}\right), &&&&
\end{aligned}
\tag{3.5}
$$

in which case:

$$
\begin{aligned}
G_5 = {} & \frac{2\lambda^3(1+\zeta^2)}{L\zeta^{5/2}} e^{01234} - \frac{\varepsilon \ell^2 \sqrt{F}\sin(2\theta)}{r^2\zeta^{5/2}} e^{01235} - \frac{\sin\theta \sin\psi A'_{1\phi}}{\zeta^{3/2}} e^{01257}\\
& - \frac{\sin\theta\cos\psi A'_{1\phi}}{\zeta^{3/2}} e^{01258} + \frac{\cos\psi A'_{1\phi}}{\sqrt{\zeta}} e^{01267} - \frac{\sin\psi A'_{1\phi}}{\sqrt{\zeta}} e^{01268} + \frac{\cos\theta A'_{3\phi}\lambda^9}{\zeta^{3/2}} e^{01259},
\end{aligned}
\tag{3.6}
$$

where we abbreviate $e^{abcdf} = e^a \wedge e^b \wedge e^c \wedge e^d \wedge e^f$. We denote with a prime the derivative with respect to the r-coordinate.

Alternatively, the five-form G_5 can be expressed in terms of a four-form potential C_4 as $G_5 = \mathrm{d}C_4$, where

$$
\begin{aligned}
C_4 = {} & \left[\frac{r^4\zeta^2}{L^4} - \frac{\ell^4}{2}\left(\frac{q_1^2}{r_\star^2} - \frac{q_2}{L}\frac{A_{3\phi}}{r^2 - r_\star^2}\frac{\lambda^6}{\lambda^6 - 1}\right)\cos(2\theta)\right]\mathrm{d}t \wedge \mathrm{d}w \wedge \mathrm{d}z \wedge \mathrm{d}\phi\\
& - \frac{\ell^2\varepsilon}{2}\cos(2\theta)\mathrm{d}t \wedge \mathrm{d}w \wedge \mathrm{d}z \wedge \Big(q_1\big(\sin^2\psi\, \mathrm{d}\phi_1 + \cos^2\psi\, \mathrm{d}\phi_2\big) - q_2\, \mathrm{d}\phi_3\Big)\\
& + \frac{q_1\ell^2\varepsilon}{2}\cos^2\psi\, \mathrm{d}t \wedge \mathrm{d}w \wedge \mathrm{d}z \wedge \mathrm{d}(\phi_1 - \phi_2)\,.
\end{aligned}
\tag{3.7}
$$

The Hodge dual of G_5 can also be written in terms of a four-form $\tilde{C}_4$ (see (C.1)) as $\star G_5 = \mathrm{d}\tilde{C}_4$. The self-dual five-form can then be expressed in terms of C_4 and $\tilde{C}_4$ as $F_5 = \mathrm{d}(C_4 + \tilde{C}_4)$. Notice that $\lambda_\star$ and $\zeta_\star$ refer to the values of the functions $\lambda(r)$ and $\zeta(r,\theta)$ at $r = r_\star$.

Lastly, we wish to comment that in this IIB background, the singular locus we described in section 2.2 is located, after setting $\hat{\nu} = -1$, along the curve:

$$
\xi^2 - \cos^2\theta = \left(\frac{r}{r_\star}\right)^2 - \cos^2\theta = 0,
\tag{3.8}
$$

as when this equation is satisfied the geometric invariants diverge. Therefore the singularity appears when $r = r_\star = \ell$ in the direction $\theta = 0$. Contrast this with the 5d gauged supergravity where there is no such angle.

Since the soliton we used for the uplift is a consistent truncation of 10d type IIB compactified on $\mathbb{S}^5$, the Killing spinors of the 5d gauged supergravity will uniquelly correspond to Killing spinors of the uplifted solution. The study of preserved supersymmetries was done in detail in [33], where two antiperiodic in ϕ complex Killing spinors were identified. Regarding the preserved $\mathcal{R}$ symmetry, it is a diagonal subgroup $\mathrm{SO}(2)^3_{\mathcal{R}} \subset \mathrm{SO}(6)_{\mathcal{R}}$.

JHEP04(2026)184

3.2 Embedding in Romans' SU(2) × U(1) 5d gauged supergravity

We will now present an embedding of (2.5) in another five-dimensional gauged supergravity introduced by Romans' in [40]. The general content of the bosonic sector of this theory consists of a metric, one scalar field X, an abelian gauge field B, an SU(2) gauge field $\mathcal{A}^i$ $(i = 1, 2, 3)$ and a complex two-form C charged under B. The field strengths for these gauge potentials are:

$$\begin{aligned} G &= \mathrm{d}B, \\ \mathcal{F}^i &= \mathrm{d}\mathcal{A}^i - \frac{1}{\sqrt{2}} m \epsilon_{ijk} \mathcal{A}^j \wedge \mathcal{A}^k, \\ F &= \mathrm{d}C + imB \wedge C, \end{aligned} \tag{3.9}$$

where the parameter m, called the Romans' mass, is related to the SU(2) coupling. The equations of motion for the theory can be derived from the following five-form Lagrangian density:

$$\begin{aligned} \mathcal{L} =& R \star 1 - 3X^{-2} \star \mathrm{d}X \wedge \mathrm{d}X - \frac{1}{2} \star G \wedge G - \frac{1}{2} X^{-2} (\star \mathcal{F}^i \wedge \mathcal{F}^i + \star C \wedge \bar{C}) \\ & - \frac{i}{2m} C \wedge \bar{F} - \frac{1}{2} \mathcal{F}^i \wedge \mathcal{F}^i \wedge B + 4m^2 (X^2 + 2X^{-1}) \star 1, \end{aligned} \tag{3.10}$$

and they read:

$$\begin{aligned} \mathrm{d}(X^{-1} \star \mathrm{d}X) &= \frac{1}{3} X^4 \star G \wedge G - \frac{1}{6} X^{-2} \left(\star \mathcal{F}^i \wedge \mathcal{F}^i + \star C \wedge \bar{C} \right) - \frac{4}{3} m^2 (X^2 - X^{-1}) \star 1, \\ \mathrm{d}(X^4 \star G) &= -\frac{1}{2} \mathcal{F}^i \wedge \mathcal{F}^i - \frac{1}{2} \bar{C} \wedge C\,, \quad D(X^{-2} \star \mathcal{F}^i) = -\mathcal{F}^i \wedge G\,, \quad X^2 \star F = imC, \end{aligned} \tag{3.11}$$

$$\begin{aligned} R_{\mu\nu} =& 3X^{-2} \partial_\mu X \partial_\nu X - \frac{4}{3} m^2 (X^2 + 2X^{-1}) g_{\mu\nu} \\ & + \frac{1}{2} X^4 (G^\rho_\mu G_{\nu\rho} - \frac{1}{6} g_{\mu\nu} G_{\rho\sigma} G^{\rho\sigma} + \frac{1}{2} X^{-2} \left(\mathcal{F}^{i\,\rho}_\mu \mathcal{F}^i_{\nu\rho} - \frac{1}{6} g_{\mu\nu} \mathcal{F}^i_{\rho\sigma} \mathcal{F}^{i\,\rho\sigma} \right) \\ & + \frac{1}{2} X^{-2} \left[C^\rho_{(\mu} \bar{C}_{\nu)\rho} - \frac{1}{6} C_{\rho\sigma} \bar{C}^{\rho\sigma} \right], \end{aligned} \tag{3.12}$$

where we defined the covariant derivative $\mathrm{D}(X^{-2} \star \mathcal{F}^i) := \mathrm{d}(X^{-2} \star \mathcal{F}^i) + \sqrt{2} m \epsilon_{ijk} \mathcal{A}^k \wedge (X^{-2} \star \mathcal{F}^j)$.

We can embed the solution (2.5) in this theory by defining the fields in the following way:

$$X = e^{-\frac{1}{\sqrt{6}}\Phi} = \lambda^2(r), \quad B = A^3, \quad \mathcal{A}^3 = \sqrt{2} A^1 \quad \mathcal{A}^1 = \mathcal{A}^2 = 0, \quad C = 0. \tag{3.13}$$

After identifying $m^2 = L^{-2}$, the equations of motion for the configuration (3.13) are satisfied, which coincide with the ones presented in the previous section (2.2)–(2.4).

3.3 Eleven dimensional supergravity backgrounds

In the following, we will present new embeddings of the solution (3.13) of Romans' 5d gauged supergravity in the 11 dimensional background of Lin, Lunin and Maldacena [41]. These are 1/2-BPS solutions in M-theory preserving 16 supercharges, that are dual to 4 dimensional SCFTs with $\mathcal{N} = 2$ supersymmetry. One key feature of these backgrounds, as well as their type IIA reductions we present in 3.4, that differentiates them from the one of section 3.1

JHEP04(2026)184

is that they come with either M5 or D-branes describing flavour degrees of freedom. This means that their dual QFTs contain fundamental matter.

We follow the uplift formula of Gauntlett and Varela, see [42] as well as [43] to translate between the notation. The resulting 11d deformed geometries take the form:[5]

$$\frac{\mathrm{d}s_{11}^2}{\kappa^{2/3}} = e^{2\hat{\lambda}}\mathcal{Z}\left\{\frac{4}{X}\mathrm{d}s_5^2 + \frac{y^2e^{-6\hat{\lambda}}}{\mathcal{Z}^3}\mathrm{D}\mu^i\mathrm{D}\mu^i + \frac{4X^3}{\mathcal{Z}^3}\frac{\mathrm{D}\chi^2}{1-y\partial_y D_0} - \frac{\partial_y D_0}{y}\mathrm{d}y^2 - \frac{\partial_y e^{D_0}}{y}(\mathrm{d}v_1^2+\mathrm{d}v_2^2)\right\} \tag{3.14}$$

where $\mathrm{d}s_5^2$ stands for the metric in (2.5) and we define the following quantities:

$$\begin{aligned}
\mathcal{Z} &= \left[1+y^2e^{-6\hat{\lambda}}(X^3-1)\right]^{1/3}, & X(r) &= \lambda^2(r),\\
\mathrm{D}\chi &= \mathrm{d}\chi + a_1 + B, & a_1 &= \frac{1}{2}(\partial_{v_2}D_0\mathrm{d}v_1 - \partial_{v_1}D_0\mathrm{d}v_2),\\
B &= A^3 = \frac{q_2L\varepsilon\ell^2(r^2-r_\star^2)}{(r_\star^2+\varepsilon\ell^2)(r^2+\varepsilon\ell^2)}\,\mathrm{d}\phi, & \mathcal{A}^{(3)} &= \sqrt{2}A^1 = \sqrt{2}q_1L\varepsilon\ell^2\left(\frac{1}{r^2}-\frac{1}{r_\star^2}\right)\mathrm{d}\phi,\\
\mathrm{D}\mu^i &= (\mathrm{d}\mu^1+\sqrt{2}\mu_2\mathcal{A}^{(3)})\delta^{i1} + (\mathrm{d}\mu^2-\sqrt{2}\mu_1\mathcal{A}^{(3)})\delta^{i2} + \mathrm{d}\mu^3\delta^{i3},\\
\mu^1 &= \sin\theta\cos\varphi, & \mu^2 &= \sin\theta\sin\varphi, & \mu^3 &= \cos\theta\,,
\end{aligned} \tag{3.15}$$

with the μ^is spanning a two-sphere. The functions $\hat{\lambda}$ and D_0 both have support on (v_1, v_2, y), are related by:

$$e^{-6\hat{\lambda}} = -\frac{\partial_y D_0}{y(1-y\partial_y D_0)}, \tag{3.16}$$

and D_0, which determines the solution, satisfies the three dimensional Toda equation:

$$(\partial_{v_1}^2+\partial_{v_2}^2)D_0 + \partial_y^2 e^{D_0} = 0. \tag{3.17}$$

The 4-form is given by:[6]

$$G_4 = \tilde{G}_4 + G\wedge\beta_2 + \mathcal{F}^{(3)}\wedge\beta_2^{(3)} + \star_5\mathcal{F}^{(3)}\wedge\beta_1^{(3)}, \tag{3.18}$$

where:

$$\begin{aligned}
\tilde{G}_4 = &-\frac{\kappa}{4}\mathrm{vol}\tilde{\mathbb{S}}^2\wedge\left\{8\mathrm{d}\left[\frac{y(1-y^2e^{-6\hat{\lambda}})}{1+y^2e^{-6\hat{\lambda}}(X^3-1)}-y\right]\wedge\mathrm{D}\chi - 4\partial_y e^{D_0}\mathrm{d}v_1\wedge\mathrm{d}v_2\right.\\
&\left.+8\frac{y(1-y^2e^{-6\hat{\lambda}})}{1+y^2e^{-6\hat{\lambda}}(X^3-1)}\mathrm{d}a_1\right\},
\end{aligned} \tag{3.19}$$

$$\begin{aligned}
\beta_2 = &-2\kappa\frac{X^3y^3e^{-6\hat{\lambda}}}{1+y^2e^{-6\hat{\lambda}}(X^3-1)}\mathrm{vol}\tilde{\mathbb{S}}^2\,, \quad \beta_1^{(3)} = -\frac{\kappa\sqrt{8}}{X^2}\mathrm{d}(y\mu^3)\,,\\
\beta_2^{(3)} = &\sqrt{8}\kappa\left\{\left[\mu^3\mathrm{d}y + \frac{y(1-y^2e^{-6\hat{\lambda}})}{1+y^2e^{-6\hat{\lambda}}(X^3-1)}\mathrm{D}\mu^3\right]\wedge\mathrm{D}\chi + \frac{1}{2}\mu^3\partial_y e^{D_0}\mathrm{d}v_1\wedge\mathrm{d}v_2\right\}.
\end{aligned} \tag{3.20}$$

[5] Where $\kappa = \frac{\pi}{2}l_p^3$. We will also set $m=1$ for simplicity from here onwards.

[6] With $G = \mathrm{d}B = \mathrm{d}A^3$, $\mathcal{F}^{(3)} = \mathrm{d}\mathcal{A}^3 = \sqrt{2}\mathrm{d}A^1$, $\mathrm{vol}\tilde{\mathbb{S}}^2 = \frac{1}{2}\varepsilon_{ijk}\mu^i\mathrm{D}\mu^j\mathrm{D}\mu^k$.

JHEP04(2026)184

According to [42], the equations of motion for this background, which we have verified to be satisfied, are equivalent to the five-dimensional equations of Romans' gauged supergravity (3.11) and (3.12). These are the Bianchi identity and Maxwell equation for the flux G_4 as well as the eleven dimensional Einstein equations:

$$\begin{aligned} &\mathrm{d}G_4 = 0, \quad \mathrm{d}\star_{11} G_4 = -\frac{1}{2} G_4 \wedge G_4, \\ &R_{AB} = \frac{1}{12} G_{4\,AC_1C_2C_3} G_{4\,B}^{C_1C_2C_3} - \frac{1}{144} g_{AB} G_{4\,C_1C_2C_3C_4} G_4^{C_1C_2C_3C_4}. \end{aligned} \tag{3.21}$$

In these families of deformed backgrounds we have two types of extended objects: colour M5 branes sourcing the AdS geometry, which wrap the Riemann surface Σ_2 extending in (v_1, v_2) and extend in the Minkowski directions, as well as flavour M5 branes extending in the holographic direction, the Minkowski subspace and the circle parametrised by χ. One can derive the quantization conditions for their charges by integrating the flux G_4 on appropriate four-cycles. There are two options available to construct such cycles given in [41], which are both isomorphic to four-spheres:

$$\mathcal{M}_4 \in \{\mathbb{S}^4_{\text{colour}}, \mathbb{S}^4_{\text{flavour}}\} \tag{3.22}$$

For the case of colour M5 branes, we can take an interval $[0, N]$ in the y coordinate and use the circle $\mathbb{S}^1[\chi]$ and the two-sphere $\mathbb{S}^2[\theta, \varphi]$. We take $y = N$ to be a point at which $\mathbb{S}^1[\chi]$ shrinks smoothly,[7] while we also have that $\mathbb{S}^2[\theta, \varphi]$ shrinks to zero at $y = 0$. For $0 < y < N$ both $\mathbb{S}^1[\chi]$ and $\mathbb{S}^2[\theta, \varphi]$ have finite size. We can therefore fiber the product $\mathbb{S}^1[\chi] \times \mathbb{S}^2[\theta, \varphi]$ over the interval to construct a total space that is a compact cycle isomorphic to a four-sphere: $\mathbb{S}^4_{\text{colour}} \cong \mathbb{S}^1[\chi] \times \mathbb{S}^2[\theta, \varphi] \times [0, N]$.

For the flavour M5s we focus on the $y = 0$ slice of the (y, v_1, v_2) subspace and take a closed curve Γ in $\Sigma_2[v_1, v_2]$ enclosing a two-surface that is isomorphic to a disc D^2 and sits slightly above $y = 0$. We can choose this curve such that $\mathbb{S}^1[\chi]$ collapses smoothly on $\partial D^2 = \Gamma$. At any point $p \in \text{int}(D^2)$ we can then fiber the $\mathbb{S}^2[\theta, \varphi]$ which has a finite size. Due to our choice of curve[8] the boundary of this four-manifold vanishes and therefore we have a compact cycle that is also isomorphic to a four-sphere: $\mathbb{S}^4_{\text{flavour}} \cong \mathbb{S}^2[\theta, \varphi] \times D^2$.

Let us perform the calculation for colour branes. In order to do so, we take the limit of the geometry to the boundary $r \to \infty$, which makes $\mathrm{d}s_5^2 \to \mathrm{d}s^2_{\text{AdS}_5}$ and $X(r) \to 1$. At the boundary the deformed sphere $\tilde{\mathbb{S}}^2[\theta, \varphi]$ can be recast as a round sphere $\mathbb{S}^2[\theta, \varphi]$, as the fibration in this limit is just a constant which can be absorbed in the definition of the coordinates. The same is true for the fibration in $\mathbb{S}^1[\chi]$. We then have:

$$\int_{\mathbb{S}^4} G_4 = -2\kappa \int_{\mathbb{S}^2} \text{vol}_{\mathbb{S}^2} \int_0^{2\pi} \mathrm{d}\chi \int_0^N \mathrm{d}\left[-y^2 e^{-6\hat{\lambda}}\right] = (4\pi)^2 \kappa N, \tag{3.23}$$

where we used that near $y \sim N$ $e^{D_0} \sim (N - y)$ and $e^{3\hat{\lambda}} = N$, which expresses that $\mathbb{S}^1[\chi]$ shrinks in a non-singular fashion. This yields the following condition:

$$\frac{1}{16\pi^2\kappa} \int_{\mathbb{S}^4} G_4 = N \in \mathbb{N}, \tag{3.24}$$

[7] smoothness holds if $e^{D_0} \sim N - y$ near $y = N$.

[8] If one does not make the choice that $\mathbb{S}^1[\chi]$ vanishes at the boundary of the "cup" D^2, the total space will have a non trivial boundary isomorphic to $\mathbb{S}^2 \times \mathbb{S}^1$ and will not be compact.

JHEP04(2026)184

which agrees with the quantization condition in [44] using their convention which sets $\kappa = \frac{\pi}{2} l_p^3$ where l_p denotes the Planck length.

The flavour M5s correspond to punctures on the Riemann surface spanned by (v_1, v_2). If one considers K_i such punctures at different positions (v_1^i, v_2^i), then the integral of G_4 over $\mathbb{S}^4_{\text{flavour}}$ surrounding each puncture will yield K_i. As $\mathbb{S}^4_{\text{flavour}}$ is difficult to parametrize in the coordinates of the solution (3.14), the quantized flux can be more easily calculated by focusing near each puncture, where an additional rotational symmetry in (v_1, v_2) is assumed [44]. We will explore the solution with this additional symmetry, which gives rise to an electrostatic description, in the following subsection.

3.4 Type IIA backgrounds

We will now present a reduction of the former 11d theory on the M-theory circle, which yields new infinite families of deformed type IIA backgrounds of Gaiotto Maldacena type. These are geometries dual to linear quiver SCFTs enjoying $\mathcal{N} = 2$ supersymmetry in four dimensions. We start by rewriting the Riemann surface coordinates as $v_1 = \rho \cos\beta$, $v_1 = -\rho \sin\beta$. To make the reduction work, we need to have rotational symmetry in the $[v_1, v_2]$ subspace, meaning that ∂_β generates[9] a U(1) isometry and $D_0 = D_0(\rho, y)$. We can now make the following change of coordinates first presented in [44], where we map the coordinates $(\rho, y) \mapsto (\sigma, \eta)$ and the Toda function $D_0(\rho, y) \mapsto V(\sigma, \eta)$, where:

$$\begin{aligned} \dot{V} = \sigma \partial_\sigma V, \qquad V' = \partial_\eta V, \\ \rho^2 e^{D_0} = \sigma^2, \qquad y = \dot{V}, \qquad \log\rho = V', \end{aligned} \tag{3.25}$$

and the new function V satisfies the three dimensional cylindrically symmetric Laplace equation:

$$\ddot{V} + \sigma^2 V'' = 0, \tag{3.26}$$

supplemented with appropriate boundary conditions dictated by regularity of the metric. With these changes made, the 11d metric (3.14) takes the form:

$$\mathrm{d}s_{11}^2 = \tilde{f}_1 \left[4\tilde{f} \mathrm{d}s_5^2 + \tilde{f}_2 \mathrm{D}\mu^i \mathrm{D}\mu^i + \tilde{f}_3 (\mathrm{d}\chi + B)^2 + \tilde{f}_4 (\mathrm{d}\sigma^2 + \mathrm{d}\eta^2) + \tilde{f}_5 (\mathrm{d}\beta + \tilde{f}_6 \mathrm{d}\chi + \tilde{f}_6 B)^2 \right], \tag{3.27}$$

where we define the various functions to be

$$\begin{aligned} &\tilde{f}_1 = \kappa^{2/3} \left(\frac{\dot{V}\tilde{\Delta}}{2V''} \right)^{1/3}, \qquad \tilde{f} = X^{-1} Z, \qquad \tilde{f}_2 = \frac{2\dot{V}V''}{Z^2 \tilde{\Delta}}, \\ &\tilde{f}_3 = \frac{4X^3 \sigma^2 V''}{2X^3 \dot{V} - \ddot{V}} Z, \qquad \tilde{f}_4 = \frac{2V''}{\dot{V}} Z, \qquad \tilde{f}_5 = \frac{2(2X^3\dot{V} - \ddot{V})}{Z^2 \dot{V} \tilde{\Delta}}, \qquad \tilde{f}_6 = \frac{2X^3 \dot{V} \dot{V}'}{2X^3 \dot{V} - \ddot{V}} \\ &\tilde{\Delta} = (\dot{V}')^2 + V''(2\dot{V} - \ddot{V}), \quad Z = \left[\frac{(\dot{V}')^2 + V''(2X^3\dot{V} - \ddot{V})}{(\dot{V}')^2 + V''(2\dot{V} - \ddot{V})} \right]^{1/3}. \end{aligned} \tag{3.28}$$

Notice that in the absence of a scalar profile, namely $X = 1$, we have $Z = 1$ and we recover the deformed background presented in [27] (see equation (5.20) in that paper), while further taking

[9] The reason for choosing this coordinate and not another available U(1) being the preservation of $\mathcal{N} = 2$ supersymmetry.

JHEP04(2026)184

$r \to \infty$ recovers the original Gaiotto-Maldacena background.[10] After defining the function:

$$g(\eta,\sigma) = \frac{\dot{V}'}{\ddot{V}V'' - (\dot{V}')^2}, \tag{3.29}$$

the expressions entering the flux take the following form

$$\begin{aligned}
\tilde{G}_4 &= 2\,\mathrm{vol}\tilde{\mathbb{S}}^2 \wedge \Big[\mathrm{d}\tilde{f}_7 \wedge (\mathrm{d}\chi + B - g\mathrm{d}\beta) + \tilde{f}_8 \mathrm{d}g \wedge \mathrm{d}\beta + \tilde{f}_9 \left(\sigma V''\mathrm{d}\eta + \dot{V}'\mathrm{d}\sigma\right) \wedge \mathrm{d}\beta\Big]\,, \\
\beta_1^{(3)} &= -\frac{\kappa\sqrt{8}}{X^2}\mathrm{d}(\mu^3\dot{V})\,, \quad \beta_2 = 2\,\tilde{f}_7\,\mathrm{vol}\tilde{\mathbb{S}}^2, \\
\beta_2^{(3)} &= \sqrt{8}\Big\{\left(\tilde{f}_8 \mathrm{D}\mu^3 + \kappa\mu^3\mathrm{d}\dot{V}\right) \wedge (\mathrm{d}\chi + B - g\mathrm{d}\beta) + \mu^3\tilde{f}_9\left(\sigma V''\mathrm{d}\eta + \dot{V}'\mathrm{d}\sigma\right) \wedge \mathrm{d}\beta\Big\},
\end{aligned} \tag{3.30}$$

where

$$\tilde{f}_7 = \frac{2\kappa X^3 \dot{V}^2 V''}{\tilde{\Delta} + 2V''\dot{V}(X^3-1)}, \quad \tilde{f}_8 = \frac{\kappa\dot{V}\left[(\dot{V}')^2 - V''\ddot{V}\right]}{\tilde{\Delta} + 2V''\dot{V}(X^3-1)}, \quad \tilde{f}_9 = \frac{\kappa\sigma V''}{(\dot{V}')^2 - V''\ddot{V}}, \tag{3.31}$$

From here, we can apply the reduction following [44], as well as [45] for a detailed derivation. The ansatz reads:

$$\mathrm{d}s_{11}^2 = e^{-\frac{2}{3}\Phi}\mathrm{d}s_{10}^2 + e^{\frac{4}{3}\Phi}(\mathrm{d}\beta + C_1)^2 \quad \text{with} \quad A_3 = C_3 + B_2 \wedge \mathrm{d}\beta \quad \text{and} \quad \mathrm{d}A_3 = G_4 \tag{3.32}$$

where:

$$\begin{aligned}
\mathrm{d}s_{10}^2 &= \tilde{f}_1^{\frac{3}{2}}\tilde{f}_5^{\frac{1}{2}}\left[4\tilde{f}\mathrm{d}s_5^2 + \tilde{f}_2 \mathrm{D}\mu_i \mathrm{D}\mu^i + \tilde{f}_3(\mathrm{d}\chi + B)^2 + \tilde{f}_4(\mathrm{d}\sigma^2 + \mathrm{d}\eta^2)\right] \\
e^{\frac{4}{3}\Phi} &= \tilde{f}_1\tilde{f}_5, \quad C_1 = \tilde{f}_6(\mathrm{d}\chi + B), \\
H_3 &= \mathrm{d}B_2 = 2\mathrm{vol}\tilde{\mathbb{S}}^2 \wedge \Big[-g\,\mathrm{d}\tilde{f}_7 + \tilde{f}_8\mathrm{d}g + \tilde{f}_9(\sigma V''\mathrm{d}\eta + \dot{V}'\mathrm{d}\sigma)\Big] \\
&\quad + \sqrt{8}\mathcal{F}^{(3)} \wedge \Big[\mu^3\tilde{f}_9(\sigma V''\mathrm{d}\eta + \dot{V}'\mathrm{d}\sigma) - g\left(\tilde{f}_8\mathrm{d}\mu^3 + \kappa\mu^3\mathrm{d}\dot{V}\right)\Big]\,, \\
F_4 &= \mathrm{d}C_3 - H_3 \wedge C_1 = -2\tilde{f}_7\mathrm{vol}\tilde{\mathbb{S}}^2 \wedge G - \frac{\kappa\sqrt{8}}{X^2} \star_5 \mathcal{F}^{(3)} \wedge \mathrm{d}(\mu^3\dot{V}) \\
&\quad + 2\mathrm{vol}\tilde{\mathbb{S}}^2 \wedge \Big[\left(1 + g\,\tilde{f}_6\right)\mathrm{d}\tilde{f}_7 - \tilde{f}_6\tilde{f}_8\mathrm{d}g - \tilde{f}_6\tilde{f}_9(\sigma V''\mathrm{d}\eta + \dot{V}'\mathrm{d}\sigma)\Big] \wedge (\mathrm{d}\chi + B) \\
&\quad + \sqrt{8}\mathcal{F}^{(3)} \wedge \Big[-\mu^3\tilde{f}_6\tilde{f}_9(\sigma V''\mathrm{d}\eta + \dot{V}'\mathrm{d}\sigma) + (1 + g\tilde{f}_6)\left(\tilde{f}_8\mathrm{d}\mu^3 + \kappa\mu^3\mathrm{d}\dot{V}\right)\Big] \wedge (\mathrm{d}\chi + B).
\end{aligned} \tag{3.33}$$

We have checked that this configuration solves the type IIA supergravity equations of motion, in units where the AdS radius is equal to one. Note that this geometry, still contains an $\tilde{\mathbb{S}}^2[\theta,\varphi]$ (expressing the $\mathrm{SU}(2)_{\mathcal{R}}$ symmetry), as well as the $\mathbb{S}^1[\chi]$. Notably, we can rewrite the NS three-form in terms of total derivatives:

$$\begin{aligned}
\kappa^{-1}H_3 &= \mathrm{d}\mathcal{K} \wedge \mathrm{d}\Omega + \sqrt{8}\mathcal{F}^{(3)} \wedge \mathrm{d}\tilde{\Omega}, & \mathcal{K} &= 4\cos\theta A_{1\phi}(r)\mathrm{d}\phi - 2\cos\theta\mathrm{d}\varphi \\
\Omega &= \eta - \frac{\sigma^2\dot{V}\dot{V}'}{\ddot{V}^2 - 2\dot{V}\ddot{V}\lambda^6(r) + \sigma^2(\dot{V}')^2}, & \tilde{\Omega} &= \mu^3(\eta - \Omega),
\end{aligned} \tag{3.34}$$

[10] The AdS_5 part of the background is recovered when $r \to \infty$, where we find $\lambda(r) \to 1, F(r) \to L^{-2}$ and $\mathrm{d}s_5^2 \to \mathrm{d}s_{\mathrm{AdS}_5}^2$.

JHEP04(2026)184

which we can integrate on appropriate cycles to get local expressions for the NS potential B_2. The four possible expressions read as follows:

$$\begin{aligned} B_2^{(\mathrm{I})} &= 4A^1 \wedge \mathrm{d}(\mu^3(\eta-\Omega)) + 2\Omega(\mathrm{vol}_{\mathbb{S}^2} + 2\mu^3 \mathrm{d}A^1), \\ B_2^{(\mathrm{II})} &= 4\mu^3 \eta\, \mathrm{d}A^1 + 2\Omega \mathrm{vol}_{\mathbb{S}^2}, \\ B_2^{(\mathrm{III})} &= 4A^1 \wedge \mathrm{d}(\mu^3(\eta-\Omega)) + 2\mu^3(2A^1 - \mathrm{d}\varphi) \wedge \mathrm{d}\Omega, \\ B_2^{(\mathrm{IV})} &= 4\mu^3(\eta-\Omega)\mathrm{d}A^1 + 2\mu^3(2A^1 - \mathrm{d}\varphi) \wedge \mathrm{d}\Omega, \end{aligned} \tag{3.35}$$

all of which satisfy $\mathrm{d}B_2 = \kappa^{-1} H_3$ and are related by a gauge transformation:

$$B_2^{(\mathrm{II})} = B_2^{(\mathrm{I})} + \mathrm{d}\Lambda, \quad B_2^{(\mathrm{IV})} = B_2^{(\mathrm{III})} + \mathrm{d}\Lambda \quad \text{with} \quad \Lambda = 4\mu^3(\eta-\Omega)A^1. \tag{3.36}$$

This will be important for the quantization of Page charges associated with D4 branes, as well as some computations for the observables.

Let us briefly comment on the connection to the dual quiver theory. The new compact coordinate η together with $\sigma \in [0,\infty)$ constitute a strip on which the function V is supported. Our approach in presenting this will be to consider a fixed superconformal linear quiver on the boundary, depicted in figure 2, whose data is encoded in the boundary conditions of $V(\sigma,\eta)$. After fixing the boundary theory, the geometry will then yield the appropriately quantized Page charges. If we let $\eta \in [0,P]$, where P is the total length of the linear quiver, the boundary conditions for (3.26) read [44]:

$$\dot{V}\Big|_{\eta=0,P} = 0, \quad \dot{V}\Big|_{\sigma=0} = \mathcal{R}(\eta), \quad V\Big|_{\sigma\to\infty} = 0, \tag{3.37}$$

where $\mathcal{R}$ is a piecewise linear and convex function with finitely many discontinuities in its derivative, $\mathcal{R}'(\eta)$, at integer values of η which satisfies $\mathcal{R}(0) = \mathcal{R}(P) = 0$. This is called the rank function for the quiver and one choice for it which yields linear quivers with $P-1$ nodes containing gauge groups $\mathrm{SU}(N_i)$ is the following [45]:

$$\mathcal{R}(\eta) = \begin{cases} N_1 \eta\,, & \eta \in [0,1] \\ N_l + (N_{l+1} - N_l)(\eta - l)\,, & \eta \in [l, l+1]\,, \quad l = 1, \ldots, P-2 \\ N_{P-1}(P-\eta)\,, & \eta \in [P-1, P], \end{cases} \quad . \tag{3.38}$$

The second derivative of the rank function contains information about the ranks of the flavour groups (we take $N_0 = 0 = N_P$):

$$\mathcal{R}''(\eta) = \sum_{j=1}^{P-1} (2N_j - N_{j-1} - N_{j+1})\delta(\eta - j) = \sum_{j=1}^{P-1} F_j \delta(\eta - j), \tag{3.39}$$

where $F_j = 2N_j - N_{j-1} - N_{j+1}$. We can think of the system (3.26) with boundary conditions (3.37), (3.38) as a two-dimensional electrostatic problem of a charge density $\mathcal{R}(\eta)$ located at $\sigma = 0$ and two conducting planes at $\eta = 0$ and $\eta = P$ with zero potential. One can then proceed using separation of variables to obtain the following solution [46]:

$$\begin{aligned} V(\sigma,\eta) &= -\sum_{k=1}^{\infty} \mathcal{R}_k \sin\left(\frac{k\pi\eta}{P}\right) K_0\left(\frac{k\pi\sigma}{P}\right), \quad \mathcal{R}(\eta) = \sum_{k=1}^{\infty} \mathcal{R}_k \sin\left(\frac{k\pi\eta}{P}\right), \\ \mathcal{R}_k &= \frac{2}{P}\int_0^P \mathcal{R}(\eta) \sin\left(\frac{k\pi\eta}{P}\right) \mathrm{d}\eta = \frac{2P}{(k\pi)^2} \sum_{j=1}^{P} F_j \sin\left(\frac{k\pi j}{P}\right), \end{aligned} \tag{3.40}$$

where K_0 is the modified Bessel function of the second kind.

JHEP04(2026)184

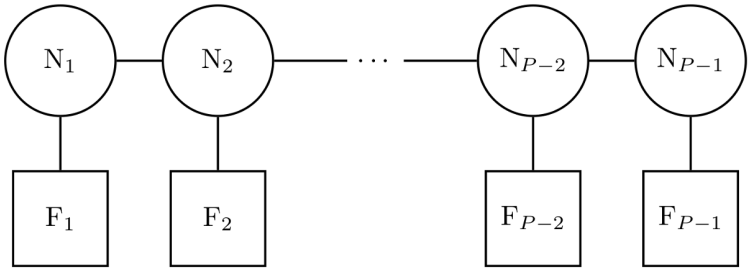

Figure 2. Quiver diagram for the linear quiver described by the rank function (3.38) with $(P-1)$ gauge nodes. The balancing conditions enforce that $F_k = 2N_k - N_{k-1} - N_{k+1}$ for each node.

	x^0 x^1 x^2 x^3	y^1 y^2 y^3	y^4 y^5	y^6
D4	——	· · ·	· ·	—
NS5	——	· · ·	——	·
D6	——	——	· ·	·

Table 1. Brane configuration for the Gaiotto-Maldacena solution when $G_N \to 0$ in flat space. A line signifies extension of the brane in the corresponding coordinate while a dot that the brane is localized there.

Page charges. In this subsection we will present the quantization of the Page charges. Unlike Maxwell fluxes, Page fluxes provide the correct quantization conditions which express the counting of branes at each stack. These are defined in terms of the RR polyform F as (setting $\alpha' = 1 = g_s$):

$$\hat{F} = e^{-B_2} \wedge F, \quad F = \sum_{n=1}^{5} F_{2n}, \quad Q_{\mathrm{D}_p} = \frac{1}{(2\pi)^{7-p}} \int_{\Sigma_{8-p}} \hat{F}_{8-p} \tag{3.41}$$

and for our purposes this gives $\hat{F}_2 = F_2$ and $\hat{F}_4 = F_4 - B_2 \wedge F_2$, as we have vanishing Romans mass $F_0 = 0$. We will follow closely [45], where the reader can find more details. The system described above contains the following extended objects at the following spacetime locations:

- A stack of NS5 branes located at $\sigma \to \infty$ extending in the coordinates of $\mathrm{d}s_5^2$ and χ,
- A stack of flavour D6 branes located at $\sigma = 0$ and at $\eta = k$ (the kinks of the rank function) and extending on $\mathrm{d}s_5^2$ and $\mathbb{S}^2$,
- A stack of colour D4 branes extending on $\mathbb{R}^{1,2} \times \mathbb{S}^1_\phi \times \mathbb{R}_\eta$.

Let us comment that from the brane configuration explained above, only the D6 flavour branes are made explicit in the solution (3.33), as they appear as localized sources, $\mathrm{d}\hat{F}_2 \propto \sum_k \delta(\eta - k)$. The rest of the branes have been replaced with units of $\hat{F}_4$ and H_3 fluxes.

One can consider a flat space $\mathbb{R}^{1,9}$ spanned by coordinates $(x^0, \ldots, x^3, y^1, \ldots, y^6)$, in which we have the brane setup depicted in table 1.

This system can be though of as the Hanany-Witten brane set-up at zero Newton constant. As one starts increasing G_N, the branes start backreacting, sourcing a curved

JHEP04(2026)184

geometry. There is a nonlinear transformation involving a near horizon limit which then maps the coordinates (x^i, y^j) to the ones appearing in the solution (3.33), with y^6 giving rise to η. The precise transformation is not known. The $\mathrm{SU}(2) \times \mathrm{U}(1) \cong \mathrm{SO}(3) \times \mathrm{SO}(2)$ $\mathcal{R}$-symmetry preserved by the QFT dual of (3.33) is initially described by isometries of the (y^1, y^2, y^3) and (y^4, y^5) subspaces.

We take again the limit $r \to \infty$ to calculate the fluxes, in which case we have $\mathrm{d}s_5^2 \to \mathrm{d}s^2_{\mathrm{AdS}_5}$ as well as:

$$\begin{aligned}
&X \to 1, && \tilde{f} \to \kappa^{2/3}, && \tilde{f}_2 \to \frac{2\dot{V}V''}{\tilde{\Delta}}, && \tilde{f}_3 \to \frac{4\sigma^2 V''}{2\dot{V} - \ddot{V}},\\
&\tilde{f}_4 \to \frac{2V''}{\dot{V}}, && \tilde{f}_5 \to \frac{2(2\dot{V} - \ddot{V})}{\tilde{\Delta}}, && \tilde{f}_6 \to \frac{2\dot{V}\dot{V}'}{2\dot{V} - \ddot{V}}, &&\\
&\tilde{f}_7 \to \frac{2\kappa \dot{V}^2 V''}{\tilde{\Delta}}, && \tilde{f}_8 \to \frac{\kappa \dot{V}\left[(\dot{V}')^2 - V''\ddot{V}\right]}{\tilde{\Delta}}, && \tilde{f}_9 \to \frac{\kappa\sigma V''}{(\dot{V}')^2 - \ddot{V}V''}. &&
\end{aligned} \tag{3.42}$$

Let us begin with the NS5 branes. In the limit where $\sigma \to \infty$ we can write the approximate form of the Laplace potential from (3.40) using the asymptotic behaviour of the Bessel function at infinity $K_0(x) \approx \sqrt{\frac{\pi}{2x}} e^{-x} + \mathcal{O}(e^{-x} x^{-3/2})$:

$$V(\sigma, \eta) \approx -\sqrt{\frac{P}{2\sigma}} \sum_{k=1}^{\infty} \frac{\mathcal{R}_k}{\sqrt{k}} \sin\left(\frac{k\pi}{P}\eta\right) e^{-\frac{k\pi\sigma}{P}} \approx -\sqrt{\frac{P}{2\sigma}} \mathcal{R}_1 \sin\left(\frac{\pi\eta}{P}\right) e^{-\frac{\pi\sigma}{P}} + \ldots, \tag{3.43}$$

where we keep only the leading term. Using this expression for V the metric takes the form:

$$\begin{aligned}
\mathrm{d}s_{10}^2 \to \kappa \Bigg\{ & 4\sigma(\mathrm{d}s^2_{\mathrm{AdS}_5} + \mathrm{d}\chi^2) + \frac{2P}{\pi} \sin^2\left(\frac{\pi\eta}{P}\right) \mathrm{d}s^2_{\mathbb{S}^2} + \frac{2\pi}{P}(\mathrm{d}\sigma^2 + \mathrm{d}\eta^2) \\
& - \frac{8LPq_1\ell^2\varepsilon \sin^2\theta}{\pi r_\star^2} \sin^2\left(\frac{\pi\eta}{P}\right) \mathrm{d}\phi \mathrm{d}\varphi + \frac{8Lq_2\ell^2\varepsilon\sigma}{r_\star^2 + \ell^2\varepsilon} \mathrm{d}\phi \mathrm{d}\chi \Bigg\},
\end{aligned} \tag{3.44}$$

The asymptotic expressions for H_3 and the dilaton take the form:

$$\begin{aligned}
\kappa^{-1} H_3 = {} & 4\sin^2\left(\frac{\pi\eta}{P}\right) \mathrm{d}\eta \wedge \mathrm{vol}_{\mathbb{S}^2} + \frac{P}{2\pi\sigma} \sin\left(\frac{2\pi\eta}{P}\right) \mathrm{d}\sigma \wedge \mathrm{vol}_{\mathbb{S}^2} \\
& - \frac{8Lq_1\ell^2\varepsilon}{r_\star^2} \sin^2\left(\frac{\pi\eta}{P}\right) \sin\theta \, \mathrm{d}\eta \wedge \mathrm{d}\theta \wedge \mathrm{d}\phi - \frac{LPq_1\ell^2\varepsilon}{\pi\sigma r_\star^2} \sin\left(\frac{2\pi\eta}{P}\right) \sin\theta \, \mathrm{d}\sigma \wedge \mathrm{d}\theta \wedge \mathrm{d}\phi,
\end{aligned} \tag{3.45}$$

$$e^{-\Phi} \to \frac{\pi^{3/2} \mathcal{R}_1 e^{-\frac{\pi\sigma}{P}}}{2P\sqrt{\sigma}}, \tag{3.46}$$

while $C_1 \to 0$ at leading order. The suitable cycle to integrate H_3, see [44], is a round unit radius three-sphere which we can construct as $\mathbb{S}^3 = \{(\frac{\pi}{P}\eta, \mathbb{S}^2) \mid \eta \in [0, P]\}$ leading to the following quantization[11] condition:

$$Q_{\mathrm{NS5}} = \frac{1}{(4\pi)^2} \int_{\mathbb{S}^3} H_3 = \frac{1}{2\pi} \int_{\mathbb{S}^2} \mathrm{vol}_{\mathbb{S}^2} \int_0^P \mathrm{d}\eta \, \sin^2\left(\frac{\pi\eta}{P}\right) = P. \tag{3.47}$$

[11] We remind the reader that we fix $\kappa = \pi/2$ (in units where $\ell_p = 1$) in order for the fluxes to be properly quantized.

JHEP04(2026)184

Moving to the stacks of D6, we will use the following coordinates for the (σ, η) subspace:

$$\eta = k - \rho\cos\alpha, \quad \sigma = \rho\sin\alpha, \tag{3.48}$$

and take $\rho \to 0$, corresponding to the limit $\sigma \to 0$ and $\eta = k \in (0, P)$. By focusing on a specific k we have the relations:

$$\dot{V} = N_k, \quad V'' = \frac{F_k}{2\rho}, \quad \dot{V}' = \frac{F_k}{2}(1+\cos\alpha) + N_{k+1} - N_k. \tag{3.49}$$

The metric in this limit takes the following form:

$$\mathrm{d}s_{10}^2 \to 2\kappa\sqrt{N_k}\left[\sqrt{\frac{\rho}{F_k}}(4\mathrm{d}s^2_{\mathrm{AdS}_5} + \mathrm{d}s^2_{\mathbb{S}^2}) + \sqrt{\frac{F_k}{\rho}}(\mathrm{d}\rho^2 + \rho^2\mathrm{d}s^2_{\mathbb{S}'^2})\right], \tag{3.50}$$

where there is second two-sphere spanned by (α, χ): $\mathrm{d}s^2_{\mathbb{S}'^2} = \mathrm{d}\alpha^2 + \sin^2\alpha\,\mathrm{d}\chi^2$. This is indeed, up to a constant factor, the near horizon metric for a stack of D6 branes extending in AdS_5 and $\mathbb{S}^2$. The RR potential and the two-form flux take the following form:

$$\begin{aligned}
C_1 &\to \left[\frac{F_k}{2}(1+\cos\alpha) + N_{k+1} - N_k\right]\mathrm{d}\chi + \frac{Lq_2\ell^2\varepsilon\left[(1+\cos\alpha)F_k - 2N_k + 2N_{k+1}\right]}{2(r_\star^2 + \ell^2\varepsilon)}\mathrm{d}\phi,\\
F_2 = \mathrm{d}C_1 &\to -\frac{F_k}{2}\mathrm{vol}_{\mathbb{S}'^2} - \frac{Lq_2\ell^2\varepsilon F_k\sin\alpha\,\mathrm{d}\alpha\wedge\mathrm{d}\phi}{2(r_\star^2+\ell^2\varepsilon)}\\
&\quad + \frac{Lq_2\ell^2\varepsilon F_k\sin^2(2\alpha)\left[F_k(1+\cos\alpha) - 2N_k + 2N_{k+1}\right]}{32(r_\star^2+\ell^2\varepsilon)N_k}\mathrm{d}\rho\wedge\mathrm{d}\phi\\
&\quad + \frac{F_k\sin^2(2\alpha)\left[F_k(1+\cos\alpha) - 2N_k + 2N_{k+1}\right]}{32N_k}\mathrm{d}\rho\wedge\mathrm{d}\chi,
\end{aligned} \tag{3.51}$$

which gives us the quantization condition:

$$Q^k_{\mathrm{D6}} = -\frac{1}{2\pi}\int_{\mathbb{S}'^2} F_2 = F_k = 2N_k - N_{k+1} - N_{k-1}, \quad k = 1, 2, \ldots, P-1, \tag{3.52}$$

with the total D6 charge being:

$$Q_{\mathrm{D6}} = \sum_{k=1}^{P-1} Q^k_{\mathrm{D6}} = N_{P-1} + N_1 = \int_0^P \mathrm{d}\eta\,\mathcal{R}''(\eta). \tag{3.53}$$

For the D4 Page charges, we construct the flux $\hat{F}_4 = F_4 - B_2\wedge F_2$ using the expressions for B_2 in (3.35), where we verify that the last two give a zero Page charge, while the first two yield asymptotically:

$$\hat{F}_4 = \kappa k F_k\sin\alpha\sin\theta\,\mathrm{d}\alpha\wedge\mathrm{d}\theta\wedge\mathrm{d}\varphi\wedge\mathrm{d}\chi = \kappa k F_k\,\mathrm{vol}_{\mathbb{S}^2}\wedge\mathrm{vol}_{\mathbb{S}'^2}. \tag{3.54}$$

This leads to the following expression for the D4 charge in a cell $[k, k+1]$:

$$Q^k_{\mathrm{D4}} = \frac{1}{(2\pi)^3}\int_{\mathbb{S}^2\times\mathbb{S}'^2}\hat{F}_4 = kF_k, \tag{3.55}$$

while the total Page charge of the D4 branes is given by:

$$Q_{\mathrm{D4}} = \sum_{k=1}^{P-1} Q^k_{\mathrm{D4}} = \sum_{k=1}^{P-1} kF_k = PN_{P-1}. \tag{3.56}$$

JHEP04(2026)184

As pointed out in [45], the calculation of the above quantity includes the induced charges of the D4s on the other stacks of branes. The "true" colour charge of the D4 branes is given by the formula [47]:

$$Q_{\rm D4}^{\rm total} = \int_0^P {\rm d}\eta\, \mathcal{R}(\eta). \tag{3.57}$$

Let us comment that the integral (3.55) does not yield the rank of the gauge group between $\eta = k$ and $\eta = k+1$, namely N_k, as opposed to (3.52) which gives off the rank of the flavour group F_k. This can be explained in two different ways. For once, the groups $\mathrm{SU}(F_k)$ represent physical symmetries of the dual theory, while the gauge groups $\mathrm{SU}(N_k)$ do not correspond to any physical symmetry and thus it is not necessarily the case that one can extract the various gauge group ranks from quantized charges. Another reason is that in the case of the D6s, one can clearly tell their location in the η coordinate (corresponding to a singularity in the metric), which is not the case for D4s, as they are replaced with fluxes. Finally, one might notice that the Page charges have similar expressions as in the undeformed Gaiotto-Maldacena background. This is due to the quantized charges being invariant under bulk deformations which respect the boundary geometry.

4 Observables of the dual field theories

In the present section we will calculate various observables in the dual field theories of the backgrounds presented in section 3. These include: the expectation value of the Wilson and 't Hooft loop operators, entanglement entropy, flow central charge, holographic complexity as well as the study of D7 brane embeddings in the case of the deformed type IIB background of Anabalon and Ross [24]. We will present the holographic calculation of said observables while emphasizing two key features. The first feature is universality. The resulting expressions are factorized into two parts, one depending on the radial direction which contains the dynamics of each object in gravity, while the other numerical factor containing details of the internal space and expressing information about the UV SCFTs. We attribute this phenomenon to the theorem of Gauntlett and Varela presented as a conjecture in [48] and later proved in [49] using G-structure techniques. The theorem states that any SUSY solution of supergravity in dimensions D=10 or D=11, which can be written as a warped product $\mathrm{AdS}_{d+1} \times_w \mathcal{M}_{D-d-1}$ consistently truncates on[12] $\mathcal{M}_{D-d-1}$ resulting in a gauged supergravity in $(d+1)$-dimensions. The field content of the gauged lower dimensional theory is dual to the superconformal current multiplet of the SCFT_d dual. The fields belonging to this multiplet are the ones responsible for the dynamical/radially dependent part of the observables. In this sense, the behaviour of these observables, even in the case where they do involve the internal space in their calculation (like the flow central charge and entanglement entropy), depends only on the underlying 5d gauged supergravity. The second feature concerns the singularity study we presented in section 2.2. We notice that even in the case of the solutions being smooth ($\hat{\nu} \approx -1$ but never -1), the Wilson loop observable is affected by the high curvature in the supergravity, signalling that the theory is not a trustable approximation in this region of parameter space. This presents itself as a first order phase transition near this region of parameter space, which

[12] $\mathcal{M}_{D-d-1}$ is required to be Riemannian.

JHEP04(2026)184

we argue is not physically relevant. Additionally, appendices A and B are dedicated to the study of Polyakov loops and the effective gauge coupling constant of each QFT.

4.1 Wilson loop

Let us first review the calculation of the Wilson loop in the context of holography [50]. Starting from a gauge theory perspective, one can define the Wilson loop as the following non local operator:

$$W(\mathcal{C}) = \frac{1}{N}\mathrm{tr}\,\mathcal{P}\exp\left(i\oint_{\mathcal{C}} A\right), \tag{4.1}$$

where N is the rank of the gauge group and $\mathcal{C}$ is any closed loop, conveniently taken to be a rectangular contour in time and one spatial coordinate. Then the vacuum expectation value of this operator provides a way of investigating the potential between a pair of non dynamical, infinitely massive, quark and anti-quark in the fundamental representation:

$$\langle W(\mathcal{C})\rangle \propto e^{-\mathcal{T}\,E(L_{\mathrm{QQ}})}, \tag{4.2}$$

where $\mathcal{T}$ is the temporal length of $\mathcal{C}$ and L_{QQ} the distance between the pair. From here one can deduce if the theory is *confining* or if it presents *screening*. This calculation is implemented in the dual string theory (in the large N limit, with $g^2_{\mathrm{YM}}N$ fixed) by embedding a probe F1 string with its endpoints fixed on the path $\mathcal{C}$ at the boundary of the spacetime ($r=\infty$), representing the quark and anti-quark, while the rest of the string enters the bulk in a U shaped fashion. In this regime, the string theory is approximated by supergravity and we can use the Nambu-Goto action of classical string embeddings whose worldsheets, with a fixed boundary $\mathcal{C}$, are minimal surfaces: $\langle W(\mathcal{C})\rangle \sim e^{-S_{\mathrm{NG}}}$, where:[13]

$$S_{\mathrm{NG}} = \frac{1}{2\pi}\int \mathrm{d}^2\hat{\sigma}\sqrt{-\det(g_{\mathrm{ind}})}, \tag{4.3}$$

with g_{ind} being the induced metric on the string.

In this section we consider, aside from the usual Wilson loop that was also presented in [1], other configurations that wrap or rotate in $\mathbb{S}^1[\phi]$. We will however restrict to embeddings that are not extended along the internal space, resulting in the universal behaviour highlighted earlier in the text. Here are the three types of configurations of interest:

- **Embedding I.** The first case we will study is the simple embedding in which we give the string a profile in r and its worldsheet coordinates are parametrized as:

$$\tau = t, \quad \hat{\sigma} = w, \quad r = r(\hat{\sigma}), \tag{4.4}$$

  while the rest of the spacetime coordinates take constant values. In the case of the type IIB background, the consistency of the embedding demands the coordinate θ_0 to be either 0 or $\frac{\pi}{2}$.

[13] We make the choice to set $\alpha' = 1$. We also denote all worldvolume coordinates as $\hat{\sigma}$ instead of σ to avoid confusion with the Gaiotto-Maldacena coordinate σ in the type IIA backgrounds.

JHEP04(2026)184

- **Embedding II.** In this embedding we consider a string with the same profile, which now is spinning along $\mathbb{S}^1[\phi]$ with constant angular velocity ω:

$$\tau = t, \quad \hat{\sigma} = w, \quad r = r(\hat{\sigma}), \quad \phi(\tau) = \omega\tau. \tag{4.5}$$

- **Embedding III.** For the final embedding we will use, we place a string that wraps the $\mathbb{S}^1[\phi]$, while still having a profile in the radial coordinate:

$$\tau = t, \quad \hat{\sigma} = w, \quad r = r(\hat{\sigma}), \quad \phi = \phi(\hat{\sigma}), \tag{4.6}$$

and in the case of the type IIB background the embedding is consistent for $\theta_0 = 0$ and $\psi_0 = \frac{\pi}{4}$.

In all the above cases, the action of the string reduces to following form:

$$S_{\rm NG} \propto \int_{-L_{\rm QQ}/2}^{L_{\rm QQ}/2} \mathrm{d}w \sqrt{\mathcal{F}^2 + \mathcal{G}^2 r'^2}, \tag{4.7}$$

with $\mathcal{F}$ and $\mathcal{G}$ being case specific functions of r. One can then derive expressions for the length and energy of the quark-anti-quark pair in terms of $\mathcal{F}$ and $\mathcal{G}$ using the formulas in [51, 52]. Below r_0 denotes the turning point of the probe:

$$\begin{aligned} V_{\rm eff}(r; r_0) &= \frac{\mathcal{F}(r)\sqrt{\mathcal{F}^2(r) - \mathcal{F}^2(r_0)}}{\mathcal{F}(r_0)\mathcal{G}(r)}, \quad L_{\rm QQ}(r_0) = 2\int_{r_0}^{\infty} \frac{\mathrm{d}r}{V_{\rm eff}(r; r_0)}, \\ E_{\rm QQ}(r_0) &= \mathcal{F}(r_0) L_{\rm QQ}(r_0) + 2\int_{r_0}^{\infty} \mathrm{d}r \frac{\mathcal{G}(r)}{\mathcal{F}(r)} \sqrt{\mathcal{F}^2(r) - \mathcal{F}^2(r_0)} - 2\int_{r_\star}^{\infty} \mathrm{d}r \mathcal{G}(r). \end{aligned} \tag{4.8}$$

These integrals are not analytically solvable, therefore we employ numerical techniques to plot them. However, one can write analytic approximate expressions for the length, developed in [52], and the energy[14] of the pair:

$$L_{\rm app}(r_0) = \left.\frac{\pi \mathcal{G}(r)}{\mathcal{F}'(r)}\right|_{r=r_0}, \quad E_{\rm app}(r_0) = \int^{r_0} \mathrm{d}s\, \mathcal{F}(s) \frac{\mathrm{d}L_{\rm app}(s)}{\mathrm{d}s}, \tag{4.9}$$

which serve as a nice way of quickly determining the behaviour of the dynamics of the quark-anti-quark system. Let us now proceed to studying the Wilson loops[15] in each case and highlight the effects of the different embeddings.

4.1.1 Wilson loop for the Type IIB background

Embedding I. For the simple embedding of case I, we have checked that it is consistent in this background if one chooses the value of the angular coordinate θ to be $\theta_0 = 0$ or $\theta_0 = \pi/2$. In each case, have the following induced metric:

$$\mathrm{d}s^2_{\rm ind} = -\frac{r^2\zeta(r,\theta_0)}{L^2}\mathrm{d}t^2 + \left[\frac{r^2\zeta(r,\theta_0)}{L^2} + \frac{\zeta(r,\theta_0) r'^2}{r^2 F(r) \lambda^6(r)}\right] \mathrm{d}w^2, \tag{4.10}$$

[14] This expression was first introduced in the context of entanglement entropy calculations in [53, 54].

[15] For the remainder of the paper we will use the SUSY condition $|q_1| = |q_2| = Q$.

JHEP04(2026)184

which yields the following action (where $\mathcal{T} = \int \mathrm{d}t$):

$$\mathrm{S_{F1}} = \frac{\mathcal{T}}{2\pi}\int_{-L_{\mathrm{QQ}}/2}^{L_{\mathrm{QQ}}/2} \mathrm{d}w\sqrt{\mathcal{F}_{\mathrm{I}}^2 + \mathcal{G}_{\mathrm{I}}^2 r'^2} \quad \text{with} \quad \mathcal{F}_{\mathrm{I}}^2 = \frac{r^4\zeta^2(r,\theta_0)}{L^4}, \quad \mathcal{G}_{\mathrm{I}}^2 = \frac{\zeta^2(r,\theta_0)}{L^2\lambda^6(r)F(r)}. \tag{4.11}$$

From these functions we can derive the various expressions of interest. It is convenient to use the dimensionless quantity $\hat{\mu} = \left(\frac{r_\star}{L}\right)^4$ together with $\hat{\nu}$ and ξ for the various expressions, in terms of which the functions in (4.11) take the following form:

$$\mathcal{F}_{\mathrm{I}}^2 = \hat{\mu}\xi^2(\xi^2 + \hat{\nu}\cos^2\theta_0), \quad \mathcal{G}_{\mathrm{I}}^2 = \frac{\xi^4(\xi^2 + \hat{\nu}\cos^2\theta_0)}{\xi^6 + \hat{\nu}\xi^4 - (1+\hat{\nu})}. \tag{4.12}$$

Using numerical integration, we plot the length L_{QQ} as a function of the turning point as well as a parametric plot of the potential energy E_{QQ} between the quark and anti-quark with respect to the length of separation. The results for the embedding with $\theta_0 = 0$ are depicted in figure 3. What we discover is that as $\hat{\nu}$ takes different values away from -1 the background displays confining behaviour, that is, E_{QQ} starts with a Coulombic law for small separations (dictated by conformality in the ultraviolet) while at large L_{QQ} it is linear, signalling confinement in the infrared. However, when $\hat{\nu}$ takes values very close to -1 and smaller than $\hat{\nu} \approx -0.95$, where the geometry becomes highly curved, the length starts becoming double-valued and there seems to be a first order phase transition appearing in the energy. We claim that what is observed in figure 3(d) is a manifestation of the supergravity approximation being not trustable in this region in parameter space and for this embedding,[16] in other words, this *is not* a trustworthy result. Finally, we comment that the approximate expressions (4.9) capture very nicely the qualitative behaviour of the system, which can be seen in the plots of figure 4.

Embedding II. The idea of the spinning string embedding is that we might be able to lift the effects observed in figure 3(d) even for the value $\hat{\nu} = -0.99$ by introducing the new parameter ω which can affect the dynamics. More specifically, the angular momentum of the probe F1 introduces restoring effects on the U shaped embedding, much like in the case of a centrifugal force. If we consider for a moment both type the IIA and type IIB metrics by writing $\mathrm{d}s_{10}^2 = -G_{tt}\mathrm{d}t^2 + G_{ww}\mathrm{d}w^2 + G_{\phi\phi}\mathrm{d}\phi^2 + G_{rr}\mathrm{d}r^2 + \ldots$, the Nambu-Goto action for embedding (4.5) has the form:

$$\mathcal{L}_{\mathrm{NG}} = \sqrt{(G_{tt} - \omega^2 G_{\phi\phi})(G_{ww} + G_{rr}r'^2)}, \tag{4.13}$$

from which stems the following bound for the Lagrangian to be real:

$$\omega^2 G_{\phi\phi} \leq G_{tt}. \tag{4.14}$$

The range of values for the radial coordinate $r \in [r_\star, \infty)$ is restricted accordingly such that the above requirement holds, which in turn is interpreted as a "restoring force" preventing the string from reaching values arbitrarily close to $r_\star$.

[16] This behaviour does not appear for $\theta_0 = \pi/2$, see figure 4(b) and (d).

JHEP04(2026)184

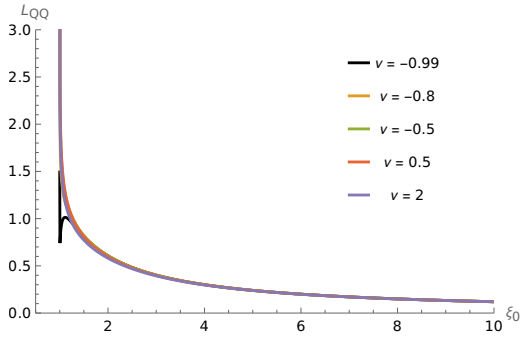

(a) Plot of the quark-anti-quark separation for various values of $\hat{\nu}$.

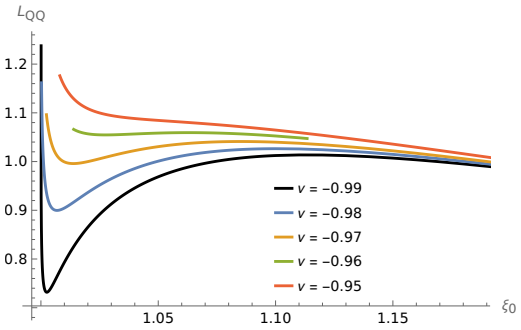

(b) Closer look at the plot of the separation length as $\hat{\nu}$ approaches -1.

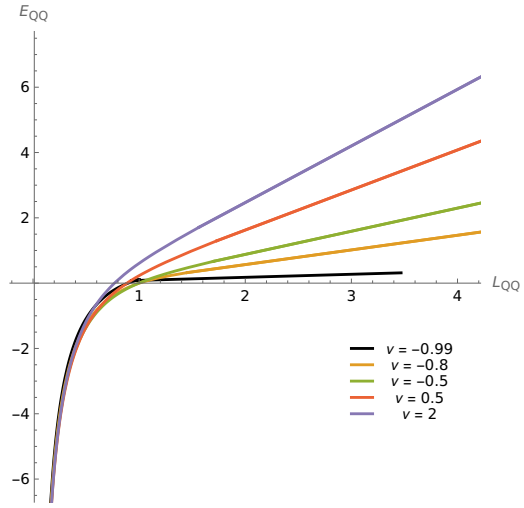

(c) Plot of the potential energy of the quark-anti-quark pair with respect to their separation for various values of $\hat{\nu}$.

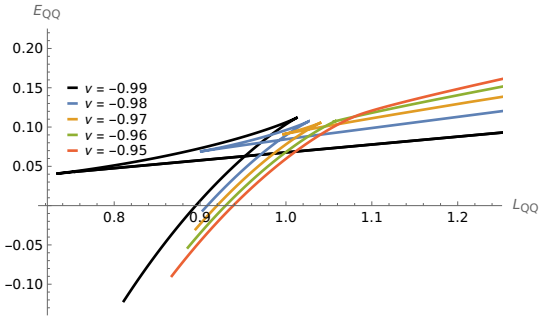

(d) Closer look at the plot of the energy as $\hat{\nu}$ approaches -1.

Figure 3. Resulting plots using numerical integration regarding the WL embedding I for different values of $\hat{\nu}$. We notice the length gradually becoming double-valued as $\hat{\nu} \to -1$. We have set $\theta_0 = 0$.

In the case of the type IIB solution, we have the induced metric:

$$\begin{aligned} \mathrm{d}s^2_{\mathrm{ind}} = \frac{1}{\zeta(r,\theta_0)} \left\{ \frac{\zeta^2(r,\theta_0) r^2 \left[L^2\omega^2 F(r) - 1\right]}{L^2} + \omega^2 \cos^2\theta_0 A_1^2 + \omega^2 \sin^2\theta_0 \lambda^6(r) A_3^2 \right\} \mathrm{d}t^2 \\ + \frac{\zeta(r,\theta_0)}{r^2} \left[\frac{r^4}{L^2} + \frac{r'^2}{F(r)\lambda^6(r)} \right] \mathrm{d}w^2 \,. \end{aligned} \tag{4.15}$$

The Nambu-Goto action then yields:

$$\mathrm{S}_{\mathrm{F1}} = \frac{\mathcal{T}}{2\pi} \int_{-L_{\mathrm{QQ}}/2}^{L_{\mathrm{QQ}}/2} \mathrm{d}w \sqrt{\mathcal{F}_{\mathrm{II}}^2 + \mathcal{G}_{\mathrm{II}}^2 r'^2}, \tag{4.16}$$

JHEP04(2026)184

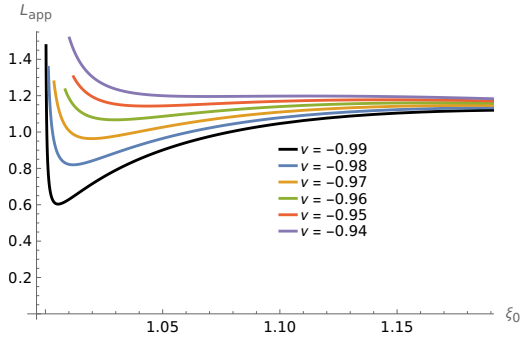

(a) Plot of the approximate length function for various values of $\hat{\nu}$ and $\theta_0 = 0$.

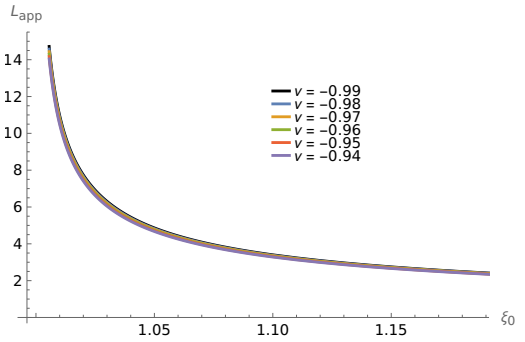

(b) Plot of the approximate length function for various values of $\hat{\nu}$ and $\theta_0 = \frac{\pi}{2}$.

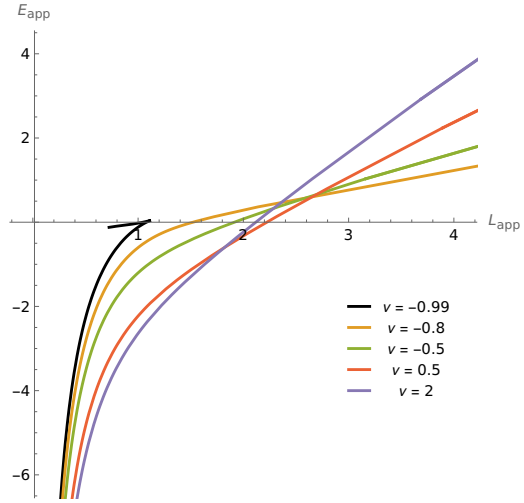

(c) Plot of the approximate potential energy as a function of the approximate length for various values of $\hat{\nu}$ and $\theta_0 = 0$.

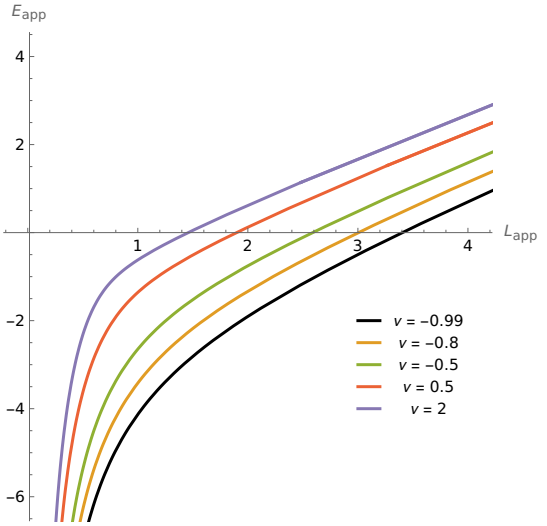

(d) Plot of the approximate potential energy as a function of the approximate length for various values of $\hat{\nu}$ and $\theta_0 = \frac{\pi}{2}$.

Figure 4. Wilson loop plots for embedding I using the approximate length and energy expressions (4.9) for various values of $\hat{\nu}$ and the two options $\theta_0 \in \{0, \pi/2\}$.

where now,

$$\begin{aligned}
\mathcal{F}_{\text{II}}^2 &= \frac{r^4\zeta^2(r,\theta_0)}{L^4} - \frac{r^2\omega^2}{L^2}\left[\cos^2\theta_0 A_1^2 + \sin^2\theta_0\lambda^6(r)A_3^2 + r^2F(r)\zeta^2(r,\theta_0)\right], \\
\mathcal{G}_{\text{II}}^2 &= \frac{\zeta^2(r,\theta_0)}{L^2F(r)\lambda^6(r)} - \frac{\omega^2}{r^2F(r)\lambda^6(r)}\left[\cos^2\theta_0 A_1^2 + \sin^2\theta_0\lambda^6(r)A_3^2 + r^2F(r)\zeta^2(r,\theta_0)\right].
\end{aligned} \tag{4.17}$$

or, in terms of the dimensionless quantities:

$$\begin{aligned}
\mathcal{F}_{\text{II}}^2 &= \hat{\mu}\xi^2(\hat{\nu}\cos^2\theta_0 + \xi^2) - \frac{\hat{\mu}(\xi^2-1)\omega^2}{2(1+\hat{\nu})}\left[4 + 5\hat{\nu} + 2\hat{\nu}^2 + 2(\hat{\nu}+1)\xi^2 + \hat{\nu}(3+2\hat{\nu})\cos(2\theta_0)\right], \\
\mathcal{G}_{\text{II}}^2 &= \frac{\xi^4\left(\xi^2 + \hat{\nu}\cos^2\theta_0\right)}{\xi^6 + \hat{\nu}\xi^4 - (1+\hat{\nu})} - \frac{\xi^2\omega^2}{2(1+\hat{\nu})}\frac{\left[4 + 5\hat{\nu} + 2\hat{\nu}^2 + 2(\hat{\nu}+1)\xi^2 + \hat{\nu}(3+2\hat{\nu})\cos(2\theta_0)\right]}{\xi^4 + \xi^2(1+\hat{\nu}) + 1 + \hat{\nu}}.
\end{aligned} \tag{4.18}$$

JHEP04(2026)184

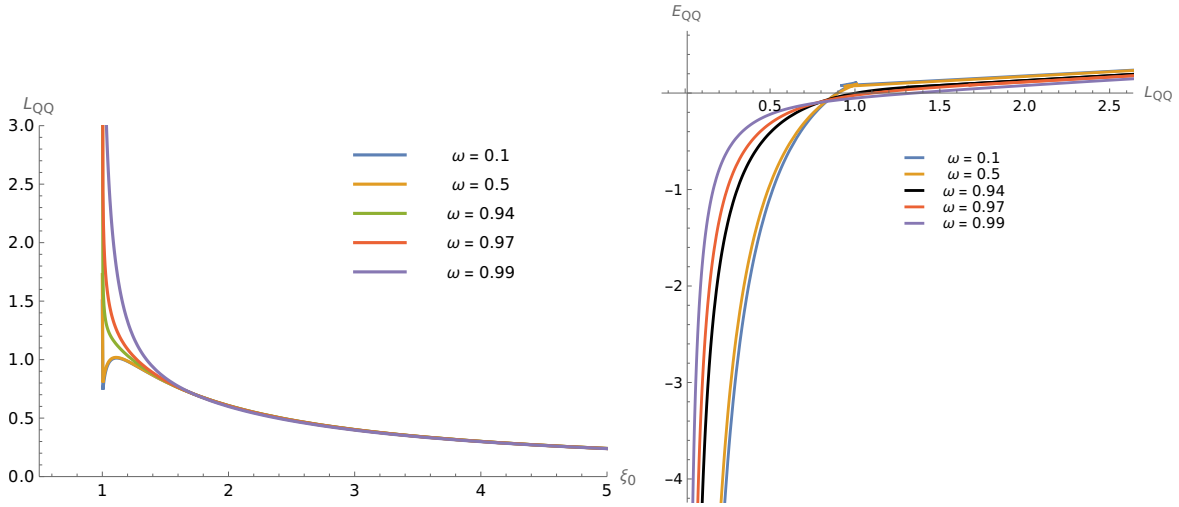

(a) Plot of the length of separation (4.19) for $\hat{\nu} = -0.99$, $\theta_0 = 0$ and various values of ω.

(b) Plot of the energy of the pair with respect to the length of separation for $\hat{\nu} = -0.99$, $\theta_0 = 0$ and various values of ω.

Figure 5. We notice that for values of ω close to 0.99 we get a single valued length and no phase transition, even when $\hat{\nu} = -0.99$ and $\theta_0 = 0$.

In the above expressions we can recognise the same functions as in the previous embedding (4.12) in the first terms, while the second terms are controlled by the new $\omega \neq 0$ parameter we introduced. The length and energy integral expressions read:[17]

$$L^{(\mathrm{II})}_{\mathrm{QQ}}(\xi_0) = 2r_\star\sqrt{\hat{\mu}}\int_{\xi_0}^{\infty}\mathrm{d}\xi\,\xi\sqrt{\frac{\xi_0^2(\hat{\nu}+\xi_0^2)-(\xi_0^2-1)\left[2(1+\hat{\nu})+\xi_0^2\right]\omega^2}{(\xi^2-\xi_0^2)\left[\xi^6+\hat{\nu}\xi^4-(1+\hat{\nu})\right]\left[\hat{\nu}+\xi^2+\xi_0^2-(1+2\hat{\nu}+\xi^2+\xi_0^2)\omega^2\right]}} \tag{4.19}$$

and

$$\begin{aligned} E^{(\mathrm{II})}_{\mathrm{QQ}}(\xi_0) =& \sqrt{\hat{\mu}}\sqrt{\xi_0^2(\hat{\nu}+\xi_0^2)-(\xi_0^2-1)\left[2(1+\hat{\nu})+\xi_0^2\right]\omega^2}\,L^{(\mathrm{II})}_{\mathrm{QQ}}(\xi_0) \\ &+ 2r_\star\int_{\xi_0}^{\infty}\mathrm{d}\xi\,\xi\sqrt{\frac{(\xi^2-\xi_0^2)\left[\hat{\nu}+\xi^2+\xi_0^2-(1+2\hat{\nu}+\xi^2+\xi_0^2)\omega^2\right]}{\xi^2+\hat{\nu}\xi^4-(1+\hat{\nu})}} \\ &- 2r_\star\int_{1}^{\infty}\mathrm{d}\xi\,\xi\sqrt{\frac{\xi^2(\hat{\nu}+\xi^2)-(\xi^2-1)\left[2(1+\hat{\nu})+\xi^2\right]\omega^2}{\xi^6+\hat{\nu}\xi^4-(1+\hat{\nu})}}\,. \end{aligned} \tag{4.20}$$

We observe in figure 5 that there is indeed a range of values for the newly introduced parameter, which is roughly $0.94 \lesssim \omega \lesssim 0.99$, that lifts the phase transition of embedding I in the case when $\hat{\nu} = -0.99$ and $\theta_0 = 0$. One can think of this phenomenon as the spinning motion introducing a "restoring force" effect on the string embedding.

[17] We specialize to the case where $\theta_0 = 0$ for convenience in writing the expressions explicitly.

JHEP04(2026)184

Embedding III. Finally, for the embedding that wraps around the cigar direction ϕ we have the following induced metric, where the embedding is constrained by (4.6):

$$\mathrm{d}s^2_{\text{ind}} = -\frac{r^2\zeta(r,0)}{L^2}\mathrm{d}t^2 + \left\{\frac{r^2\zeta(r,0)}{L^2} + \frac{\zeta(r,0)r'^2}{r^2F(r)\lambda^6(r)} + \phi'^2\left[r^2F(r)\zeta(r,0) + \frac{A_1^2}{\zeta(r,0)}\right]\right\}\mathrm{d}w^2, \tag{4.21}$$

with:

$$\begin{aligned} \mathrm{S}_{\mathrm{F1}} &= \frac{\mathcal{T}}{2\pi}\int_{-L_{\mathrm{QQ}}/2}^{L_{\mathrm{QQ}}/2}\mathrm{d}w\sqrt{\mathcal{A}^2+\mathcal{B}^2r'^2+\mathcal{C}^2\phi'^2}, \\ \mathcal{A}^2 &= \frac{r^4\zeta^2(r,0)}{L^4}, \quad \mathcal{B}^2 = \frac{\zeta^2(r,0)}{L^2F(r)\lambda^6(r)}, \quad \mathcal{C}^2 = \frac{r^2}{L^2}\left[A_1^2 + r^2F(r)\zeta^2(r,0)\right]. \end{aligned} \tag{4.22}$$

We can use the equation of motion for $\phi(w)$ to integrate it out, as the corresponding Hamiltonian is conserved:

$$\frac{\mathrm{d}}{\mathrm{d}w}\frac{\delta\mathcal{L}_{\mathrm{F1}}}{\delta\phi'} = \frac{\mathrm{d}}{\mathrm{d}w}\left[\frac{\mathcal{C}^2\phi'}{\sqrt{\mathcal{A}^2+\mathcal{B}^2r'^2+\mathcal{C}^2\phi'^2}}\right] = 0, \tag{4.23}$$

and calling the constant in the last expression c_ϕ, we get:

$$\phi'^2(w) = \frac{c_\phi^2(\mathcal{A}^2+\mathcal{B}^2r'^2)}{\mathcal{C}^2(\mathcal{C}^2-c_\phi^2)}. \tag{4.24}$$

Plugging this back into the action, one arrives at the following expressions:

$$\begin{aligned} \mathrm{S}_{\mathrm{F1}} &= \frac{\mathcal{T}}{2\pi}\int_{-L_{\mathrm{QQ}}/2}^{L_{\mathrm{QQ}}/2}\mathrm{d}w\sqrt{\mathcal{F}_{\mathrm{III}}^2+\mathcal{G}_{\mathrm{III}}^2r'^2}, \\ \mathcal{F}_{\mathrm{III}}^2 &= \frac{r^6\zeta^2(r,0)\left[A_1^2+r^2F(r)\zeta^2(r,0)\right]}{L^4\left[r^2A_1^2+r^4F(r)\zeta^2(r,0)-c_\phi^2L^2\right]}, \\ \mathcal{G}_{\mathrm{III}}^2 &= \frac{r^2\zeta^2(r,0)\left[A_1^2+r^2F(r)\zeta^2(r,0)\right]}{L^2F(r)\left[r^2A_1^2+r^4F(r)\zeta^2(r,0)-c_\phi^2L^2\right]\lambda^6(r)}, \end{aligned} \tag{4.25}$$

or, in terms of the dimensionless quantities:

$$\begin{aligned} \mathcal{F}_{\mathrm{III}}^2 &= \frac{\hat{\mu}^2\xi^2(\xi^2-1)(\xi^2+\hat{\nu})\left[\xi^2+2(1+\hat{\nu})\right]}{\hat{\mu}(\xi^2-1)\left[\xi^2+2(1+\hat{\nu})\right]-c_\phi^2}, \\ \mathcal{G}_{\mathrm{III}}^2 &= \frac{\hat{\mu}\xi^4(\xi^2+\hat{\nu})\left[\xi^2+2(1+\hat{\nu})\right]}{\left[\xi^4+\xi^2(1+\hat{\nu})+1+\hat{\nu}\right]\left[\hat{\mu}(\xi^2-1)\left(\xi^2+2(1+\hat{\nu})\right)-c_\phi^2\right]}, \end{aligned} \tag{4.26}$$

which agree with (4.12) when $c_\phi = 0$ and $\theta_0 = 0$ (the later imposed by the consistency of the embedding). Similarly to the previous embedding of a spinning string, non zero values of the integration constant c_ϕ allow the length to become single valued and therefore there is no phase transition in the energy of the configuration, see figure 6(a). The effect of c_ϕ is clear when one observes the behaviour of the string profiles: in figure 6(b) we see that as the string approaches the end of space (ξ_0 monotonically approaching 1), its U shaped embedding "opens" and then "closes" again, in other words the profiles are not ordered with

JHEP04(2026)184

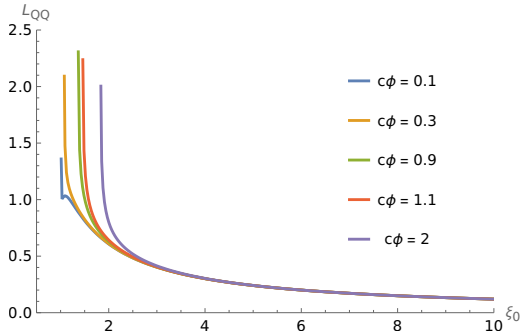

(a) Plot of the length of separation as a function of the turning point for various values of c_ϕ and $\hat{\nu} = -0.99$.

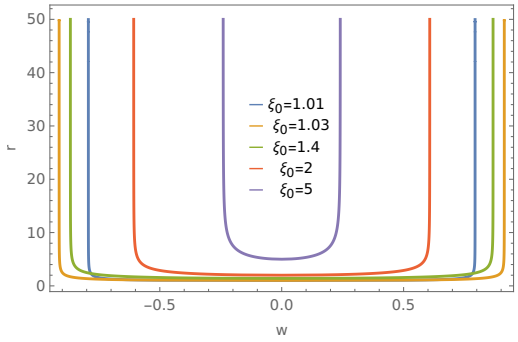

(b) Plot of the string profiles in the (r, w) plane for embedding I ($c_\phi = 0$), for different turning points and $\hat{\nu} = -0.99$.

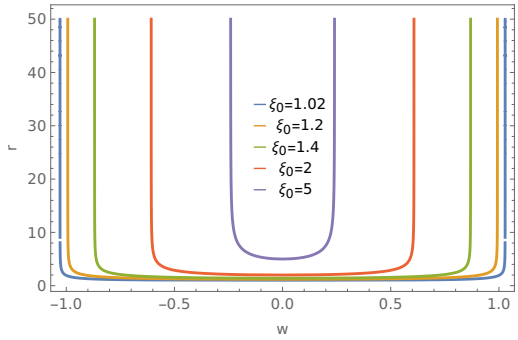

(c) String profiles for embedding III and various values of ξ_0, $\hat{\nu} = -0.99$ and $c_\phi = 0.1$.

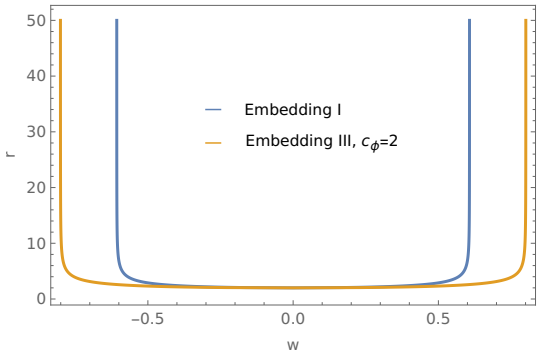

(d) String profiles for both embeddings (I and III), the same turning point $\xi_0 = 2$, $\hat{\nu} = -0.99$ and $c_\phi = 2$.

Figure 6. We notice that for values of the parameter $c_\phi \gtrapprox 0.3$ the length becomes a single valued function of the turning point when $\hat{\nu} = -0.99$.

the monotonically decreasing ξ_0, in contrast with the embedding III profiles seen in 6(c). This signals the lift of the double-valuedness of $L_{\rm QQ}(\xi_0)$. The final plot 6(d) shows the profiles for a specific ξ_0 in both embeddings, given the value $c_\phi = 2$ for embedding III. We note that for the same ξ_0 embedding III gives a smaller length of separation than embedding I, or conversely c_ϕ has the effect of obstructing the string from reaching values closer to the end of space compared to embedding I (for the same fixed length).

4.1.2 Wilson loop for the 11d backgrounds

In order to study the dynamics of a Wilson loop-like object in the M-theory background (3.14)–(3.15), the first step we take is making the change of coordinates to write the Riemann surface in polar coordinates:

$$\mathrm{d}v_1^2 + \mathrm{d}v_2^2 = \mathrm{d}\rho^2 + \rho^2 \mathrm{d}\beta^2, \tag{4.27}$$

without making any extra assumptions about a symmetry in β. We can then use a probe M2 brane whose worldvolume coordinates $\hat{\sigma}$ extend in the submanifold $\Sigma_3[t, w, \beta]$, while it

JHEP04(2026)184

also has a w-dependent profile in the radial direction: $r = r(w)$. The rest of the coordinates are kept constant, however one should choose a suitable location for the M2 brane in y such that $y\,\partial_y D_0(y,\rho,\beta)$ approaches infinity. This allows us to compute the y and D_0 dependent prefactor that enter in the action of the brane and get an answer in terms of r. The induced metric on the brane can be compactly written as:

$$\begin{aligned} \mathrm{d}s^2_{\mathrm{M2}} &= G_{tt}\mathrm{d}t^2 + (G_{ww} + G_{rr}r'^2)\mathrm{d}w^2 + G_{\beta\beta}\mathrm{d}\beta^2, \\ G_{tt} &= -e^{2\hat{\lambda}}\mathcal{Z}\frac{4}{X}\frac{r^2\lambda^2(r)}{L^2}, \quad G_{rr} = e^{2\hat{\lambda}}\mathcal{Z}\frac{4}{X}\frac{1}{r^2\lambda^4(r)F(r)}, \\ G_{\beta\beta} &= -e^{2\hat{\lambda}}\mathcal{Z}\frac{\partial_y e^{D_0}}{y}\rho^2, \quad G_{ww} = -G_{tt}. \end{aligned} \tag{4.28}$$

We can use a specific solution for $D_0(y,\rho,\beta)$ in order to illustrate the calculation. Consider the simple solution presented in [44]:

$$e^{D_0} = 4\frac{N^2 - y^2}{(1-\rho^2)^2}, \quad y\,\partial_y D_0(y,\rho) = \frac{2y^2}{y^2 - N^2}, \tag{4.29}$$

suggesting we place the probe M2 at $y = N$. We then have[18]

$$\begin{aligned} -\det g_{\mathrm{ind,M2}} &= -\frac{16\rho^2 e^{6\hat{\lambda}\mathcal{Z}^3}}{X^2(r)}\frac{\partial_y e^{D_0(y,\rho_0)}}{y}\left[\frac{r^4\lambda^4(r)}{L^4} + \frac{r'^2}{L^2\lambda^2(r)F(r)}\right], \\ \text{with} \quad -\frac{16\rho_0^2 e^{6\hat{\lambda}\mathcal{Z}^3}}{X^2(r)}\frac{\partial_y e^{D_0(y,\rho_0)}}{y} &= \frac{128N^2\rho_0^2}{(1-\rho_0^2)^2}X(r)\left[\frac{r^4\lambda^4(r)}{L^4} + \frac{r'^2}{\lambda^2(r)L^2F(r)}\right] \end{aligned} \tag{4.30}$$

and substituting $X(r) = \lambda^2(r)$, the action reads:

$$\begin{aligned} \mathrm{S}_{\mathrm{M2}} &\propto T_{\mathrm{M2}}\int_{\Sigma_3}\mathrm{d}^3\hat{\sigma}\sqrt{-\det g_{\mathrm{ind,M2}}} \propto 2\pi\mathcal{T}T_{\mathrm{M2}}\int_{-L_{\mathrm{QQ}}/2}^{L_{\mathrm{QQ}}/2}\mathrm{d}w\sqrt{\mathcal{F}^2 + \mathcal{G}^2 r'^2}, \\ \mathcal{F}^2 &= \frac{r^4\lambda^6(r)}{L^4}, \quad \mathcal{G}^2 = \frac{1}{L^2F(r)}. \end{aligned} \tag{4.31}$$

We notice that the functions appearing in the dynamical part of the expression are indeed the same as (4.11) for $\theta_0 = 0$, therefore the analysis of the previous subsection yields the same results in this case. We conclude that the dynamics of the effective string described by the M2 in these backgrounds is the same as the F1 string of the Type IIB solution and it captures confinement.

4.1.3 Wilson loop for the Type IIA backgrounds

We now wish to apply the same analysis for the family of backgrounds presented in (3.33). This calculation proves to be more subtle, however it too contains the same dynamical part as the previous two cases. The complication with this backgrounds enters because of the various functions $\tilde{f}_i$ which after our deformation have acquired a non-trivial dependence on r. To circumvent this and extract the r-dependent part out of the expression, which holds the

[18] We place the brane at ρ_0.

JHEP04(2026)184

information of the dynamics, we choose to localise the probe in the (σ, η) subspace by taking $\eta = \eta_\star$ to be an integer in $(0, P)$ and $\sigma \to 0$. The later will offer us a clearer interpretation of the dual quiver data, as we have $\dot{V}(\sigma,\eta)\Big|_{\sigma=0} = \mathcal{R}(\eta)$, where $\mathcal{R}$ contains information about the location of each gauge group on the quiver. To calculate the various expressions involving the $\tilde{f}_i$s we can first expand the Laplace potential[19] V and its derivatives in Fourier-Bessel series as:

$$\begin{aligned}
V(\sigma,\eta) &= -\sum_{k=1}^{\infty}\left(\frac{P}{k\pi}\right) a_k \sin\left(\frac{k\pi}{P}\eta\right) K_0\left(\frac{k\pi}{P}\sigma\right),\\
\dot{V}(\sigma,\eta) &= \sigma\sum_{k=1}^{\infty} a_k \sin\left(\frac{k\pi}{P}\eta\right) K_1\left(\frac{k\pi}{P}\sigma\right),\\
V''(\sigma,\eta) &= \sum_{k=1}^{\infty}\left(\frac{k\pi}{P}\right) a_k \sin\left(\frac{k\pi}{P}\eta\right) K_0\left(\frac{k\pi}{P}\sigma\right),\\
\ddot{V}(\sigma,\eta) &= -\sigma^2\sum_{k=1}^{\infty}\left(\frac{k\pi}{P}\right) a_k \sin\left(\frac{k\pi}{P}\eta\right) K_0\left(\frac{k\pi}{P}\sigma\right),\\
\dot{V}'(\sigma,\eta) &= \sigma\sum_{k=1}^{\infty}\left(\frac{k\pi}{P}\right) a_k \cos\left(\frac{k\pi}{P}\eta\right) K_1\left(\frac{k\pi}{P}\sigma\right),
\end{aligned} \tag{4.32}$$

and use the known asymptotic behaviour of the modified Bessel functions:

$$\text{As } x\to 0: \quad xK_1(x)\to 1,\ K_0(x)\approx -\gamma_{\text{EM}} + \log\frac{2}{x} + \mathcal{O}(x^2). \tag{4.33}$$

One can notice that all of the above expressions are finite as $\sigma \to 0$, except V''. Let us write $\sigma = \epsilon$ with $\epsilon \to 0$, which then gives the following asymptotic behaviour:

$$\begin{aligned}
&\lim_{\epsilon\to 0}\dot{V}(\epsilon,\eta) = \mathcal{R}(\eta), \qquad &&\lim_{\epsilon\to 0}\dot{V}'(\epsilon,\eta) = \mathcal{R}'(\eta),\\
&\lim_{\epsilon\to 0}\ddot{V}(\epsilon,\eta) = 0, &&V''(\epsilon,\eta)\approx \hat{M}(\epsilon),
\end{aligned} \tag{4.34}$$

where we denoted as $\hat{M}(\epsilon)$ the limiting expression of V'' which diverges as $\log\epsilon^{-1}$. This in turn, allows us to write:

$$\begin{aligned}
&\text{As } \sigma\to 0: \qquad \tilde{\Delta}\approx 2\hat{M}(\epsilon)\mathcal{R}(\eta), \qquad Z^3\to X^3, \qquad \tilde{f}_1\to \mathcal{R}^{2/3}(\eta)\\
&\tilde{f}\to 1, \qquad \tilde{f}_1^3\tilde{f}_5\approx 2X\mathcal{R}(\eta)\hat{M}^{-1}(\epsilon)\to 0, \qquad \tilde{f}_2\to X^{-2}, \qquad \tilde{f}_3\to 0,
\end{aligned} \tag{4.35}$$

which we will make use of in our calculations.

In the following we introduce probe fundamental strings and consider all the different embeddings that were studied in subsection 4.1.1.

Embedding I. Let us start by the simplest F1 embedding with a profile $r = r(w)$, $t = \tau$ and $w = \hat{\sigma}$. We find the induced metric to be:

$$\mathrm{d}s^2_{\text{ind}} = 4\tilde{f}_1^{3/2}\tilde{f}_5^{1/2}\tilde{f}\frac{r^2\lambda^2(r)}{L^2}\left\{-\mathrm{d}t^2 + \left[1+\frac{L^2 r'^2}{r^4 F(r)\lambda^6(r)}\right]\mathrm{d}w^2\right\}, \tag{4.36}$$

[19] With boundary conditions in the η direction: $\dot{V}(\sigma,\eta)\Big|_{\eta=0} = 0 = \dot{V}(\sigma,\eta)\Big|_{\eta=P}$. The connection with (3.40) can be made by setting $\mathcal{R}_k = \frac{Pa_k}{k\pi}$.

JHEP04(2026)184

and the Nambu-Goto action:[20]

$$\mathrm{S_{F1}}=\frac{\mathcal{T}}{2\pi}\int_{-L_{\rm QQ}/2}^{L_{\rm QQ}/2}\mathrm{d}w\sqrt{\hat{\mathcal{F}}_{\rm I}^2+\hat{\mathcal{G}}_{\rm I}^2 r'^2}\quad\text{with}\quad\hat{\mathcal{F}}_{\rm I}^2=16\tilde{f}_1^3\tilde{f}_5\tilde{f}^2\frac{r^4\lambda^4(r)}{L^4},\quad\hat{\mathcal{G}}_{\rm I}^2=\frac{16\tilde{f}_1^3\tilde{f}_5\tilde{f}^2}{L^2F(r)\lambda^2(r)}. \tag{4.37}$$

By employing (4.35) we get as $\sigma=\epsilon\to 0$:

$$\hat{\mathcal{F}}_{\rm I}^2\approx\frac{32\mathcal{R}(\eta_\star)}{\hat{M}(\epsilon)}X(r)\frac{r^4\lambda^4(r)}{L^4},\quad\hat{\mathcal{G}}_{\rm I}^2\approx\frac{32\mathcal{R}(\eta_\star)}{\hat{M}(\epsilon)}\frac{X(r)}{L^2F(r)\lambda^2(r)}. \tag{4.38}$$

We notice again the radial part of the expressions being the same as the one found in the 11d and type IIB backgrounds and therefore the behaviour of the Wilson loops in this case is also described by figure 3. Moreover, The numerical factor describing the conformal quiver in the UV, contains the rank of the gauge group in which we choose to compute the Wilson loop, $N_\star=\mathcal{R}(\eta_\star)$.

Embedding II. Here we repeat the study of the spinning string embedding in this background by taking:

$$\begin{aligned}&t=\tau,\qquad\hat{\sigma}=w,\qquad\phi=\omega\tau,\qquad r=r(w),\qquad z=z_0,\\&\theta=\theta_0,\qquad\varphi=\varphi_0,\qquad\chi=\chi_0,\qquad\sigma=\epsilon\to 0,\qquad\eta=\eta_\star\,.\end{aligned} \tag{4.39}$$

Then the induced metric on the string is:

$$\begin{aligned}\mathrm{d}s_{\rm ind}^2=&(\tilde{f}_1^3\tilde{f}_5)^{1/2}\left[-4\tilde{f}\frac{r^2\lambda^2(r)}{L^2}+\omega^2\left(\tilde{f}_3A_3^2+2\tilde{f}_2\sin^2\theta_0A_1^2+4L^2\tilde{f}F(r)\frac{r^2\lambda^2(r)}{L^2}\right)\right]\mathrm{d}t^2\\&+4(\tilde{f}_2^3\tilde{f}_5)^{1/2}\tilde{f}\left[\frac{r^2\lambda^2(r)}{L^2}+\frac{r'^2}{r^2F(r)\lambda^4(r)}\right]\mathrm{d}w^2,\end{aligned} \tag{4.40}$$

and the Nambu-Goto action reads:

$$S_{\rm F1}=\frac{1}{2\pi}\int\mathrm{d}t\mathrm{d}w\sqrt{-\det g_{\rm ind}}=\frac{\mathcal{T}}{2\pi}\int_{-L_{\rm QQ}/2}^{L_{\rm QQ}/2}\mathrm{d}w\sqrt{\hat{\mathcal{F}}_{\rm II}^2+\hat{\mathcal{G}}_{\rm II}^2r'^2}, \tag{4.41}$$

where:

$$\begin{aligned}\hat{\mathcal{F}}_{\rm II}^2&=4\tilde{f}_1^3\tilde{f}_5\tilde{f}\frac{r^2\lambda^2}{L^2}\left[4\tilde{f}\frac{r^2\lambda^2}{L^2}-\omega^2\left(\tilde{f}_3A_3^2+2\tilde{f}_2\sin^2\theta_0A_1^2+4\tilde{f}Fr^2\lambda^2\right)\right],\\\hat{\mathcal{G}}_{\rm II}^2&=4\tilde{f}_1^3\tilde{f}_5\tilde{f}\left[\frac{4\tilde{f}}{L^2\lambda^2F}-\omega^2\frac{\tilde{f}_3A_3^2+2\tilde{f}_2\sin^2\theta_0A_1^2+4F\tilde{f}r^2\lambda^2}{r^2\lambda^4F}\right].\end{aligned} \tag{4.42}$$

We can now take the limit $\epsilon\to 0$ using (4.35) to obtain the following expressions:

$$\begin{aligned}\hat{\mathcal{F}}_{\rm II}^2&\approx\frac{32\mathcal{R}(\eta_\star)}{\hat{M}(\epsilon)}\left[X(r)\frac{r^4\lambda^4}{L^4}-\omega^2\frac{r^2\lambda^2X(r)}{4L^2}\left(2X^{-2}(r)\sin^2\theta_0A_1^2+4F(r)r^2\lambda^2(r)\right)\right],\\\hat{\mathcal{G}}_{\rm II}^2&\approx\frac{32\mathcal{R}(\eta_\star)}{\hat{M}(\epsilon)}\left[\frac{X(r)}{L^2\lambda^2(r)F(r)}-\frac{\omega^2}{2}\frac{\sin^2\theta_0A_1^2+2F(r)X^2(r)r^2\lambda^2(r)}{r^2X(r)\lambda^4(r)F(r)}\right].\end{aligned} \tag{4.43}$$

[20] We use the shorthand notation $\tilde{f}_i\equiv\tilde{f}_i(\sigma,\eta_\star,r)$.

JHEP04(2026)184

We first notice that when $\omega = 0$ the above agree with the case of embedding I (4.38), which in turn agrees with the type IIB results of embedding I (4.11). The expressions appearing in the ω^2 terms also match the ones in (4.17) when one imposes $\theta_0 = 0$ for the IIB case and $\theta_0 = \pi/2$ for the IIA (notice that the angle θ_0 is not the same coordinate for the two backgrounds). Consequently, one gets the same behaviour as the one depicted in the figure 5 for the case of the type IIB version of this embedding.

Embedding III. We will now study the third and final embedding for the type IIA backgrounds, that is a string wrapping the shrinking circle. In this case (4.6) gives the following induced metric on the string:

$$\begin{aligned} \mathrm{d}s^2_{\rm ind} = &\tilde{f}_1^{3/2}\tilde{f}_5^{1/2}4\tilde{f}\frac{r^2\lambda^2(r)}{L^2} \\ &\times\left\{-\mathrm{d}t^2+\left[1+\frac{L^2r'^2}{r^4\lambda^6(r)F(r)}+\left(F(r)+\frac{\tilde{f}_2L^2\cos^2\theta_0(\mathcal{A}^{(3)})^2}{2\tilde{f}r^2\lambda^2(r)}\right)\phi'^2\right]\mathrm{d}w^2\right\}. \end{aligned} \tag{4.44}$$

After taking limits of the various functions as $\sigma = \epsilon \to 0$ we obtain the Nambu-Goto action:

$$\mathrm{S}_{\rm F1} = \frac{1}{2\pi}\int \mathrm{d}t\mathrm{d}w\sqrt{-\det g_{\rm ind}} \approx \frac{\mathcal{T}}{2\pi}\sqrt{\frac{32\mathcal{R}(\eta_\star)}{\hat{M}(\epsilon)}}\int_{-L_{\rm QQ}/2}^{L_{\rm QQ}/2}\mathrm{d}w\sqrt{\hat{\mathcal{A}}^2+\hat{\mathcal{B}}^2r'^2+\hat{\mathcal{C}}^2\phi'^2}, \tag{4.45}$$

with

$$\hat{\mathcal{A}}^2 = \frac{r^4\lambda^6(r)}{L^4}, \quad \hat{\mathcal{B}}^2 = \frac{X(r)}{\lambda^2(r)F(r)L^2}, \quad \hat{\mathcal{C}}^2 = \frac{r^4\lambda^4(r)}{L^4}X(r)\left[F(r)+\frac{L^2\cos^2\theta_0A_1^2}{X^2(r)r^2\lambda^2(r)}\right]. \tag{4.46}$$

Once again, these functions are the same as the ones found in the corresponding embedding in the type IIB case (4.22) when we set $\theta_0 = 0$. One can then follow the same procedure of using the conserved momentum of ϕ to integrate it out and introduce the new parameter c_ϕ to the problem. The results are the same as in the type IIB case, modulo the divergent prefactor in the action, and can be seen in figure 6.

Let us summarize our findings regarding the Wilson loop observable. Our previous study in section 2.2 revealed that the supergravity background in the case where $\varepsilon = -1$ has a singularity when $\hat{\nu} = -1$ at $r = r_\star$. We deduced that this happens when $q_1 = q_2 = 0$, in which case the gauge fields A_1, A_2 and A_3 are set to zero and there is no fibration. We therefore decided to accept the *smooth* supergravity solutions in the regime $\hat{\nu} > -1$ with nonzero gauge fields.

There is however the following interesting phenomenon: for values of $\hat{\nu}$ very close to -1 Wilson loop embeddings start "feeling" the need for higher curvature corrections in the action, which results in a first order phase transition making its appearance, much like the one in the singular background of [39]. This happens for the case of embedding I in the type IIB background in a specific direction $\theta = 0$.

Our analysis however, shows that the backgrounds are dual to confining field theories,[21] since the energy as a function of the length of separation for a probe quark-anti-quark pair

[21] As long as one does not allow the string embedding to explore the η direction, where there are localized sources describing fundamental degrees of freedom. In this case the Wilson loop will probably undergo screening, as was shown in a different system in [55].

JHEP04(2026)184

interpolates from a Coulombic behaviour in the UV, due to the solutions being asymptotically AdS, to a linear one in the IR. This holds for all values of the parameters of the theory as well as all values of $\hat{\nu} > -1$. The later is supported by the study of different types of embeddings, which introduce new parameters allowing us to reveal the confining behaviour and lift the apparent phase transition for $\hat{\nu} \approx -1$.

4.2 't Hooft loop

In this section we will study the 't Hooft loop, which is the non local operator associated with magnetic charges, in analogy with its electric equivalent, the Wilson loop. The idea is to probe the background with some suitable brane[22] that effectively looks like a magnetic string in the submanifold spanned by the field theory coordinates $\mathbb{R}^{1,2}[t, w, \phi]$, which in turn captures the dynamics of monopole-anti-monopole pairs. One can then deduce if screening takes place, that is, if the pair moves freely at no energy cost, or equivalently, the tension of the "chromomagnetic string" is zero. In the gravity picture this amounts to the system energetically preferring a disconnected embedding of the probe, unlike a U shaped one, which can happen when two different values of the parameter r_0 correspond to the same value for the length of separation $L_{\rm MM}(r_0)$.

The action for the 't Hooft loop will have a similar form as the one for the Wilson loop in the effective two dimensional worldsheet part:

$$S_{\rm D_p} = T_{\rm D_p} \int_{\Sigma_{p+1}} {\rm d}^{p+1}\hat{\sigma} \sqrt{-e^{-2\Phi} {\rm det}(g_{\rm ind})} \propto \int_{-L_{\rm MM}/2}^{L_{\rm MM}/2} {\rm d}w \sqrt{\mathcal{F}_t^2 + \mathcal{G}_t^2 r'^2}, \tag{4.47}$$

where one can relate the value of the function $\mathcal{F}_t$ at the end of space with the tension of the string:

$$T_{\rm eff} \propto \mathcal{F}_t(r_0). \tag{4.48}$$

The inclusion of the shrinking coordinate in the induced metric will typically contribute a multiplicative factor of the warping function $F(r)$ in $\mathcal{F}_t$, which vanishes smoothly as $r \to r_\star$. This is the case when a theory is in the confining phase, where the potential for Wilson loop obeys the area law, while the one for the 't Hooft loop the perimeter law [56].

In the following, we study the dynamics of the effective string using various type IIB brane embeddings. Up to constant prefactors, we find that all the different probes give the same 't Hooft loop observable.

4.2.1 't Hooft loop for the Type IIB background

D3 probe. First, we look at a D3 probe extended in $\Sigma_4 = [t, w, \phi, \phi_3]$ with the following embedding ansatz:

$$r = r(w), \quad \theta = \theta_0 = \frac{\pi}{2}, \quad \phi_1 = \phi_2 = \text{constant}, \quad z = z_0, \quad \psi = \psi_0. \tag{4.49}$$

The equations of motion are satisfied and the embedding is consistent as long as $\theta_0 = \frac{\pi}{2}$.

[22] One usually aims to wrap the shrinking circle $\mathbb{S}^1[\phi]$ which plays an important role in the IR dynamics, as well as some closed submanifold of the internal space.

JHEP04(2026)184

We have the induced metric

$$\begin{aligned} \mathrm{d}s^2_{\mathrm{ind,D3}} = \frac{\zeta(r,\theta_0)}{L^2}\left[-r^2\mathrm{d}t^2 + F(r)r^2L^2\mathrm{d}\phi^2 + \mathrm{d}w^2\left(r^2 + \frac{L^2r'^2}{F(r)\lambda(r)^6r^2}\right)\right] \\ + \frac{L^2}{\zeta(r,\theta_0)}\lambda^6(r)\left(\mathrm{d}\phi_3 + \frac{A_3}{L}\right)^2. \end{aligned} \tag{4.50}$$

Here we have $\zeta(r,\theta_0 = \frac{\pi}{2}) = 1$, and the dilaton is trivial. The Dirac-Born-Infeld action for the D3 yields the following:

$$S_{\mathrm{D3}} = \mathrm{T}_{\mathrm{D3}}\int_{\Sigma_4}\mathrm{d}^4\hat{\sigma}\sqrt{-e^{-2\Phi}\det(g_{\mathrm{ind,D3}})} = \hat{\mathcal{N}}_{\mathrm{D3}}\int_{-L_{\mathrm{MM}}}^{L_{\mathrm{MM}}}\mathrm{d}w\,\sqrt{\mathcal{F}_t^2 + \mathcal{G}_t^2r'^2}, \tag{4.51}$$

where we once again notice the universal nature of the observable. The functions appearing in the dynamical part are:

$$\mathcal{F}_t^2 = r^6\lambda(r)^6F(r), \quad \mathcal{G}_t^2 = L^2r^2 \tag{4.52}$$

and the constant UV prefactor reads:

$$\hat{\mathcal{N}}_{\mathrm{D3}} = \frac{T_{D3}}{L}\int\mathrm{d}t\,\mathrm{d}\phi\,\mathrm{d}\phi_3 = \frac{\mathcal{T}T_{\mathrm{D3}}}{L}2\pi L_\phi, \tag{4.53}$$

where $\mathcal{T}$ is the extent of the time coordinate. In terms of the dimensionless parameters we have:

$$\mathcal{F}_t^2 = \frac{r_\star^6}{L^2}\left[\xi^4(\hat{\nu}+\xi^2) - (1+\hat{\nu})\right], \quad \mathcal{G}_t^2 = L^2r_\star^2\xi^2, \tag{4.54}$$

from which we can form the length and energy integrals using the same equations as in the case of the Wilson loop (4.8), (4.9). The resulting expressions are listed in appendix C, in equations (C.2), (C.3) and (C.4).

The resulting plots of both the approximate and exact expressions are depicted in figure 7, where we once more notice how well the approximate expressions capture the dynamics of the system. The double-valuedness of the length for any value of $\hat{\nu}$ leads to a phase transition and monopole screening taking place. The system prefers energetically the disconnected embedding in which the monopole-anti-monopole pair moves freely. This phase transition in the 't Hooft loop (that can be interpreted as the screening of non-dynamical monopoles) further supports our claims for quark confinement in the dual field theory [56].

D5 probe. Next we consider a D5 brane extended in the submanifold $\Sigma_6 = [t, w, \phi, \phi_1, \phi_2, \phi_3]$, with:[23]

$$r = r(w), \quad z = z_0, \quad \theta = \theta_0 = \frac{1}{2}\arccos\left(\frac{1}{3}\right), \quad \psi_0 = \frac{\pi}{4}. \tag{4.55}$$

The induced metric on the brane is:

$$\begin{aligned} \mathrm{d}s^2_{\mathrm{ind}} = \frac{\zeta(r,\theta_0)r^2}{L^2}\left(-\mathrm{d}t^2 + F(r)L^2\mathrm{d}\phi^2\right) + \frac{L^2}{\zeta(r,\theta_0)}\cos^2\theta_0\sin^2\psi_0\left(\mathrm{d}\phi_1 + \frac{A_1}{L}\mathrm{d}\phi\right)^2 \\ + \frac{L^2}{\zeta(r,\theta_0)}\cos^2\theta_0\cos^2\psi_0\left(\mathrm{d}\phi_2 + \frac{A_2}{L}\mathrm{d}\phi\right)^2 + \frac{L^2\lambda^6(r)}{\zeta(r,\theta_0)}\sin^2\theta_0\left(\mathrm{d}\phi_3 + \frac{A_3}{L}\mathrm{d}\phi\right)^2 \\ + \left[\frac{r^2\zeta(r,\theta_0)}{L^2} + \frac{\zeta(r,\theta_0)r'^2}{r^2F(r)\lambda^6(r)}\right]\mathrm{d}w^2, \end{aligned} \tag{4.56}$$

[23] The full equations of motion enforce $\cos(2\psi_0) = 0$ and $-1 + 3\cos(2\theta_0) = 0$, in order for the embedding to be consistent.

JHEP04(2026)184

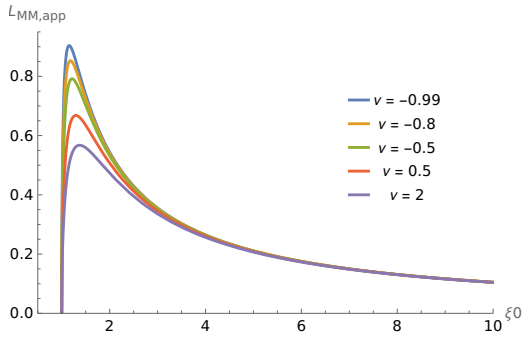

(a) Plot of the approximate length of separation of a monopole-anti-monopole pair as a function of the turning point for different values of $\hat{\nu}$.

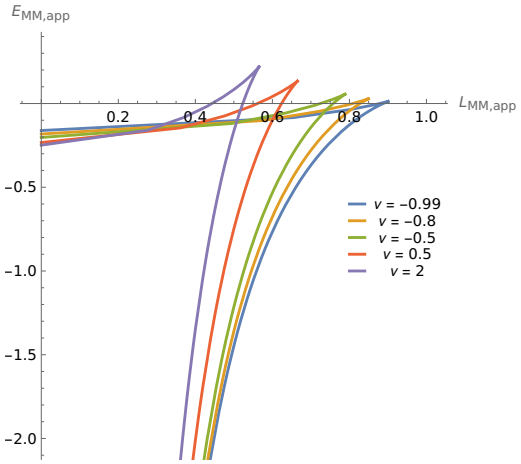

(b) Plot of the approximate energy of the pair as a function of the approximate length for different values of $\hat{\nu}$.

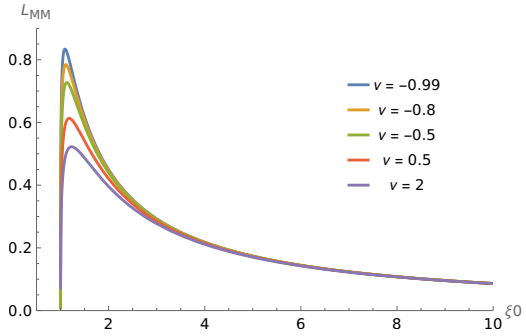

(c) Plot of the length as a function of the turning point for different values of $\hat{\nu}$.

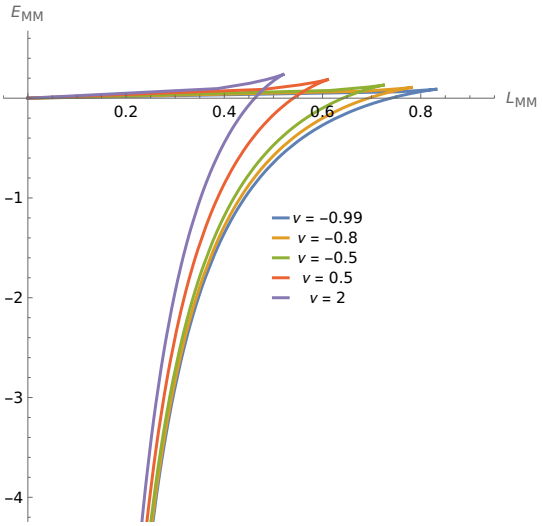

(d) Plot of the energy with respect to the lenth of separation for different values of $\hat{\nu}$.

Figure 7. Resulting plots for the 't Hooft loop length and energy expressions, given in (C.2)–(C.4).

and its action gives the following expression:

$$S_{\rm D5} = \mathrm{T}_{\rm D5}\int_{\Sigma_6} \mathrm{d}^6\hat{\sigma}\sqrt{-e^{-2\Phi}\det(g_{\rm ind,D5})} = \hat{\mathcal{N}}_{\rm D5}\int_{-L_{\rm MM}/2}^{L_{\rm MM}/2}\mathrm{d}w\sqrt{\mathcal{F}_t^2+\mathcal{G}_t^2 r'^2},$$
$$\mathcal{F}_t = r^3\lambda^3(r)\sqrt{F(r)},\quad \mathcal{G}_t = Lr,\quad \hat{\mathcal{N}}_{\rm D5} = \frac{8\pi^3}{3\sqrt{3}}L\mathcal{T}T_{\rm D5}L_\phi. \tag{4.57}$$

We see that the dynamical part, comprising of the w-integral, is the same as the one in the previous embedding as we find the same functions as in (4.52), and therefore the same plots of figure 7 apply here.

JHEP04(2026)184

D7 probe. Let us consider a D7 that extends in the following coordinates $\Sigma_8 = [t, w, \phi, \theta, \psi, \phi_1, \phi_2, \phi_3]$ with $r = r(w)$ and $z = z_0$ kept fixed. The embedding is consistent and the equations of motion are satisfied. The induced metric on the D7 is:

$$\begin{aligned} \mathrm{d}s^2_{\mathrm{ind,D7}} = &\frac{\zeta(r,\theta)}{L^2}\left[-r^2\mathrm{d}t^2 + F(r)L^2r^2\mathrm{d}\phi^2 + \mathrm{d}w^2\left(r^2 + \frac{L^2r'^2}{F(r)\lambda(r)^6r^2}\right) + L^4\mathrm{d}\theta^2\right] \\ &+ \frac{L^2}{\zeta(r,\theta)}\left[\cos^2\theta\mathrm{d}\psi^2 + \cos^2\theta\sin^2\psi\left(\mathrm{d}\phi_1 + \frac{A_1}{L}\right)^2 + \cos^2\theta\cos^2\psi\left(\mathrm{d}\phi_2 + \frac{A_2}{L}\right)^2\right. \\ &\left.+\lambda(r)^6\sin^2\theta\left(\mathrm{d}\phi_3 + \frac{A_3}{L}\right)^2\right], \end{aligned} \tag{4.58}$$

while the DBI yields:

$$\begin{aligned} &S_{\mathrm{D7}} = T_{\mathrm{D7}}\int_{\Sigma_8}\mathrm{d}^8\hat{\sigma}\sqrt{-e^{-2\Phi}\det(g_{\mathrm{ind,D7}})} = \hat{\mathcal{N}}_{\mathrm{D7}}\int_{-L_{\mathrm{MM}}}^{L_{\mathrm{MM}}}\mathrm{d}w\,\sqrt{\mathcal{F}_t^2 + \mathcal{G}_t^2r'^2}, \\ &\mathcal{F}_t = r^3\lambda^3(r)\sqrt{F(r)}, \quad \mathcal{G}_t = Lr, \quad \hat{\mathcal{N}}_{\mathrm{D7}} = \frac{4}{3}\pi^3L^3\mathcal{T}T_{\mathrm{D7}}L_\phi. \end{aligned} \tag{4.59}$$

Once again, we obtain the same dynamics and therefore this probe captures the same effects of the 't Hooft loop as the previous ones.

4.2.2 't Hooft loop for the Type IIA backgrounds

Here, we study a probe in the Type IIA family of backgrounds that can be associated with the 't Hooft loop and displays screening of the monopole-anti-monopole pair. The dynamics as we argue is analogous to the one in the Type IIB system.

D2 probe. We will first use a D2 probe brane extended in $\Sigma_3[t, w, \phi]$ with the direction $r = r(w)$ and the rest of the coordinates being fixed to constant values:

$$z = z_0, \quad \theta = \theta_0, \quad \varphi = \varphi_0, \quad \chi = \chi_0, \quad \eta = \eta_\star, \quad \sigma = \epsilon \to 0, \tag{4.60}$$

with $0 < \eta_\star < P$. This is the simplest choice one can have for describing the 't Hooft loop, as the pullback of the NS potential B_2 on Σ_3 is zero and therefore the DBI action is easy to handle. The induced metric on the brane reads:

$$\begin{aligned} \mathrm{d}s^2_{\mathrm{ind}} = &-4\tilde{f}_1^{3/2}\tilde{f}_5^{1/2}\tilde{f}\frac{r^2\lambda^2}{L^2}\,\mathrm{d}t^2 + 4\tilde{f}_1^{3/2}\tilde{f}_5^{1/2}\tilde{f}\left(\frac{r^2\lambda^2}{L^2} + \frac{r'^2}{r^2F\lambda^4}\right)\mathrm{d}w^2 \\ &+ \tilde{f}_1^{3/2}\tilde{f}_5^{1/2}\left[\tilde{f}_3A_{3\phi}^2 + 2\left(\tilde{f}_2\sin^2\theta_0A_{1\phi}^2 + 2F\tilde{f}r^2\lambda^2\right)\right]\mathrm{d}\phi^2. \end{aligned} \tag{4.61}$$

where in the above expression all the functions are to be taken at the values of the ansatz (4.60): $\tilde{f}_i \equiv \tilde{f}_i(r, \eta_\star, \sigma_0)$, etc. We can now choose the value for $\theta_0 = 0$ and take $\sigma_0 \to 0$. Using coordinates $\hat{\sigma} \in \{t, w, \phi\}$ where $t \in [0, \mathcal{T}]$ on the worldvolume Σ_3, we have:

$$\begin{aligned} S_{\mathrm{D2}} &= T_{\mathrm{D2}}\int_{\Sigma_3}\mathrm{d}^3\hat{\sigma}\sqrt{-e^{-2\Phi}\det(g_{\mathrm{ind,D2}})} \\ &= 8LT_{\mathrm{D2}}L_\phi\mathcal{T}\lim_{\epsilon\to 0}\tilde{f}_1^{3/2}(\epsilon,\eta_\star)\tilde{f}(\epsilon,\eta_\star)\int_{-L_{\mathrm{MM}}}^{L_{\mathrm{MM}}}\mathrm{d}w\sqrt{F\frac{r^4\lambda^4}{L^4}\left(\frac{r^2\lambda^2}{L^2} + \frac{r'^2}{r^2F\lambda^4}\right)} \\ &= \hat{\mathcal{N}}_{\mathrm{D2}}\int_{-L_{\mathrm{MM}}}^{L_{\mathrm{MM}}}\mathrm{d}w\sqrt{\mathcal{F}_t^2 + \mathcal{G}_t^2r'^2}, \qquad \hat{\mathcal{N}}_{\mathrm{D2}} = \frac{8T_{\mathrm{D2}}L_\phi\mathcal{T}\mathcal{R}(\eta_\star)}{L^2} \end{aligned} \tag{4.62}$$

JHEP04(2026)184

where the functions $\mathcal{F}_t$ and $\mathcal{G}_t$ are the same as the ones found in the Type IIB background (4.52). Consequently, the plots are similar to figure 7, indicating the screening of monopole-anti-monopole pairs in this background as well.

One could also study the 't Hooft loops obtained by suitably probing the geometry with D4 and D6 branes. In these cases, the non-zero pull back of the NS two form makes the calculation more cumbersome. We do not discuss these further in this paper. Instead, we focus on another relevant observable.

4.3 Entanglement entropy

In this section, we study the entanglement entropy of the QFTs dual to our backgrounds. We consider codimension two submanifolds which explore the bulk, while their boundary at $r = \infty$ divides the dual theory in two entangled regions. Following the proposal of Ryu and Takayanagi [57], the action for the minimization of the hypersurface for the 10d theories is given by

$$S_{\rm EE} = \frac{1}{4G_N}\int_{\Sigma_8} \mathrm{d}^8\hat{\sigma}\sqrt{e^{-4\Phi}\det(g_{\Sigma_8})}, \tag{4.63}$$

where G_N is the ten dimensional Newton constant and Φ the dilaton of the theory. In 11d we propose the following formula[24]

$$S_{\rm EE} = \frac{1}{4G_N^{(11)}}\int_{\Sigma_9} \mathrm{d}^9\hat{\sigma}\sqrt{\det(g_{\Sigma_9})}, \tag{4.64}$$

where $G_N^{(11)}$ denotes the eleven dimensional Newton constant and Σ_9 a codimension two manifold in eleven dimensions. The above reduces to (4.63) in the case of a U(1) isometry in the M-theory solution. In that case, using (3.32) one can indeed verify that[25]

$$\sqrt{\det(g_{\Sigma_9})} = \sqrt{e^{-4\Phi}\det(g_{\Sigma_8})}. \tag{4.65}$$

In the absence of a U(1) isometry we expect that (4.64) will yield a similar dynamical integral as (4.63), which if we consider giving the RT surface a profile in the radial coordinate will have the same form as the integral found in the previous observables (4.7), with the constant of proportionality in this case being related to the central charge.

In the following, we study this observable in the three different backgrounds presented in this work.

4.3.1 Entanglement entropy for the Type IIB background

For the case of the type IIB background, we choose an eight-manifold Σ_8 that extends in the directions $[w, z, \phi, \theta, \psi, \phi_1, \phi_2, \phi_3]$ with the profile of the radial coordinate being $r = r(w)$. At $r = \infty$ we take this manifold to have a boundary which splits the field theory in two regions: one being a strip of length $L_{\rm EE}$, and the other the rest of the space.

[24] To the best of our knowledge this definition for 11d geometries has not been written down explicitly.

[25] One can choose to write the expression of the metric in type II theories either in the string or Einstein frame, the difference being $\mathrm{d}s_E^2 = e^{-\Phi/2}\mathrm{d}s_S^2$.

JHEP04(2026)184

The induced metric on Σ_8 is then

$$\begin{aligned} \mathrm{d}s^2_{\rm ind} = \frac{\zeta(r,\theta) r^2}{L^2}\left[\mathrm{d}z^2 + L^2 F(r)\mathrm{d}\phi^2 + \left(1+\frac{L^2 r'^2}{F(r)\lambda^6(r) r^4}\right)\mathrm{d}w^2\right] \\ + L^2\left[\zeta(r,\theta)\mathrm{d}\theta^2 + \frac{\cos^2\theta}{\zeta(r,\theta)}\mathrm{d}\psi^2 + \frac{\cos^2\theta\sin^2\psi}{\zeta(r,\theta)}\left(\mathrm{d}\phi_1 + \frac{A_1}{L}\right)^2\right. \\ \left. + \frac{\cos^2\theta\cos^2\psi}{\zeta(r,\theta)}\left(\mathrm{d}\phi_2 + \frac{A_2}{L}\right)^2 + \frac{\lambda^6(r)\sin^2\theta}{\zeta(r,\theta)}\left(\mathrm{d}\phi_3 + \frac{A_3}{L}\right)^2\right], \end{aligned} \tag{4.66}$$

and the determinant of this yields

$$\det(g_{\Sigma_8}) = L^6 r^6 F(r)\lambda^6(r)\cos^6\theta\cos^2\psi\sin^2\theta\sin^2\psi\left[1+\frac{L^2 r'^2}{\lambda^6(r)F(r)r^4}\right]. \tag{4.67}$$

Given that the dilaton for this background is trivial, we arrive at the following expression for the entanglement entropy action

$$\begin{aligned} S_{\rm EE} &= \hat{\mathcal{N}}^{\rm EE}_{\rm IIB}\int_{-L_{\rm EE}/2}^{L_{\rm EE}/2}\mathrm{d}w\sqrt{\mathcal{F}^2_{\rm EE} + \mathcal{G}^2_{\rm EE} r'^2}, \\ \mathcal{F}^2_{\rm EE} &= r^6 F(r)\lambda^6(r), \quad \mathcal{G}^2_{\rm EE} = L^2 r^2, \quad \hat{\mathcal{N}}^{\rm EE}_{\rm IIB} = \frac{L^3 L_\phi L_z \pi^3}{4 G_N}. \end{aligned} \tag{4.68}$$

We find the same functions as the ones appearing in the integrand on the 't Hooft loop observable in (4.52). From this it follows that the entanglement entropy undergoes a phase transition as well, since the plots for the length of the strip $L_{\rm EE}$ and the corresponding energy are identical to the ones presented in figure 7, where a phase transition in the energy $E(L_{\rm EE})$ is apparent. There is a critical length after which the system prefers to have zero entanglement entropy, corresponding to two disconnected Ryu-Takayanagi surfaces that are attached at $w = \pm L_{\rm EE}/2$ at the boundary ($r = \infty$) and extend deep in the bulk, reaching the end of space. This behaviour of the entanglement entropy further supports the confinement-deconfinement phase transition [52, 58, 59].

4.3.2 Entanglement entropy for the Type IIA background

For this background, we will choose an eight manifold Σ_8 extended in the coordinates $[w, z, \phi, \theta, \varphi, \chi, \sigma, \eta]$ with $r = r(w)$. The induced metric on this manifold is

$$\begin{aligned} \mathrm{d}s^2_{\Sigma_8} = \tilde{f}_1^{3/2}\tilde{f}_5^{1/2}\left[4\tilde{f}\frac{r^2\lambda(r)^2}{L^2}(\mathrm{d}z^2 + L^2 F\mathrm{d}\phi^2 + 4\tilde{f}\tilde{f}_1^{3/2}\tilde{f}_5^{1/2}\left(\frac{r'^2}{r^2\lambda^4 F} + \frac{r^2\lambda(r)^2}{L^2}\right)\mathrm{d}w^2\right. \\ \left. + \tilde{f}_2 \mathrm{D}\mu^i\mathrm{D}\mu^i + \tilde{f}_3(\mathrm{d}\chi + B)^2 + \tilde{f}_4(\mathrm{d}\sigma^2 + \mathrm{d}\eta^2)\right]. \end{aligned} \tag{4.69}$$

Taking the determinant of the above metric, we arrive at

$$\det(g_{\Sigma_8}) = 4^3 F(r)\frac{r^6\lambda(r)^6}{L^4}\sin^2\theta\tilde{f}_1^{12}\tilde{f}_2^2\tilde{f}_3\tilde{f}_4^2\tilde{f}_5^4\tilde{f}^3\left[1+\frac{L^2 r'^2}{r^4 F(r)\lambda^6(r)}\right], \tag{4.70}$$

JHEP04(2026)184

which in turn yields the following action for the surface (setting $\kappa = 1$):

$$\begin{aligned} S_{\rm EE} &= \hat{\mathcal{N}}^{\rm EE}_{\rm IIA}\int_{-L_{\rm EE}/2}^{L_{\rm EE}/2} {\rm d}w\sqrt{\mathcal{F}^2_{\rm EE}+\mathcal{G}^2_{\rm EE}r'^2}, \\ \mathcal{F}^2_{\rm EE} &= r^6F(r)\lambda^6(r), \quad \mathcal{G}^2_{\rm EE} = L^2r^2, \quad \hat{\mathcal{N}}^{\rm EE}_{\rm IIA} = \frac{64\pi^2\kappa^3 L_\phi L_z}{L^2G_N}\int_0^\infty {\rm d}\sigma\int_0^P {\rm d}\eta\,\sigma\dot{V}V'', \end{aligned} \tag{4.71}$$

Once again we arrive at the same dynamical part as in the type IIB background and the 't Hooft loops, hence this systems also exhibits a phase transition in the entanglement entropy. In addition to the constant numerical prefactor, we also obtain an integral in the subspace spanned by σ and η, which makes its appearance in many of these systems when one calculates the entanglement entropy or other observables that encode the degrees of freedom of the dual field theory, like the c-function [26, 45, 60]. We further comment on this in the next section where we calculate the flow central charge.

4.3.3 Entanglement entropy in 11d supergravity

To calculate the entanglement entropy directly in the 11d system (3.27), we take the codimension 2 manifold Σ_9 with t constant and $r = r(w)$. The induced metric on this subspace is then

$$\begin{aligned} {\rm d}s_9^2 = e^{2\lambda}\Bigg\{&\frac{4Z}{X^3}\left[\frac{r^2\lambda(r)^2}{L^2}\left({\rm d}z^2+L^2F(r){\rm d}\phi^2\right)+\left(\frac{r^2\lambda(r)^2}{L^2}+\frac{r'^2}{r^2\lambda(r)^4F(r)}\right){\rm d}w^2\right] \\ &+\frac{y^2e^{-6\lambda}}{Z^2}(D\mu^i)^2+\frac{4X^3}{Z^2}\frac{(D\chi^2)}{1-y\partial_yD_0}-\frac{Z}{y}\partial_yD_0{\rm d}y^2-\frac{Z^2}{y}\partial_ye^{D_0}({\rm d}v_1^2+{\rm d}v_2^2)\Bigg\}. \end{aligned} \tag{4.72}$$

where we have again set $\kappa = 1 = m$. The determinant of this metric is

$$\det g_{\Sigma_9} = 256L^2e^{2D_0}y^2(\partial_yD_0)^2\sin^2\theta\left[F(r)\frac{r^6\lambda(r)^6}{L^6}+\frac{r^2r'^2}{L^2}\right] \tag{4.73}$$

and the action is written as

$$S_{\rm EE} = \hat{\mathcal{N}}^{\rm EE}_{\rm LLM}\int_{-L_{\rm EE}/2}^{L_{\rm EE}/2}{\rm d}w\,\sqrt{\mathcal{F}^2_{\rm EE}+\mathcal{G}^2_{\rm EE}r'^2}, \tag{4.74}$$

$$\mathcal{F}^2_{\rm EE} = r^6F(r)\lambda^6(r), \quad \mathcal{G}^2_{\rm EE} = r^2L^2, \quad \hat{\mathcal{N}}^{\rm EE}_{\rm LLM} = \frac{32\pi^2L_zL_\phi}{G_N^{(11)}}\int {\rm d}y{\rm d}v_1{\rm d}v_2\,y\partial_ye^{D_0}. \tag{4.75}$$

Once again, the observable factorizes itself in a universal manner and the r-dependent factor is the same as in the previous cases. An interesting comment here is that the integral in the subspace spanned by y, v_1 and v_2 appearing in the UV factor above, is the 11d version of the integral found in the electrostatic case (4.71). To see this in detail, we make use of the change of coordinates (3.25) to translate this subspace to the "electrostatic variables": $(y, v_1, v_2) \mapsto (\sigma, \eta, \beta)$. Writting the (v_1, v_2) plane in polar coordinates (ρ, β) and differentiating these relations, we find:

$${\rm d}y = \dot{V}'{\rm d}\eta - \sigma V''{\rm d}\sigma, \quad {\rm d}v_1\wedge{\rm d}v_2 = -\rho\,{\rm d}\rho\wedge{\rm d}\beta \quad \text{and} \quad e^{\frac{D_0}{2}}{\rm d}\rho = \sigma V''{\rm d}\eta + \dot{V}'{\rm d}\sigma, \tag{4.76}$$

and then we write the integrand as:

$$y\partial_ye^{D_0} = \frac{2V''\dot{V}\sigma^2}{\rho^2\left[\ddot{V}V''-(\dot{V}')^2\right]}. \tag{4.77}$$

JHEP04(2026)184

This maps the integral in (y, v_1, v_2) to the following:

$$\int \mathrm{d}y\ \mathrm{d}v_1\ \mathrm{d}v_2\ y\partial_y e^{D_0} = -2\int \mathrm{d}\beta\ \mathrm{d}\eta\ \mathrm{d}\sigma\ \dot{V}V''\sigma, \quad \text{with } V = V(\beta,\eta,\sigma), \tag{4.78}$$

which is indeed proportional to the integral in (4.68) in the electrostatic case, that is when the extra SO(2) symmetry in the v_1, v_2 plane renders V independent of β. The same integral appears also in flow central charge calculation, carried out below.

4.4 Flow central charge

We now study an observable called flow central charge. The calculation details are included in [1, 27, 60, 61]. This is a monotonic quantity related to the number of degrees of freedom of the flow and asymptotes to the UV central charge value. It provides an effective number of degrees of freedom for every value of the holographic coordinate along the flow from the CFT_4 to the strongly coupled 3d systems in the IR.

Interestingly, notice that this quantity is monotonic for the backgrounds here studied, in which Lorentz invariance SO(1, 3) is broken to SO(1, 2) × SO(2) under the RG flow. In summary, we write a quantity that detects the four dimensional fixed point, the gapped character of the three-dimensional QFT (giving a vanishing result) and is monotonic along the flow.

Consider a dilaton and metric of the form

$$\mathrm{d}s^2 = -a_0\mathrm{d}t_0^2 + \sum_{i=1}^{d} a_i\mathrm{d}x_i^2 + \prod_{i=1}^{d}(a_i)^{\frac{1}{d}}\,\tilde{b}(r)\mathrm{d}r^2 + h_{ab}(\mathrm{d}y^a - A^a)(\mathrm{d}y^b - A^b), \quad \Phi(\vec{y}, r). \tag{4.79}$$

To calculate the holographic flow central charge we use [60–62]

$$G_{ij}\mathrm{d}X^i\mathrm{d}X^j = \sum_{i=1}^{d} a_i\mathrm{d}x_i^2 + h_{ab}(\mathrm{d}y^a - A^a)(\mathrm{d}y^b - A^b) \tag{4.80}$$

$$\hat{H} = \left(\int \prod_{a=1}^{8} \mathrm{d}X^a \sqrt{e^{-4\Phi}\det\left(G_{ij}\right)}\right)^2, \quad c_{\text{flow}} = \mathrm{Vol}_d\, d^d \frac{\tilde{b}(r)^{\frac{d}{2}}\hat{H}^{\frac{2d+1}{2}}}{G_N^{(10)}\left(\hat{H}'\right)^d}. \tag{4.81}$$

For G_{ij} the 8-dimensional internal space and field theory directions and Vol_d the volume of the field theory subspace spanned by $\{x_i\}$.

4.4.1 Flow central charge in Type IIB Background

Calculating the flow central charge in the IIB background, we find with $d = 3$,

$$\tilde{b}(r) = \frac{L^{\frac{4}{3}}}{F(r)^{\frac{4}{3}}\lambda(r)^6 r^4}. \tag{4.82}$$

The 8-dimensional space is

$$\begin{aligned} G_{ij}\mathrm{d}x^i\mathrm{d}x^j = {} & \frac{\zeta(r,\theta)r^2}{L^2}\left[\mathrm{d}w^2 + \mathrm{d}z^2 + L^2F(r)\mathrm{d}\phi^2\right] \\ & + \frac{L^2}{\zeta(r,\theta)}\Big[\zeta(r,\theta)^2\mathrm{d}\theta^2 + \cos^2\theta\mathrm{d}\psi^2 + \cos^2\theta\sin^2\psi\mathrm{D}\phi_1^2 + \cos^2\theta\cos^2\psi\mathrm{D}\phi_2^2 \\ & + \lambda^6(r)\sin^2\theta\mathrm{D}\phi_3^2\Big]. \end{aligned}$$

JHEP04(2026)184

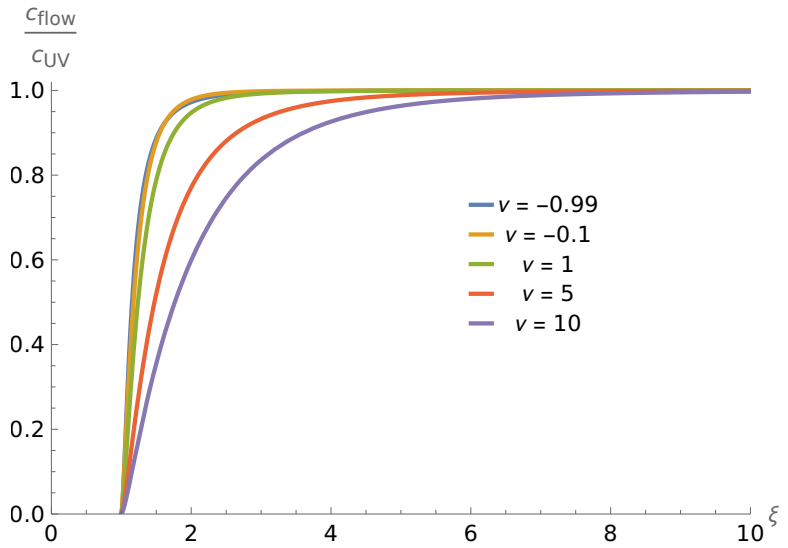

Figure 8. Plot of the normalised flow central charge in eq. (4.85) as a function of ξ for different values of $\hat{\nu}$ and $L = 1$. The c_{flow} goes to the UV central charge $c_{\text{UV}} = \hat{\mathcal{N}}^{c}_{\text{IIB}}$ for large values of ξ. This plot is the same for all of the three backgrounds.

Taking the determinant we find:

$$\begin{aligned} \det G_{ij} &= r^6 L^6 F(r)\lambda(r)^6 \sin^2\theta \cos^6\theta \cos^2\psi \sin^2\psi, \\ \int \mathrm{d}^8x \sqrt{e^{-4\Phi}\det G_{ij}} &= \pi^3 L^3 r^3 \lambda(r)^3 \sqrt{F(r)} L_w L_z L_\phi = \hat{H}^{1/2}, \end{aligned} \tag{4.83}$$

and the flow central charge takes the form

$$c_{\text{flow}} = \frac{3^3\, \tilde{b}(r)^{\frac{3}{2}} \hat{H}^{\frac{7}{2}} L_\phi L_z L_w}{G_N^{(10)} (\hat{H}')^3}. \tag{4.84}$$

We write the radially dependent part in terms of dimensionless variables $\xi, \hat{\nu}$ defined in (2.2) and the final expression takes the universal form:

$$c_{\text{flow}} = 27 \hat{\mathcal{N}}^{c}_{\text{IIB}} \frac{\xi^6 \left(1 + \frac{\hat{\nu}}{\xi^2}\right)^2 \left(\frac{\xi^6 - 1 + \hat{\nu}(\xi^4 - 1)}{\xi^4(\hat{\nu} + \xi^2)}\right)^{\frac{3}{2}}}{(2\hat{\nu} + 3\xi^2)^3} \quad \text{with} \quad \hat{\mathcal{N}}^{c}_{\text{IIB}} = \frac{\pi^3 L^8 L_w L_z L_\phi}{8 G_N^{(10)}}. \tag{4.85}$$

In figure 8 we observe that the point $r = r_\star$ corresponds to an energy scale in the dual field theory below which there are no dynamical degrees of freedom. This indicates that the system has a gapped spectrum and $r_\star$ is associated with the gap scale.

Moreover, we notice that the non-universal part $\hat{\mathcal{N}}^{c}_{\text{IIB}}$ of the observable which equals the central charge of the UV theory, is also contained in the UV factor of the entanglement entropy calculation (4.68). The two are related as:

$$\hat{\mathcal{N}}^{c}_{\text{IIB}} = c_{\text{UV}} = \frac{L^2 L_w^2 L_z L_\phi}{2} \hat{\mathcal{N}}^{\text{EE}}_{\text{IIB}}. \tag{4.86}$$

Similar relations hold for the rest of the backgrounds under study. The interested reader can consult [63] for more on the relation between c-functions and entanglement entropy.

JHEP04(2026)184

4.4.2 Flow central charge for Type IIA background

In the same way as above, we calculate the flow central charge for the 11d and IIA backgrounds. We have the same $\tilde{b}(r)$ as in eq. (4.82). The 8-manifold metric reads

$$G_{ij}\mathrm{d}x^i\mathrm{d}x^j = \tilde{f}_1^{3/2}\tilde{f}_5^{1/2}\Big[\frac{4\tilde{f}\ r^2\lambda(r)^2}{L^2}(\mathrm{d}w^2+\mathrm{d}z^2+L^2F(r)\mathrm{d}\phi^2) + \tilde{f}_2\mathrm{D}\mu^i\mathrm{D}\mu^i+\tilde{f}_3(\mathrm{d}\chi+B)^2+\tilde{f}_4(\mathrm{d}\sigma^2+\mathrm{d}\eta^2)\Big], \tag{4.87}$$

and we find

$$e^{-4\Phi}\det(G_{ij}) = 64\tilde{f}_1^9\tilde{f}_2^2\tilde{f}_3\tilde{f}_4^2\tilde{f}_5\tilde{f}^3\frac{r^6\lambda(r)^6}{L^4}F(r) \tag{4.88}$$

Setting $\kappa = 1$ and utilising

$$\tilde{f}_1^9\tilde{f}_2^2\tilde{f}_3\tilde{f}_4^2\tilde{f}_5\tilde{f}^3 = 16\dot{V}^2V''^2\sigma^2, \tag{4.89}$$

we get:

$$\hat{H}^{\frac{1}{2}} = \frac{265\pi^2L_\phi}{L^2}\int \mathrm{d}\sigma\mathrm{d}\eta\ \dot{V}V''\sigma\ r^3\lambda(r)^3\sqrt{F(r)}. \tag{4.90}$$

This yields the result:

$$c_{\text{flow}} = \hat{\mathcal{N}}^c_{\text{IIA}}\ 27\frac{\xi^6\left(1+\frac{\hat{\nu}}{\xi^2}\right)^2\left(\frac{\xi^6-1+\hat{\nu}(\xi^4-1)}{\xi^4(\hat{\nu}+\xi^2)}\right)^{\frac{3}{2}}}{(2\hat{\nu}+3\xi^2)^3}, \quad \hat{\mathcal{N}}^c_{\text{IIA}} = \frac{32\pi^2L_\phi^2L_z^2L_w^2L^2}{G_N}\int_0^\infty \mathrm{d}\sigma\int_0^P \mathrm{d}\eta\dot{V}V''\sigma, \tag{4.91}$$

where the flow factor matches that of the type IIB calculation above. The normalized flow central charge for this solution will also be depicted by figure 8. Again, one observes that the expression $\int \mathrm{d}\sigma\mathrm{d}\eta\,\dot{V}\sigma$ makes its appearance in the corresponding constant in the entanglement entropy calculation. More specifically,

$$c_{\text{UV}} = \hat{\mathcal{N}}^c_{\text{IIA}} = \frac{L^4L_\phi L_wL_z}{2}\hat{\mathcal{N}}^{\text{EE}}_{\text{IIA}}. \tag{4.92}$$

4.4.3 Flow central charge in 11d supergravity

For the calculation in 11d, we compute a 9-volume and there is no dilaton. Here we find:

$$\hat{H}^{\frac{1}{2}} = \frac{256\pi^2L_\phi}{L^2}\int \mathrm{d}y\ \mathrm{d}v_1\mathrm{d}v_2\ y\partial_y e^{D_0}\ r^3\lambda(r)^3\sqrt{F(r)}, \tag{4.93}$$

and therefore

$$c_{\text{flow}} = \hat{\mathcal{N}}^c_{\text{LLM}}\ 27\frac{\xi^6\left(1+\frac{\hat{\nu}}{\xi^2}\right)^2\left(\frac{\xi^6-1+\hat{\nu}(\xi^4-1)}{\xi^4(\hat{\nu}+\xi^2)}\right)^{\frac{3}{2}}}{(2\hat{\nu}+3\xi^2)^3}, \quad \hat{\mathcal{N}}^c_{\text{IIA}} = \frac{32\pi^2L_w^2L_z^2L_\phi^2}{G_N^{(11)}}\int \mathrm{d}y\ \mathrm{d}v_1\mathrm{d}v_2y\partial_y e^{D_0}, \tag{4.94}$$

in which case we have the connection with the entanglement entropy UV factor:

$$c_{\text{UV}} = \hat{\mathcal{N}}^c_{\text{LLM}} = L_zL_\phi L_w^2\hat{\mathcal{N}}^{\text{EE}}_{\text{LLM}}. \tag{4.95}$$

JHEP04(2026)184

4.5 D7 brane embeddings in the Anabalon-Ross deformed $AdS_5 \times \mathbb{S}^5$ solution

The main objective of this subsection is to study the properties of a D7-brane probe embedded in a confined background. To facilitate the analysis we will focus on the type IIB confined solution and set to zero the Coulomb branch parameter ℓ. In this way we essentially analyze the addition of D7-brane probes to the Anabalon-Ross deformed $AdS_5 \times \mathbb{S}^5$ background [24]. The background in this case is

$$\begin{aligned} \mathrm{d}s_{10}^2 = \frac{r^2}{L^2}\left[\mathrm{d}x_{1,2}^2 + f(r)\, L^2\, \mathrm{d}\phi^2 + \frac{L^2\, \mathrm{d}r^2}{r^4\, f(r)}\right] + L^2\Bigg\{\mathrm{d}\theta^2 + \sin^2\theta\, \left(\mathrm{d}\phi_3 + \frac{A_3}{L}\right)^2 \\ + \cos^2\theta\left[\mathrm{d}\psi^2 + \sin^2\psi\left(\mathrm{d}\phi_1 + \frac{A_1}{L}\right)^2 + \cos^2\psi\left(\mathrm{d}\phi_2 + \frac{A_2}{L}\right)^2\right]\Bigg\}, \end{aligned} \tag{4.96}$$

with[26]

$$f(r) = \frac{1}{L^2} - \frac{L^2\, Q^2}{r^6} \quad \text{and} \quad A_1 = A_2 = A_3 = -\frac{Q^{1/3}}{L^{1/3}}\mathrm{d}\phi + \frac{LQ}{r^2}\mathrm{d}\phi, \tag{4.97}$$

where we have explicitly used the expression for $r_\star = L^{2/3}Q^{1/3}$ coming from the condition $F(r_\star) = 0$. A consistent ansatz for a D7-brane probe with the following worldvolume coordinates

$$\zeta^\alpha = (t, y, z, \phi, r, \psi, \phi_1, \phi_2) \quad \text{is} \quad \theta = \theta(r) \quad \text{and} \quad \phi_3 = \frac{L^{2/3}Q^{1/3}}{L^2}\,\phi\,. \tag{4.98}$$

Notice that in the limit of $Q \to 0$, in which case we obtain the familiar $AdS_5 \times \mathbb{S}^5$ solution, the ansatz for the embedding function ϕ_3 becomes zero, and we obtain the D7-brane embedding of [64]. To simplify the study of the embeddings, it is convenient to introduce an isotropic system of coordinates, along the lines of [65, 66]. To identify these coordinates, we have to isolate the (r, θ) part of the induced metric

$$\frac{\mathrm{d}r^2}{r^2\, f(r)} + L^2\mathrm{d}\theta^2 = L^2\left[\frac{\mathrm{d}r^2}{r^2\, L^2\, f(r)} + \mathrm{d}\theta^2\right] \tag{4.99}$$

and exchange the radial coordinate r with a new radial coordinate ρ, such that such the first term inside the brackets becomes $\mathrm{d}\rho^2/\rho^2$. This means

$$\frac{\mathrm{d}r}{r\sqrt{1 - \frac{L^4\, Q^2}{r^6}}} = \frac{\mathrm{d}\rho}{\rho} \quad \Rightarrow \quad r = \frac{L^{\frac{2}{3}}\, Q^{\frac{1}{3}}}{2^{\frac{1}{3}}\, \rho}\left(1 + \rho^6\right)^{\frac{1}{3}} \quad \text{with} \quad \rho \in [1, \infty)\,. \tag{4.100}$$

Describing the embedding in terms of the function $\chi(\rho) = \sin\theta(\rho)$ simplifies the analysis, and the Euclidean D7-brane action becomes

$$\frac{I}{\mathcal{N}} = \int \frac{\mathrm{d}\rho}{\rho^5}\left(1 + \rho^6\right)^{\frac{1}{3}}\sqrt{(1 - \rho^6)^2 + 4\,\rho^6\,\chi^2}\left(1 - \chi^2\right)\sqrt{1 - \chi^2 + \rho^2\,\chi'^2} \tag{4.101}$$

with

$$\mathcal{N} = \frac{\pi^2 L^{\frac{8}{3}} Q^{\frac{4}{3}}}{\sqrt[3]{2}}\, T_{D_7} \tag{4.102}$$

[26] The metric in (4.96) is the $\ell \to 0$ limit of (6.3). Due to the redefinition of equation (6.1), the parameter Q has dimensions of length.

JHEP04(2026)184

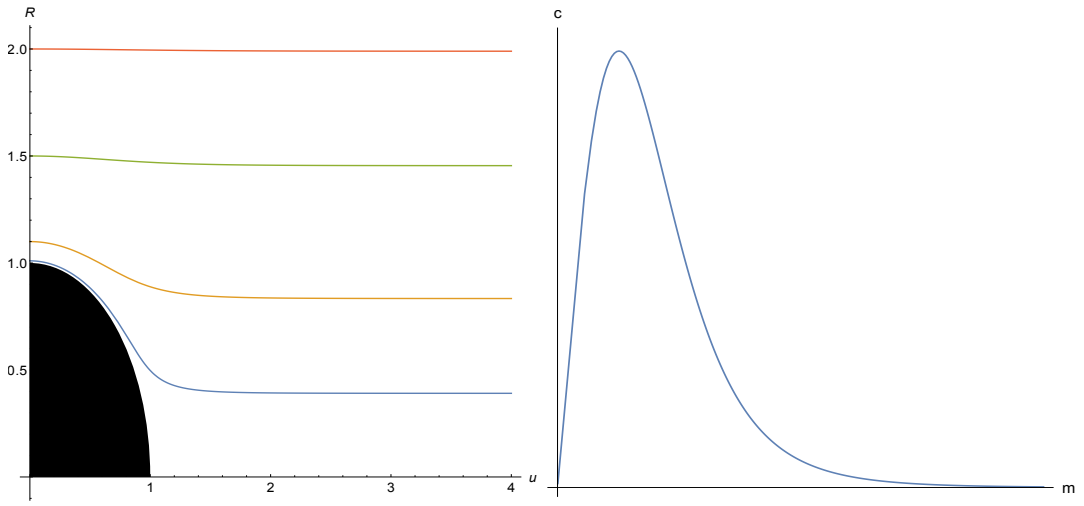

Figure 9. In the left panel, plots of the D7-brane embeddings for different values of the constant R_0. The black region indicates the end of space which is an inaccessible region of the geometry. In the right panel, qualitative plot of the parameter c versus the parameter m, as they are read off from the boundary behaviour of the solution.

The equation of motion for $\chi(\rho)$ can be obtained from the Euclidean D7-brane action and implies that the behaviour of the field at infinity is

$$\chi = \frac{m}{\rho} + \frac{c}{\rho^3} + \cdots \tag{4.103}$$

where the dimensionless constants m and c are related to the quark mass and condensate. Let us now introduce a system of Cartesian-like coordinates (u, R), defined as follows

$$R = \rho\,\chi \quad \text{and} \quad u = \rho\sqrt{1-\chi^2}\,. \tag{4.104}$$

The Euclidean D7-brane action becomes

$$\frac{I}{\mathcal{N}'} = \int \mathrm{d}u\, \frac{u^3\left[1+\left(u^2+R^2\right)^3\right]^{\frac{1}{3}}}{\left(u^2+R^2\right)^4} \sqrt{4R^2\left(u^2+R^2\right)^2 + \left[1-\left(u^2+R^2\right)^3\right]^2}\sqrt{1+R'^2} \tag{4.105}$$

where the embedding of the D7-brane is given by $R = R(u)$. For large values of u we have

$$R(u) \;=\; m + \frac{c}{u^2} + \cdots\,. \tag{4.106}$$

Even if there are two free parameters in solving the equation of motion for the embedding function $R(u)$, the dynamics in the IR of the theory allows that for a given value of m a finite number of values for c exist, in order to have solutions that are well behaved. In the current case, there is only one value of c for every m. To solve numerically the equation of motion for $R(u)$ from (4.105), we integrate from the IR with boundary conditions $R(0) = R_0$ and $R'(0) = 0$. In the left panel of figure 9, some of these solutions are presented for different values of the constant R_0. The values of the parameters m and c are read off at the boundary and are presented in the right panel of figure 9.

JHEP04(2026)184

In other confining backgrounds (see e.g. [67]), the interior singularity triggers repulsion, causing the D7-branes to avoid the central region. We observe similar avoidance behavior for the probe brane in our case (see the left panel of figure 9), even without an interior singularity. Moreover, the plot of the condensate with respect to the quark mass (in the right panel of figure 9), shows an interesting non monotonic behaviour. The condensate flows to zero both when the quark mass is large (something that is expected since away from the singularity the embeddings are flat), but also for very small quark masses. And all this without "jumping" from Minkowski to Black hole embeddings, as it happens in the presence of the temperature [65]. Notice here that in the embeddings that are studied in [67], in a Gubser dilaton flow geometry [68] that is not supersymmetric, the condensate is finite for zero quark mass indicating spontaneous chiral symmetry. In our case, there is a finite value of the quark mass that the condensate obtains a maximal value. This behaviour has to be investigated further. First we have to determine the exact relation between the parameters m, c with the quark mass and the condensate. This should be followed by a holographic renormalization, in order to calculate the "on-shell" action, and by the computation of the meson spectrum.

5 Holographic renormalization

5.1 Anabalon-Ross solution

In this section we will study the holographic renormalization of the solution presented by Anabalon and Ross in [24], using the methods developed by Skenderis et al. in [16–18, 69]. The configuration we wish to study is a solution of five-dimensional gauged $\mathcal{N}=2$ supergravity with the following action:

$$S=\frac{1}{16\pi G}\int \mathrm{d}^5x\sqrt{-g}\left(R+\frac{12}{L^2}-\frac{3}{4}\mathcal{F}_{\mu\nu}\mathcal{F}^{\mu\nu}\right)+\frac{1}{16\pi G}\int\sqrt{-g}\mathcal{F}\wedge\mathcal{F}\wedge\mathcal{A}, \tag{5.1}$$

with a gauge field

$$\mathcal{A}=Q\left(\frac{1}{r^2}-\frac{1}{r_\star^2}\right)\mathrm{d}\phi,\quad \mathcal{F}=\mathrm{d}\mathcal{A}. \tag{5.2}$$

The equations of motion for the gauge field and the metric read:

$$\mathrm{d}\star_5\mathcal{F}+\mathcal{F}\wedge\mathcal{F}=0,\quad G_{\mu\nu}=\tilde{T}_{\mu\nu}(\mathcal{A})\quad\text{with}\quad \tilde{T}_{\mu\nu}(\mathcal{A})=\frac{3}{2}\left(\mathcal{F}_{\mu\rho}\mathcal{F}^{\rho}_{\nu}-\frac{1}{6}g_{\mu\nu}\mathcal{F}_{\rho\sigma}\mathcal{F}^{\rho\sigma}\right)+\frac{6}{L^2}g_{\mu\nu}. \tag{5.3}$$

The metric is given by

$$\mathrm{d}s^2=\frac{r^2}{L^2}\Big(-\mathrm{d}t^2+\mathrm{d}x_1^2+\mathrm{d}x_2^2+f(r)\mathrm{d}\phi^2\Big)+\frac{L^2\mathrm{d}r^2}{r^2f(r)}\quad\text{with}\quad f(r)=1-\frac{\mu\, l^2}{r^4}-\frac{Q^2L^2}{r^6}. \tag{5.4}$$

The configuration preserves four real supercharges when $\mu=0$, or equivalently when $r_\star=(QL)^{1/3}$. Following the steps leading to holographic renormalization [16–18], we first transform our coordinate system to Fefferman-Graham coordinates:

$$\mathrm{d}s_5^2=\frac{L^2}{\rho^2}\Big(\mathrm{d}\rho^2+g_{ij}(x,\rho)\mathrm{d}x^i\mathrm{d}x^j\Big), \tag{5.5}$$

where the variable ρ is defined such that the boundary is now at $\rho = 0$. To achieve this we will treat the coordinate change asymptotically near the boundary. First we use $r \mapsto z^{-1}$ and expand around $z = 0$. The radial part of the metric then becomes (notice that we have to go up to fifth order for the parameter Q to appear):

$$\frac{L\mathrm{d}r}{r\sqrt{f(r)}} \approx -\left(\frac{L}{z} + \frac{L^3\mu}{2}z^3 + \frac{L^3Q^2}{2}z^5 + \mathcal{O}(z^7)\right)\mathrm{d}z = \frac{L\mathrm{d}\rho}{\rho}, \tag{5.6}$$

which we can integrate to find $\rho(z)$ asymptotically:

$$\begin{aligned} &\Rightarrow \rho = \exp\left\{\frac{1}{L}\int \mathrm{d}z\left(\frac{L}{z} + \frac{L^3\mu}{2}z^3 + \frac{L^3Q^2}{2}z^5 + \mathcal{O}(z^7)\right)\right\} \\ &\Rightarrow \rho \approx z + \frac{L^2\mu}{8}z^5 + \frac{L^2Q^2}{12}z^7 + \mathcal{O}(z^9), \end{aligned} \tag{5.7}$$

and inverting this we get the relation for $z(\rho)$:

$$z \approx \rho - \frac{L^2\mu}{8}\rho^5 - \frac{L^2Q^2}{12}\rho^7 + \mathcal{O}(\rho^9). \tag{5.8}$$

We can now expand the expressions of the boundary metric g_{ij} around $\rho = 0$:

$$|g_{tt}| = g_{x_1x_1} = g_{x_2x_2} \approx \frac{1}{L^2} + \frac{\mu}{4}\rho^4 + \frac{Q^2}{6}\rho^6 + \mathcal{O}(\rho^8)\,, \quad g_{\phi\phi} \approx \frac{1}{L^2} - \frac{3\mu}{4}\rho^4 - \frac{5Q^2}{6}\rho^6 + \mathcal{O}(\rho^8). \tag{5.9}$$

One can then use the following formula to calculate the vacuum expectation value of the stress energy momentum tensor in the four-dimensional boundary field theory [16]:

$$\langle T_{ij}\rangle = \frac{4L^3}{16\pi G_{\mathrm{N}}}g_{(4)ij}, \tag{5.10}$$

where $g_{(4)ij}$ denotes the coefficient of the fourth order in ρ term in the expansion. The result reads:

$$-\langle T_{tt}\rangle = \langle T_{x_1x_1}\rangle = \langle T_{x_2x_2}\rangle = -\frac{L^3\mu}{16\pi G_{\mathrm{N}}}, \quad \langle T_{\phi\phi}\rangle = \frac{3L^3\mu}{16\pi G_{\mathrm{N}}}. \tag{5.11}$$

As expected, the SUSY point $\mu = 0$ has vanishing vev for the energy momentum tensor. As for the gauge field, its near boundary expansion in these variables is:

$$\mathcal{A} \approx \left(-\frac{Q}{r_\star^2} + Q\rho^2 - \frac{L^2Q\mu}{4}\rho^6 + \mathcal{O}(\rho^8)\right)\mathrm{d}\phi, \tag{5.12}$$

yielding the vev for the current:

$$\langle J_\phi\rangle = Q, \tag{5.13}$$

which couples to a global current expressing the $\mathcal{R}$-symmetry of the dual theory. We comment that the preserved $\mathcal{R}$ symmetry is still realized by internal cycles inside the deformed $\mathbb{S}^5$, namely the $\mathrm{U}(1)^3 \cong \mathbb{S}^1 \times \mathbb{S}^1 \times \mathbb{S}^1 \subset \mathbb{S}^5$.

JHEP04(2026)184

5.2 Anabalon-Nastase-Oyarzo

The same procedure can be carried for the solution of [33]. In this case the change of variables bringing the metric of (2.5) asymptotically to the Fefferman-Graham form (5.5), as well as its inverse, read:[27]

$$\begin{aligned}\rho &\approx z - \frac{\ell^2\varepsilon}{6}z^3 + \frac{9L^4(q_1^2-q_2^2)\ell^2\varepsilon + 5\ell^4}{72}z^5 + \mathcal{O}(z^7),\\ z &\approx \rho + \frac{\ell^2\varepsilon}{6}\rho^3 - \frac{9L^4(q_1^2-q_2^2) - 5\ell^4}{72}\rho^5 + \mathcal{O}(\rho^7).\end{aligned} \tag{5.14}$$

Let us now look at the expansions of the 4d metric coefficients near the boundary. We have:

$$\begin{aligned}|g_{tt}| = g_{ww} = g_{zz} = \frac{r^2\lambda^2(r)}{L^2} &\approx \frac{1}{L^2} + \left[-\frac{L^4\ell^2\varepsilon(q_1^2-q_2^2)}{4L^2} - \frac{\ell^4}{18L^2}\right]\rho^4\\ &+ \left[-\frac{L^2\ell^4(q_1^2-q_2^2)}{8} + \frac{13\ell^6\varepsilon}{648L^2}\right]\rho^6 + \mathcal{O}(\rho^8),\\ g_{\phi\phi} = r^2\lambda^2(r)F(r) &\approx \frac{1}{L^2} + \left[-\frac{3L^4\ell^2(q_1^2-q_2^2)\varepsilon}{4L^2} - \frac{\ell^4}{18L^2}\right]\rho^4\\ &+ \frac{-27L^4\ell^4(19q_1^2+5q_2^2) + 13\ell^6\varepsilon}{648L^2}\rho^6 + \mathcal{O}(\rho^8).\end{aligned} \tag{5.15}$$

We notice that the boundary expansions contain constant isotropic terms, highlighted in blue. In order to ensure that the VEV of the stress-energy-momentum tensor vanishes, as it should for a SUSY theory, we can remove these terms by adding the following boundary expression to the supergravity action:

$$S_{\text{c.t.}} = \frac{1}{8\pi G_N}\left(\frac{L\ell^4}{9}\right)\int_{\mathbb{R}^{1,3}} \mathrm{d}^4x\sqrt{\gamma}, \tag{5.16}$$

where γ is the induced metric on the boundary of AdS_5. Such a term respects all the symmetries of the theory, is covariant and does not interfere with the equations of motion. It only results in a shifting of the VEV of T_{ij}. The final expression reads:

$$\langle T_{ij}\rangle = \frac{4L^3}{16\pi G_N}\left(g_{(4)ij} + \eta_{ij}\frac{\ell^4}{18L^2}\right) = \frac{L^3\mu}{16\pi G_N}\,\mathrm{diag}(-1,1,1,-3), \tag{5.17}$$

where $\mu = -\eta L^4(q_1^2-q_2^2)$, $g_{(4)ij}$ refers to the fourth order coefficients in (5.15) and the second term is the effect of (5.16). Clearly, in the supersymmetric case where $q_1 = q_2$ we get $\langle T_{ij}\rangle = 0$. Let us note that counterterms of this form were first introduced in [70] for the purpose of removing divergences from physical observables like the AdS mass density. As noted in [70] as well as [16], it is often necessary to fix such terms, expressing ambiguities, in order to match

[27] Again, after letting $r = z^{-1}$ to bring the boundary at $z = 0$.

JHEP04(2026)184

the ground state energy. As for the scalar and gauge fields, their near boundary behaviour is:

$$\begin{aligned}
\Phi(r) &= \sqrt{\frac{2}{3}}\ln\lambda^{-6}(r) \approx -\sqrt{\frac{2}{3}}\ell^2\varepsilon\rho^4 + \frac{\ell^4}{3\sqrt{6}}\rho^6 + \mathcal{O}(\rho^8),\\
A^1_\phi &= A^2_\phi \approx \frac{L\ell^2\varepsilon q_1}{r_\star^2} - L\ell^2\varepsilon q_1\rho^2 - \frac{L\ell^4 q_1}{3}\rho^4 + \frac{L\ell^4 q_1}{36}\left[9L^4(q_1^2-q_2^2) - 2\ell^2\varepsilon\right]\rho^6 + \mathcal{O}(\rho^8),\\
A^3_\phi &\approx \frac{L\ell^2\varepsilon q_2}{r_\star^2+\ell^2\varepsilon} - L\ell^2\varepsilon q_2\rho^2 + \frac{2L\ell^4 q_2}{3}\rho^4 - \frac{Lq_2}{36}\left[-9L^4(q_1^2-q_2^2)\ell^4 + 14\ell^6\varepsilon\right]\rho^6 + \mathcal{O}(\rho^8).
\end{aligned} \tag{5.18}$$

From these we can read the VEV of the dimension two[28] operator dual to the scalar field:[29]

$$\langle O_2\rangle = 2\times\left(-\sqrt{\frac{2}{3}}\ell^2\varepsilon\right) = \frac{2\sqrt{2}L^2}{\sqrt{3}}\eta, \tag{5.19}$$

as well as the VEVs of the currents contained in the $\mathcal{O}(\rho^2)$ coefficients of the gauge fields:

$$\langle J_1\rangle = -L\ell^2\varepsilon q_1, \quad \langle J_3\rangle = -L\ell^2\varepsilon q_2, \tag{5.20}$$

which are equal at the SUSY point where $q_1 = q_2 = q$. We see that one can recover the results of the previous subsection by setting $Q = \ell^2 Lq$ and taking the limit $\ell \to 0$ which maps the Anabalon-Nastase-Oyarzo solution to the Anabalon-Ross one as explained in [1].

6 The stability analysis of the classical solution for the Wilson loops

In this subsection we will examine the stability of some of the Wilson loop configurations that were calculated in [1]. The analysis will be for Wilson loops in the Type IIB case, however we expect that the conclusions of the subsequent analysis will be valid also for the other cases.

6.1 The classical solution

We consider the ten-dimensional supergravity background constructed in section 5 of [33], presented here in 3.1 (we are especially interested in the supersymmetric case, in which the parameters q_1 and q_2 are equal) and we perform the following redefinition (see also [1])

$$q_1 = q_2 = \frac{Q}{\ell^2}\,, \tag{6.1}$$

where Q has dimensions of length. In this way the background functions and the gauge fields become[30]

$$\begin{aligned}
&\zeta(r,\theta)^2 = 1 - \frac{\ell^2}{r^2}\cos^2\theta\,, \qquad \lambda(r)^6 = 1 - \frac{\ell^2}{r^2}\,, \qquad F(r) = \frac{1}{L^2}\left[1 - \frac{L^4\,Q^2}{r^4(r^2-\ell^2)}\right]\\
&A_1 = A_2 = -\,L\,Q\,\frac{r^2-r_\star^2}{r_\star^2\,r^2}\,d\phi\,, \qquad A_3 = -\,L\,Q\,\frac{r^2-r_\star^2}{(r_\star^2-\ell^2)\,(r^2-\ell^2)}\,d\phi\,.
\end{aligned} \tag{6.2}$$

[28] The prefactor of 2 in the VEV expression enters because in this special case where $\Delta = 2$ we have $(2\Delta - d) = 0$, as explained in [16].

[29] We remind the reader that $\eta = -\varepsilon\ell^2/L^2$.

[30] For simplicity we have chosen $\varepsilon = -1$. Notice that we can reverse this choice at any time by $\ell \to i\,\ell$.

JHEP04(2026)184

The background metric is given by (3.1), see [1, 33], which we repeat here for convenience

$$\begin{aligned} \mathrm{d}s^2 \,=\, & \frac{r^2}{L^2}\,\zeta(r,\theta)\left[\mathrm{d}x_{1,2}^2 + L^2 F(r)\mathrm{d}\phi^2 + \frac{L^2\mathrm{d}r^2}{F(r)\,r^4\,\lambda^3(r)}\right] + L^2\,\zeta(r,\theta)\,\mathrm{d}\theta^2 \\ & + \frac{L^2}{\zeta(r,\theta)}\Bigg\{\cos^2\theta\left[\mathrm{d}\psi^2 + \sin^2\psi\left(\mathrm{d}\phi_1 + \frac{A_1}{L}\right)^2 + \cos^2\psi\left(\mathrm{d}\phi_2 + \frac{A_2}{L}\right)^2\right] \\ & + \lambda^6(r)\sin^2\theta\left(\mathrm{d}\phi_3 + \frac{A_3}{L}\right)\Bigg\}. \end{aligned} \tag{6.3}$$

with C_4 given in (3.7) which does not participate in the calculation of the Wilson loops and their stability analysis.

To obtain generic expressions for the string configuration and for the equations of the fluctuation modes, we consider the following general form for the metric

$$\mathrm{d}s^2 = G_{tt}\mathrm{d}t^2 + G_{ww}\mathrm{d}w^2 + G_{zz}\mathrm{d}z^2 + G_{\phi\phi}\mathrm{d}\phi^2 + G_{rr}\mathrm{d}r^2 + G_{\theta\theta}\mathrm{d}\theta^2 + \dots \tag{6.4}$$

Notice that in the cases we will consider G_{tt} will be negative and y denotes the spatial side of the Wilson loop along which the Wilson loop extends. To write down the expression for the string trajectory in a compact form, we introduce the following functions

$$g(r,\theta) = -G_{tt}G_{rr}\,, \quad f_y(r,\theta) = -G_{tt}G_{yy}\,. \tag{6.5}$$

The Nambu-Goto action for a string that propagates in the gravity background becomes

$$S = -\frac{1}{2\pi}\int \mathrm{d}\tau\mathrm{d}\sigma\sqrt{-\det g_{\alpha\beta}} \quad \text{with} \quad g_{\alpha\beta} = G_{\mu\nu}\partial_\alpha x^\mu \partial_\beta x^\nu\,. \tag{6.6}$$

To fix reparametrization invariance, we make the choice: $t=\tau$ and $r=\sigma$, and the ansatz for the string embedding corresponds to that of embedding I (with $\phi_0=0$) studied in section 4.1.1

$$y = y(\sigma)\,, \quad \phi = 0\,, \quad \theta = \theta_0 = \left\{0 \text{ or } \frac{\pi}{2}\right\} \quad \text{and} \quad \text{rest} = \text{constant}\,. \tag{6.7}$$

Notice here that the two values for the angle θ came from the substitution of the ansatz (6.7) into the equations of motion, that are derived from (6.6). The equation that the embedding obeys becomes

$$\frac{f_y\,y'_{\rm cl}}{\sqrt{g + f_y\,y'^2_{\rm cl}}} = \pm\left(f_y^0\right)^{1/2} \quad \Rightarrow \quad y'_{\rm cl} = \pm\frac{\sqrt{f_y^0\,F}}{f_y} \quad \text{with} \quad F = \frac{g\,f_y}{f_y - f_y^0}\,. \tag{6.8}$$

All the functions are calculated at $\theta=\theta_0$ and r_0 is the value of the holographic coordinate at the turning point. Moreover, $f_y^0 \equiv f_y(r_0,\theta_0)$, $y_{\rm cl}$ is the classical solution and $y'_{\rm cl}$ is the derivative of the classical solution with respect to σ at $\theta=\theta_0$. The two signs denote the two symmetric branches of the string trajectory around the turning point. Integrating (6.8) we obtain the expression for the separation length and inserting the solution for $y'_{\rm cl}$ into the Nambu-Goto action (and properly subtracting the contribution from two straight strings

JHEP04(2026)184

extending until the end of the geometry), we obtain the expression for the energy. This is the same procedure we followed to obtain equations (4.8) and in this context they read

$$L = 2\sqrt{f_y^0}\int_{r_0}^{\infty} \mathrm{d}r \frac{\sqrt{F}}{f_y} \,. \quad \text{and} \quad E = \frac{1}{\pi}\int_{r_0}^{\infty} \mathrm{d}r\sqrt{F} - \frac{1}{\pi}\int_{r_\star}^{\infty} \mathrm{d}r\sqrt{g}\,. \tag{6.9}$$

In principle, we would like to analytically evaluate the preceding integrals, express the parameter r_0 as a function of the separation length L and then insert that expression into the expression for the energy. In that way, we would obtain an expression of the energy in terms of the separation length, $E(L)$. In practice this can be done only for a limited amount of "cases" (i.e. backgrounds), and the confined background is not one of those cases. Alternatively, we consider the expressions of (6.9) as parametric equations of the length and of the energy with parameter r_0.

In figure 3 (c) and (d) we have plotted the energy of the Wilson loop as a function of the separation length for different values of $\hat{\nu}$, or equivalently, different values of Q (the case $\hat{\nu} = -1$ corresponding to $Q = 0$). For large values of the separation length, which is equivalent to small values of the parameter r_0 (i.e. the turning point of the string approaches the confinement scale Q), the energy has a confining behaviour. This means that it increases linearly with the separation length. In this section we are going to investigate the perturbative stability of the string configuration, paying special attention to the region of small r_0. We are going to analyze the case with $\theta_0 = 0$, but the main conclusion will be also valid for the other cases. Notice that in the $\theta_0 = 0$ case and for very small values of Q (or $\hat{\nu} \approx -1^+$), there is a region in the $E(L)$ plot (figure 3 (d)) in which a "swallow tail" is observed. In [1] we have plotted the quantities $R_{ab}R^{ab}$ and $R_{abcd}R^{abcd}$ for different values of θ_0 and Q and we have observed that when both θ_0 and Q approach zero, those quantities become very large, almost infinite. As a result, background corrections are needed since the supergravity approximation is not valid. It is in this regime that the "swallow tail" appears, and for this reason we argue that the phase transition that is seen in the behaviour of the Wilson loop does not correspond to an actual physical situation. Based on these arguments we are not considering this region of the parametric space for Q in the following analysis.

6.2 Expansion of the action and equations of motion for the fluctuations

To investigate the stability of the string configuration that is described in (6.8), we consider small fluctuations about the classical solution. We are going to fluctuate all the coordinates, either transverse or longitudinal to the quark-antiquark axis. We perturb the embedding ansatz as follows

$$\begin{aligned} &z = z_0 + \delta z(\tau,\sigma)\,, \quad y = y_{\rm cl}(\sigma) + \delta y(\tau,\sigma)\,, \quad \theta = \theta_0 + \delta\theta(\tau,\sigma)\,, \quad \phi = \delta\phi(\tau,\sigma) \\ &\varphi_1 = \delta\varphi_1(\tau,\sigma)\,, \quad \varphi_2 = \delta\varphi_2(\tau,\sigma)\,, \quad \varphi_3 = \delta\varphi_3(\tau,\sigma)\,, \quad \psi = \delta\psi(\tau,\sigma)\,. \end{aligned} \tag{6.10}$$

Notice that we keep the expansion ansatz for the angle θ general. In this way we will obtain a system of equations for the fluctuations that could be potentially applied for both values of θ_0. The next step is to substitute the ansatz (6.10) into the Nambu-Goto action and expand in powers of the fluctuations. In this way we obtain an expression of the form

$$S = S_0 + S_1 + S_2 + \ldots \tag{6.11}$$

JHEP04(2026)184

where the zeroth order term is the classical action and the first order contribution is

$$S_1 = -\frac{1}{2\pi}\int \mathrm{d}\tau\mathrm{d}\sigma\left\{\sqrt{f_y^0}\,\delta y' + \left[\frac{1}{2F^{1/2}}\partial_\theta g + \frac{f_y^0\,F^{1/2}}{2f_y^2}\partial_\theta f_y\right]\delta\theta\right\} \tag{6.12}$$

where $\partial_\theta g$ and $\partial_\theta f_y$ denote derivatives of the functions g and f_y with respect to θ evaluated at the value $\theta = \theta_0$, while $\delta y'$ denotes derivative with respect to σ. In the cases that we consider the derivatives of the functions g and f_y vanish and the first term is a surface contribution that will not affect the equations of motion. The second order contribution can split to a sum of terms. Some of them contain contribution from just one fluctuation

$$\begin{aligned}
S_2^{\delta z} &= \frac{f_z}{2\,F^{1/2}}\delta z'^2 - \frac{h\,f_z\,F^{1/2}}{2\,g\,f_y}\delta\dot{z}^2 \quad \& \quad S_2^{\delta y} = \frac{g f_y}{2\,F^{3/2}}\delta y'^2 - \frac{h}{2\,F^{1/2}}\delta\dot{y}^2\\
S_2^{\delta\theta} &= \frac{f_\theta}{2\,F^{1/2}}\delta\theta'^2 - \frac{h\,f_\theta\,F^{1/2}}{2\,g\,f_y}\delta\dot{\theta}^2 + \left(\frac{1}{4\,F^{1/2}}\partial_\theta^2 g + \frac{f_y^0\,F^{1/2}}{4\,f_y^2}\partial_\theta^2 f_y\right)\delta\theta^2\\
S_2^{\delta\psi} &= \frac{f_\psi}{2\,F^{1/2}}\delta\psi'^2 - \frac{h\,f_\psi\,F^{1/2}}{2\,g\,f_y}\delta\dot{\psi}^2 \quad \& \quad S_2^{\delta\phi} = \frac{f_\phi}{2\,F^{1/2}}\delta\phi'^2 - \frac{h\,f_\phi\,F^{1/2}}{2\,g\,f_y}\delta\dot{\phi}^2\\
S_2^{\delta\varphi_i} &= \frac{f_{\varphi_i}}{2\,F^{1/2}}\delta\varphi_i'^2 - \frac{h\,f_{\varphi_i}\,F^{1/2}}{2\,g\,f_y}\delta\dot{\varphi}_i{}^2 \quad \text{with} \quad i = 1,2,3
\end{aligned} \tag{6.13}$$

and there are three more that contribute to the coupling between the modes $\delta\phi$ and $\delta\varphi_i$, for $i = 1,2,3$

$$\begin{aligned}
S_2^{\delta\phi\,\delta\varphi_i} &= f_{12}\left[\frac{f_{\varphi_i}}{F^{1/2}}\,\delta\phi'\,\delta\varphi_i' - \frac{h\,f_{\varphi_i}\,F^{1/2}}{g\,f_y}\,\delta\dot{\phi}\,\delta\dot{\varphi}_i\right] \quad \text{for} \quad i = 1,2 \ \text{ with } f_{12} = -\,Q\,\frac{r^2 - r_\star^2}{r_\star^2\,r^2}\\
S_2^{\delta\phi\,\delta\varphi_3} &= f_3\left[\frac{f_{\varphi_3}}{F^{1/2}}\,\delta\phi'\,\delta\varphi_3' - \frac{h\,f_{\varphi_3}\,F^{1/2}}{g\,f_y}\,\delta\dot{\phi}\,\delta\dot{\varphi}_3\right] \ \text{with } f_3 = -\,Q\,\frac{r^2 - r_\star^2}{(r_\star^2 - \ell^2)\,(r^2 - \ell^2)}\,.
\end{aligned} \tag{6.14}$$

The definitions of the functions f_z, f_θ, f_ϕ, f_ψ, h and f_{φ_i} with $i = 1,2,3$, are listed in (C.5). The equations for the fluctuations δz, $\delta\psi$, δy and $\delta\theta$ are decoupled, while the equations for $\delta\phi$, $\delta\varphi_{12}$ and $\delta\varphi_3$ are coupled. After introducing a time dependence of the form $e^{-\mathrm{i}\,\omega\,\tau}$ (see (C.6)), they take the form that is listed in (C.7), (C.8) and (C.9). Therefore, we have reduced the problem of examining the stability of the string trajectory to an eigenvalue problem for the differential operators that refer to the different types of fluctuation modes. The differential equations are of the general Sturm-Liouville type

$$\left\{-\frac{\mathrm{d}}{\mathrm{d}\sigma}\left[p(\sigma)\frac{\mathrm{d}}{\mathrm{d}\sigma}\right] - r(\sigma)\right\}\Phi(\sigma) = \omega^2\,q(\sigma)\Phi(\sigma) \quad \text{with} \quad \sigma_{\min} \le \sigma < \infty \tag{6.15}$$

where the functions $p(\sigma)$, $q(\sigma)$ and $r(\sigma)$ are read off from the corresponding fluctuation equation and depend on r_0 and the confinement parameter Q. Summarizing, the task is to solve the Sturm-Liouville problem and determine the range of values of r_0 and Q, for which ω^2 is negative. For this range of values the classical solution will be perturbatively unstable.

6.3 Transformation to a Schrödinger potential

To perform the stability analysis it is often more convenient to transform the problem to a Schrödinger one. For this reason we perform the following change of variable and change

JHEP04(2026)184

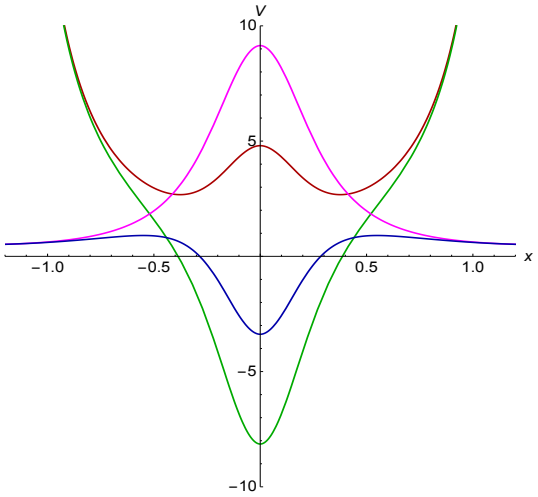

Figure 10. Plots of the Schrödinger potentials from (C.10) as a function of x from (6.19) for $Q = 0$ and $r_0 = 1.2$. The red, green, magenta and blue solid lines correspond to $V_{\delta z}$, $V_{\delta y}$, $V_{\delta\theta}$ and $V_{\delta\psi}$.

of function

$$x = \pm \int_{r_0}^{\sigma} \mathrm{d}\sigma' \sqrt{\frac{q}{p}} \quad \text{with} \quad \Phi = (pq)^{-1/4}\Psi \tag{6.16}$$

where the two different signs for the new variable x, correspond to the two different branches of the U-shaped string embedding. Now equation (6.15) becomes

$$\left[-\frac{\mathrm{d}^2}{\mathrm{d}x^2} + V(x)\right]\Psi(x) = \omega^2\Psi(x) \tag{6.17}$$

and the expression for the potential is

$$V = -\frac{r}{q} + \frac{p^{1/4}}{q^{3/4}}\frac{\mathrm{d}}{\mathrm{d}\sigma}\left[\left(\frac{p}{q}\right)^{1/2}\frac{\mathrm{d}}{\mathrm{d}\sigma}(pq)^{1/4}\right] = -\frac{r}{q} + (pq)^{-1/4}\frac{\mathrm{d}^2}{\mathrm{d}x^2}(pq)^{1/4}\,. \tag{6.18}$$

In the first part of the above relation the potential is a function of the "old" variable σ, while in the second part the potential depends on the 'new" variable x.

Toy model — $Q = 0$ case — reproducing the results of [71]. To set-up the conventions and compare with existing results in the literature, we begin the analysis with the $Q = 0$ case and consider $\theta_0 = 0$. The expressions for the Schrödinger potentials in each fluctuation mode are presented in (C.10). Notice that the analysis of the $\delta\psi$ mode was absent in [71]. For all the cases that we consider, the change of variables (6.16) in this case becomes[31]

$$x(\sigma, r_0) = \pm \int_{r_0}^{\sigma} \frac{\mathrm{d}\xi}{\sqrt{(\xi^2 - r_0^2)\,(\xi^2 + r_0^2 - 1)}}\,. \tag{6.19}$$

To decide about the stability of the solution against perturbations, in figure 10, we are plotting the expressions of the different potentials from (C.10) as a function of x from (6.19).

[31] Notice that in the following analysis we have set $\ell = 1$. This means that all the values of r that we consider are with respect to ℓ: i.e. $r_0 = 1.2$ for $\ell = 1$, transforms to $r_0 = 1.2\,\ell$ for generic ℓ.

JHEP04(2026)184

We have chosen to plot for $r_0 = 1.2$, but the conclusions we draw are valid for any value of $r_0 > 1$. Notice that the $Q = 0$ case corresponds to the Coulomb branch (i.e. without confinement) and there is a singularity at $r = 1$. Since $V_{\delta z}$ and $V_{\delta\theta}$ are positive for every value of r_0, the solution is stable under fluctuations along z and θ. Contrary to the above behaviour, $V_{\delta y}$ and $V_{\delta\psi}$ are positive for large values of x and turn negative as x approaches zero. Because of those negative values for the potential, a numerical computation of the spectrum is needed, in order to decide whether tachyonic modes are produced or not. As we will see from the analysis of the next subsection, the small negative part of the potential $V_{\delta\psi}$ is not sufficient to produce tachyons for that mode, however we will identify tachyons, below a critical value of r_0, for the mode δy.

Finite Q — confining geometry. For finite Q, as can be seen from equations (C.8) and (C.9), two of the modes (namely $\delta\phi$ and $\delta\varphi_{12}$ for $\theta = 0$) are coupled and all the rest are decoupled.

The expressions for the potentials of the decoupled modes are complicated and in (C.11) we are presenting their expansions for small value of Q. The change of variables for finite Q becomes

$$x(\sigma, r_0, Q) = \pm \int_{r_0}^{\sigma} \frac{\xi^2 \sqrt{\xi^2 - 1}\, \mathrm{d}\xi}{\sqrt{(\xi^6 - \xi^4 - Q^2)\,(\xi^2 - r_0^2)\,(\xi^2 + r_0^2 - 1)}}\,. \tag{6.20}$$

Notice that this expression holds both for the coupled and the decoupled modes and in the limit of $Q \to 0$, it reduces to (6.19). In figure 11 we are plotting the decoupled potentials for small values of Q. From this plot it is clear that the presence of the confinement contributes to the stability of the system, since increasing the value of Q is decreasing the region within which some of the potentials have negative values. Moreover the potentials that were positive for $Q = 0$ remain positive for finite Q. In the next subsection we will solve numerically the fluctuation equations for δy and $\delta\psi$ (that have regions of x with negative values or the corresponding potentials) to confirm the absence of tachyonic modes for finite Q.

The coupled system of $\delta\phi$ and $\delta\varphi_{12}$ can be brought into a Schrödinger form with the following transformation

$$\begin{pmatrix} \delta\phi \\ \delta\varphi_{12} \end{pmatrix} = \begin{pmatrix} \Omega_1 & \Omega_2 \\ \Omega_3 & \Omega_4 \end{pmatrix} \cdot \begin{pmatrix} \Delta_1 \\ \Delta_2 \end{pmatrix} \tag{6.21}$$

together with the change of variables of (6.20). The differential equations to determine the functions Ω_i, with $i = 1, \cdots, 4$ are coupled and cannot be solved analytically. Alternatively, one can expand in powers of Q and solve the coupled system order by order in Q. Until the linear in Q term, the expressions of the functions Ω_i, with $i = 1, \cdots, 4$ are listed in (C.12). The coupled system becomes

$$\partial_x^2 \begin{pmatrix} \Delta_1 \\ \Delta_2 \end{pmatrix} + \left(\omega^2\, \hat{1} - V\right) \cdot \begin{pmatrix} \Delta_1 \\ \Delta_2 \end{pmatrix} = 0 \quad \text{with} \quad V = \begin{pmatrix} V_{11} & V_{12} \\ V_{21} & V_{22} \end{pmatrix} \tag{6.22}$$

where the expressions for V_{11}, V_{12}, V_{21} and V_{22} are listed in (C.13). For normalizable solutions of (6.22) that vanish at infinity, ω^2 is positive if the matrix potential V is positively definite.

JHEP04(2026)184

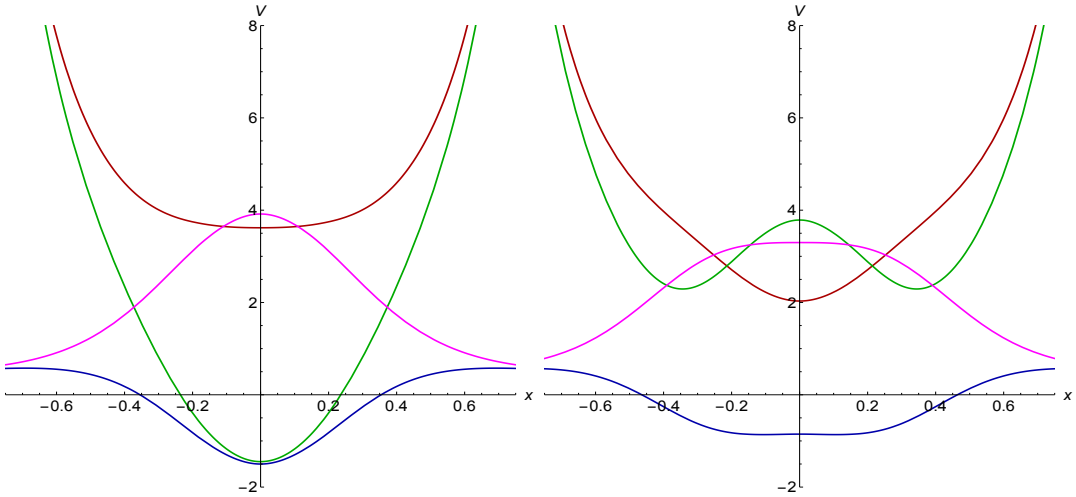

Figure 11. Plots of the decoupled Schrödinger potentials for finite values of Q as a function of x from (6.20). In the left panel $Q = 1/2$ and in the right panel $Q = 1$. The value of the parameter r_0 is fixed to $r_0 = 1.3$, for all the plots. The red, green, magenta and blue solid lines correspond to $V_{\delta z}$, $V_{\delta y}$, $V_{\delta\theta}$ and $V_{\delta\psi}$. Notice that increasing Q, decreases the region of potential instability. If we keep increasing the value of Q, all the potentials will become positive for any value of x. To produce the plots of this figure, we have the used the full expression for each potential and not the perturbative expansions of (C.11).

This means that $\mathrm{Tr}\, V > 0$ and $\det V > 0$. In figure 12 we have plotted the determinant and the trace of the potential V, including terms of order Q^4. While the trace is positive even for $Q = 0$, the negative values of the determinant, in the left panel of figure 12, reduce and eventually disappear when the value of Q increases. As a result it is plausible to expect that the spectrum is tachyon free. Solving numerically the coupled system of equations for $\delta\phi$ and $\delta\varphi_{12}$, we will verify this expectation.

6.4 Solving for the fluctuations

The final step in the investigation of the stability of the Wilson loop configuration is to solve numerically the equations of motion for the fluctuations. We will focus to fluctuation modes for which the corresponding Schrödinger potential had regions of potential instability, i.e. regions of negative values.

Toy model — $Q = 0$ case — reproducing the results of [71]. To describe the steps we have to follow in order to solve numerically the fluctuation equations, we start the analysis from the simpler $Q = 0$ case. In this way we will reproduce the results of the analysis of [71].

Solving from (C.7) the equation of motion for $\delta\psi$ approximately around $\sigma = r_0$ reveals two classes of solutions, namely

$$\delta\psi = A + B\sqrt{\sigma - r_0}\,. \tag{6.23}$$

In a parallel approach, it is possible to solve perturbatively the Schrödinger equation for $\delta\psi$ with the potential $V_{\delta\psi}$ from (C.10) around $x = 0$ (as it is defined in (6.19)). From this

JHEP04(2026)184

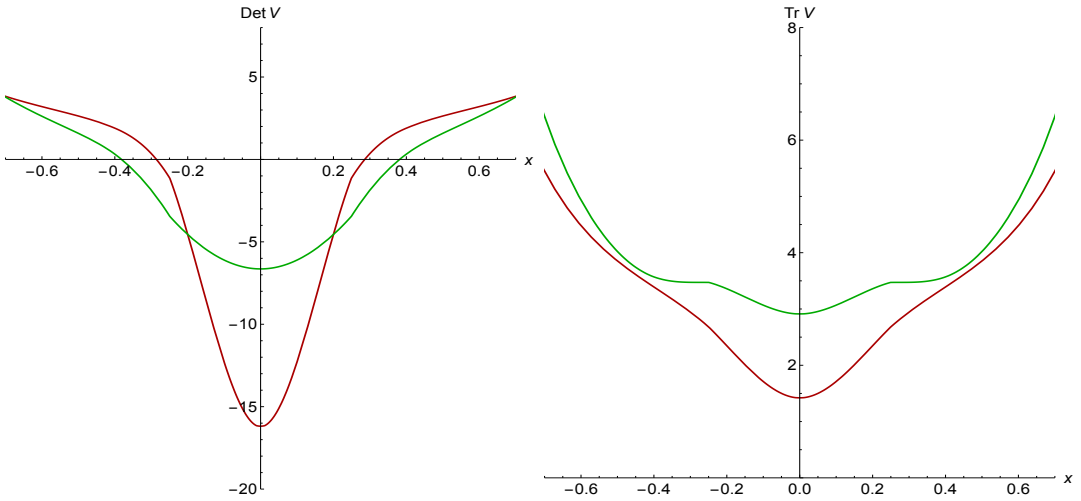

Figure 12. Plots of the determinant (left panel) and of the trace (right panel) of the matrix potential V for two values of the parameter Q. The red and green solid lines correspond to $Q = 0$ and $Q = 1/2$. While the trace is always positive, the determinant is initially negative (i.e. for small values of Q), but as the value of Q increases the region that could potentially lead to an instability is shrinking. To produce the plots of this figure, we have used a perturbative expansion for the trace and the determinant that includes more terms than those that appear in (C.13). In particular we have included terms of order Q^4.

analysis two types of modes arise, namely even and odd ones [72, 73]. Inverting (6.19) to express σ as a function of x when σ approaches r_0, we can relate the even and the odd types of modes with the two classes of solutions of (6.23). From this identification, we have

$$\begin{aligned} A \neq 0 \ \text{and} \ B = 0 \quad &\Rightarrow \quad \Psi^{'}(0) = 0 \ \text{and} \ \Psi(0) \neq 0 \quad \Rightarrow \text{even modes} \\ A = 0 \ \text{and} \ B \neq 0 \quad &\Rightarrow \quad \Psi^{'}(0) \neq 0 \ \text{and} \ \Psi(0) = 0 \quad \Rightarrow \text{odd modes}\,. \end{aligned} \tag{6.24}$$

Solving numerically the equation of motion for $\delta\psi$, and imposing either odd or even boundary conditions, we find a spectrum that is free of instabilities for any value of r_0. This happens even if the Schrödinger potential for $\delta\psi$, as can be seen in figure 10, becomes negative for a range of values of r_0. For $r_0 = 1.1$ the first several excited states are,

$$\begin{aligned} \omega_{\text{even}} &= 0.928,\, 3.440,\, 5.774,\, 8.084,\, 10.390,\, \ldots \\ \omega_{\text{odd}} &= 2.442,\, 4.650,\, 6.936,\, 9.238,\, 11.544,\, \ldots \end{aligned} \tag{6.25}$$

From the analysis of the previous subsection we know that the other mode that could potentially lead to an instability is δy. Analysing the behaviour of δy around $\sigma = r_0$, we obtain the following behaviour

$$\delta y = A + \frac{B}{\sqrt{\sigma - r_0}} \tag{6.26}$$

and performing a similar analysis as before, we identify odd and even modes in the following fashion

$$\begin{aligned} A = 0 \ \text{and} \ B \neq 0 \quad &\Rightarrow \quad \Psi^{'}(0) = 0 \ \text{and} \ \Psi(0) \neq 0 \quad \Rightarrow \text{even modes} \\ A \neq 0 \ \text{and} \ B = 0 \quad &\Rightarrow \quad \Psi^{'}(0) \neq 0 \ \text{and} \ \Psi(0) = 0 \quad \Rightarrow \text{odd modes}\,. \end{aligned} \tag{6.27}$$

JHEP04(2026)184

Computation of the spectrum reveals a critical value for the parameter r_0, namely $r_0^{\rm crit} = 1.125$, below which the spectrum is tachyonic. This is in agreement with the findings from [71]. Notice that exactly for this critical value of r_0, the spectrum has a zero mode

$$\begin{aligned}\omega_{\rm even}^{\rm crit} &= 0.000,\, 4.391,\, 6.881,\, 9.299,\, 11.692,\, \ldots \\ \omega_{\rm odd}^{\rm crit} &= 3.154,\, 5.665,\, 8.096,\, 10.497,\, 12.885,\, \ldots\end{aligned} \tag{6.28}$$

Finite Q — confining geometry. Now we move to the case that we are interested in, namely of finite Q, and start solving numerically from the mode $\delta\psi$. Similarly to the $Q = 0$ case, we find no sign of instability and the first several excited states for $Q = 1$ and $r_0 = r_0^{\rm min}(Q = 1) + 0.1 = 1.31$ are,

$$\begin{aligned}\omega_{\rm even} &= 1.192,\, 4.014,\, 6.678,\, 9.346,\, 12.015,\, \ldots \\ \omega_{\rm odd} &= 2.704,\, 5.340,\, 8.011,\, 10.680,\, 13.350\, \ldots\end{aligned} \tag{6.29}$$

For the δy modes, one has to separate the analysis is two cases. When $Q < 0.22$, in agreement with the analysis of the $Q = 0$ case, there is always a critical value of r_0 (that depends on Q) where a tachyon appears and for this value there is a zero mode. However, as we extensively discussed in [1], these WL trajectories are pathological since the string is "touching" the Coulomb branch singularity. The reason is that the values of the Coulomb scale and of the confining scale are close to each other. Remarkably when $Q > 0.22$ the tachyons disappear from the spectrum for any value above the $r_0^{\rm min}(Q)$. For $Q = 1$ and $r_0 = r_0^{\rm min}(Q = 1) + 0.1 = 1.31$ the first several excited states that we find are,

$$\begin{aligned}\omega_{\rm even} &= 2.388,\, 5.163,\, 7.851,\, 10.521,\, 13.183,\, \ldots \\ \omega_{\rm odd} &= 3.727,\, 6.505,\, 9.188,\, 11.853,\, 14.511\, \ldots\end{aligned} \tag{6.30}$$

Finally we solve numerically the coupled system of equations (C.8) and the first of (C.9) (this is the one that survives when $\theta = 0$). As previously the modes are either even or odd depending on the boundary conditions and it turns out that even/odd modes of $\delta\phi$ couple to even/odd modes of $\delta\varphi_{12}$, respectively. From the numerical solution, no presence of tachyon appears and the first several excited states that we find, for $Q = 1$, $r_0 = r_0^{\rm min}(Q = 1) + 0.1 = 1.31$, are

$$\begin{aligned}\omega_{\rm even-even} &= 1.177,\, 2.687,\, 4.002,\, 5.146\,, 6.652,\, \ldots \\ \omega_{\rm odd-odd} &= 2.680,\, 3.780,\, 5.278,\, 6.270,\, 7.814\, \ldots\end{aligned} \tag{6.31}$$

7 Penrose limits of the Anabalon-Ross deformed $AdS_5 \times \mathbb{S}^5$ solution

Here we review the uplift of the supersymmetric Anabalon-Ross solution [24] in type-IIB supergravity, following the notation of [27]. This consists of a $10D$ metric and a self-dual RR 5-form. As mentioned in [1] this solution can be reached by taking the limit $\ell \to 0$ with $\ell^2 Q$ fixed in the solution of section 3.1 (considering the SUSY case where $Q = |q_1| = |q_2|$).

JHEP04(2026)184

For the metric we have[32]

$$
\begin{aligned}
L^{-2}\mathrm{d}s^2 = r^2(-\mathrm{d}t^2 + \mathrm{d}x_1^2 + \mathrm{d}x_2^2) + \frac{\mathrm{d}r^2}{r^2 f(r)} + r^2 f(r)\mathrm{d}\phi^2 \\
+ \mathrm{d}\theta^2 + \sin^2\theta \mathrm{d}\varphi^2 + \sin^2\theta \sin^2\varphi \Big(\mathrm{d}\varphi_1 + \frac{1}{L}\mathcal{A}\Big)^2 \\
+ \sin^2\theta\cos^2\varphi\Big(\mathrm{d}\varphi_2 + \frac{1}{L}\mathcal{A}\Big)^2 + \cos^2\theta\Big(\mathrm{d}\varphi_3 + \frac{1}{L}\mathcal{A}\Big)^2 ,
\end{aligned}
\tag{7.1}
$$

where

$$
f(r) = 1 - \Big(\frac{Q}{r}\Big)^6 , \qquad \mathcal{A} = LQ\left(1 - \Big(\frac{Q}{r}\Big)^2\right)\mathrm{d}\phi = LA(r)\mathrm{d}\phi\,. \tag{7.2}
$$

The periodicities of the various angular coordinates are

$$
0 \le \theta \le \frac{\pi}{2}\,, \qquad 0 \le \varphi \le \frac{\pi}{2}\,, \qquad 0 \le \varphi_i \le 2\pi \quad (i = 1,2,3)\,. \tag{7.3}
$$

The RR 5-form is given by the formula below

$$
F_5 = (1 + \star)G_5\,, \qquad G_5 = 4L^4\,\mathrm{vol}_5 - L^3\sum_{i=1}^{3}\mu_i \mathrm{d}\mu_i \wedge \Big(\mathrm{d}\varphi_i + \frac{1}{L}\mathcal{A}\Big) \wedge \star_5 \mathrm{d}\mathcal{A}\,. \tag{7.4}
$$

In the above expression, the operator $\star_5$ stands for Hodge duality in the $5D$ space with line element given by the first line in (7.1). Also, with vol_5 we refer to the volume form of the aforementioned $5D$ space. Therefore

$$
\mathrm{vol}_5 = r^3\,\mathrm{d}t \wedge \mathrm{d}x_1 \wedge \mathrm{d}x_2 \wedge \mathrm{d}r \wedge \mathrm{d}\phi\,, \qquad \star_5 \mathrm{d}\mathcal{A} = 2LQ^3\,\mathrm{d}t \wedge \mathrm{d}x_1 \wedge \mathrm{d}x_2\,. \tag{7.5}
$$

Moreover, $\mu_i\,(i = 1,2,3)$ are the embedding coordinates in $\mathbb{R}^3$ of a unit two-sphere parametrised by (θ, φ). In particular

$$
\mu_1 = \sin\theta\sin\varphi\,, \qquad \mu_2 = \sin\theta\cos\varphi\,, \qquad \mu_3 = \cos\theta\,. \tag{7.6}
$$

Given the ranges of the coordinates (θ, φ) in (7.3), the embedding coordinates $\mu_i\,(i = 1,2,3)$ cover only the $\frac{1}{8}$ of the sphere surface.

Notice that we factor out the scale L^2 in the line element (7.1). This is done by redefining the radial coordinate r of [27] as $r \to L^2 r$ and the parameter Q as $Q \to LQ$. The reason behind this redefinition is that we will use the scale L later to compute Penrose limits in the geometry (7.1).

Besides the time-like Killing vector, the $10D$ geometry (7.1) admits four more Killing vectors representing the symmetry under shifts in the directions ϕ and $\varphi_i\,(i = 1,2,3)$. In this section, we will consider the Penrose limits that correspond to null geodesics that are associated with the motion of a point particle in t and the Killing directions ϕ and $\varphi_i\,(i = 1,2,3)$.

[32]Notice that the internal coordinates $(\theta,\, \varphi, \varphi_i)$ here correspond to $(\theta - \frac{\pi}{2},\, \psi,\, \phi_i)$ in section 3.1.

JHEP04(2026)184

7.1 Motion along (t, ϕ, φ_1)

Let us start with the case where a particle moves in the spacetime (7.1) with fixed x_1, x_2, r, θ, φ. In particular, if we take $\theta = \varphi = \frac{\pi}{2}$ then the particle does not "feel" the presence of φ_2 and φ_3. The geodesic equations of motion, except that for r, require

$$t = \mathcal{E}u\,, \qquad \phi = \left(\mathcal{J} + \frac{r_0^2}{Q^2 - r_0^2}\mathcal{J}_1\right)u\,, \qquad \varphi_1 = Q\mathcal{J}_1 u\,, \tag{7.7}$$

where r_0 is the fixed value of the r direction and $\mathcal{E}$, $\mathcal{J}$, $\mathcal{J}_1$ are integration constants. The geodesic equation for the r direction provides an algebraic constraint for the constants $\mathcal{E}$, $\mathcal{J}$ and $\mathcal{J}_1$, which is

$$\mathcal{E}^2 = \left(1 + 2\frac{Q^4}{r_0^4}\right)\mathcal{J}^2 + \frac{2}{r_0^4}\frac{Q^6 + Q^4 r_0^2 + r_0^6}{Q^2 - r_0^2}\mathcal{J}\mathcal{J}_1 + \frac{2Q^6 + r_0^6}{\left(Q^2 - r_0^2\right)^2}\frac{\mathcal{J}_1^2}{r_0^2}\,. \tag{7.8}$$

Moreover, the null condition implies that $\mathcal{J}$ and $\mathcal{J}_1$ are related as

$$\mathcal{J} = -\frac{Q^2}{Q^2 - r_0^2}\mathcal{J}_1 \qquad \text{or} \qquad \mathcal{J} = -\frac{3Q^2 r_0^2}{4Q^4 - 5Q^2 r_0^2 + r_0^4}\mathcal{J}_1\,. \tag{7.9}$$

The above values for $\mathcal{J}$ correspond to

$$\mathcal{E}^2 = \mathcal{J}_1^2 \qquad \text{and} \qquad \mathcal{E}^2 = \frac{8Q^6 + r_0^6}{\left(4Q^2 - r_0^2\right)^2}\frac{\mathcal{J}_1^2}{r_0^2} \tag{7.10}$$

respectively.

For the Penrose limit we will adopt the rescalings

$$x_1 \to \frac{x_1}{L}\,, \qquad x_2 \to \frac{x_2}{L}\,, \qquad r \to r_0 + \frac{\rho}{L}\,, \qquad \theta \to \frac{\pi}{2} + \frac{y_1}{L}\,, \qquad \varphi \to \frac{\pi}{2} + \frac{y_2}{L} \tag{7.11}$$

together with

$$t \to \mathcal{E}u\,, \qquad \phi \to \left(\mathcal{J} + \frac{r_0^2}{Q^2 - r_0^2}\mathcal{J}_1\right)u + \frac{w}{L}\,, \qquad \varphi_1 \to Q\mathcal{J}_1 u + c\frac{w}{L} + \frac{v}{L^2}\,. \tag{7.12}$$

Here c is a constant which will be specified later, while $\mathcal{E}$ and $\mathcal{J}$ take the values (7.9) and (7.10). Therefore, we have the following two cases[33]

$$\begin{aligned} &\textbf{Case A:} \qquad \mathcal{E}^2 = \mathcal{J}_1^2\,, && \mathcal{J} = -\frac{Q^2}{Q^2 - r_0^2}\mathcal{J}_1\,, \\ &\textbf{Case B:} \qquad \mathcal{E}^2 = \frac{8Q^6 + r_0^6}{\left(4Q^2 - r_0^2\right)^2}\frac{\mathcal{J}_1^2}{r_0^2}\,, && \mathcal{J} = -\frac{3Q^2 r_0^2}{4Q^4 - 5Q^2 r_0^2 + r_0^4}\mathcal{J}_1\,. \end{aligned} \tag{7.13}$$

Let us examine each case separately.

[33] Of course one can also consider the case where $\mathcal{J} + \frac{r_0^2}{Q^2 - r_0^2}\mathcal{J}_1 = 0$, which amounts to rescaling ϕ as $\phi \to \frac{\phi}{L}$. This would just correspond to motion along t and φ_1 only.

JHEP04(2026)184

Case A. In order for the Penrose limit to be valid the constant c must take the value[34]

$$c = \frac{r_0^4 - Q^4}{Q^3}\,. \tag{7.14}$$

Sending L to infinity, one derives a pp-wave geometry, which can be cast in Brinkman form after the following sequence of transformations

i Rescalings

$$\begin{aligned} &x_1 \to \frac{x_1}{r_0}\,, \quad x_2 \to \frac{x_2}{r_0}\,, \quad w \to \frac{Q^3}{r_0\sqrt{r_0^6 - Q^6}}\, w\,, \\ &\rho \to \frac{\sqrt{r_0^6 - Q^6}}{r_0^2}\,\rho\,, \qquad v \to \omega_1\, v + \omega_2\, \rho\, w\,, \end{aligned} \tag{7.15}$$

with

$$\omega_1 = \frac{r_0^2}{Q^3 \mathcal{J}_1}\,, \qquad \omega_2 = 2\,. \tag{7.16}$$

ii Rotation

$$\begin{pmatrix} w \\ \rho \end{pmatrix} \to \begin{pmatrix} \cos\left(\frac{\omega_2}{\omega_1} u\right) & \sin\left(\frac{\omega_2}{\omega_1} u\right) \\ -\sin\left(\frac{\omega_2}{\omega_1} u\right) & \cos\left(\frac{\omega_2}{\omega_1} u\right) \end{pmatrix} \cdot \begin{pmatrix} w \\ \rho \end{pmatrix}\,. \tag{7.17}$$

iii Shifts

$$\varphi_2 \to \varphi_2 + Q\mathcal{J}_1\left(1 - \frac{Q^2}{r_0^2}\right) u\,, \qquad \varphi_3 \to \varphi_3 + Q\mathcal{J}_1\left(1 - \frac{Q^2}{r_0^2}\right) u\,. \tag{7.18}$$

As a result one finds

$$\begin{aligned} \mathrm{d}s^2 = {} & 2\mathrm{d}u\mathrm{d}v + \mathrm{d}x_1^2 + \mathrm{d}x_2^2 + \mathrm{d}y_1^2 + y_1^2\,\mathrm{d}\varphi_3^2 + \mathrm{d}y_2^2 + y_2^2\,\mathrm{d}\varphi_2^2 + \mathrm{d}w^2 + \mathrm{d}\rho^2 \\ & - \frac{Q^6 \mathcal{J}_1^2}{r_0^4}(y_1^2 + y_2^2 + 4w^2 + 4\rho^2)\mathrm{d}u^2\,. \end{aligned} \tag{7.19}$$

Notice that each of the pairs (y_1, φ_3) and (y_2, φ_2) parametrise an $\mathbb{R}^2$.

The above transformations, when applied to the self-dual five-form give

$$\begin{aligned} F_5 = \frac{2Q^3\mathcal{J}_1}{r_0^2} \Big(& 2\,\mathrm{d}u \wedge \mathrm{d}x_1 \wedge \mathrm{d}x_2 \wedge \mathrm{d}\rho \wedge \mathrm{d}w + y_1\,\mathrm{d}u \wedge \mathrm{d}y_1 \wedge \mathrm{d}\varphi_3 \wedge \mathrm{d}\rho \wedge \mathrm{d}w \\ & + y_2\,\mathrm{d}u \wedge \mathrm{d}y_2 \wedge \mathrm{d}\varphi_2 \wedge \mathrm{d}\rho \wedge \mathrm{d}w - y_1\,\mathrm{d}u \wedge \mathrm{d}x_1 \wedge \mathrm{d}x_2 \wedge \mathrm{d}y_1 \wedge \mathrm{d}\varphi_3 \\ & - y_2\,\mathrm{d}u \wedge \mathrm{d}x_1 \wedge \mathrm{d}x_2 \wedge \mathrm{d}y_2 \wedge \mathrm{d}\varphi_2 - 2\,y_1 y_2\,\mathrm{d}u \wedge \mathrm{d}y_1 \wedge \mathrm{d}y_2 \wedge \mathrm{d}\varphi_2 \wedge \mathrm{d}\varphi_3 \Big)\,. \end{aligned} \tag{7.20}$$

Case B. Now the Penrose limit makes sense when

$$c = -Q + \frac{4Q^3}{3r_0^2} - \frac{r_0^4}{3Q^3}\,. \tag{7.21}$$

The associated pp-wave geometry can be expressed in Brinkman coordinates after the following operations

[34]This value ensures the vanishing of the term that is proportional to L in the expansion of the line element for large L.

JHEP04(2026)184

i Rescalings

$$x_1 \to \frac{x_1}{r_0}\,, \quad x_2 \to \frac{x_2}{r_0}\,, \quad w \to \frac{3Q^3 r_0^2}{\sqrt{r_0^{12}+7Q^6 r_0^6-8Q^{12}}}\,w\,,$$
$$\rho \to \frac{\sqrt{r_0^6-Q^6}}{r_0^2}\,\rho\,, \qquad v \to \omega_1\, v + \omega_2 \rho\, w\,, \tag{7.22}$$

where

$$\omega_1 = \frac{4Q^2-r_0^2}{3Q^3\mathcal{J}_1}\,, \qquad \omega_2 = -\frac{2}{3r_0^3}\sqrt{\frac{r_0^{12}+7Q^6r_0^6-8Q^{12}}{r_0^6-Q^6}}\,. \tag{7.23}$$

ii Rotation in the $(\rho,\, w)$-plane as in (7.17), where now the parameters ω_1 and ω_2 are given in (7.23).

iii Shifts

$$\varphi_2 \to \varphi_2 + Q\,\mathcal{J}_1\,\frac{Q^2-r_0^2}{4Q^2-r_0^2}u\,, \qquad \varphi_3 \to \varphi_3 + Q\,\mathcal{J}_1\,\frac{Q^2-r_0^2}{4Q^2-r_0^2}u\,. \tag{7.24}$$

The outcome of this is

$$\begin{aligned} \mathrm{d}s^2 &= 2\mathrm{d}u\mathrm{d}v + \mathrm{d}x_1^2 + \mathrm{d}x_2^2 + \mathrm{d}y_1^2 + y_1^2\,\mathrm{d}\varphi_3^2 + \mathrm{d}y_2^2 + y_2^2\,\mathrm{d}\varphi_2^2 + \mathrm{d}w^2 + \mathrm{d}\rho^2 \\ &\quad - \frac{Q^6\mathcal{J}_1^2}{r_0^6(r_0^2-4Q^2)^2}\Big(9r_0^6(y_1^2+y_2^2) + 4(4Q^6+5r_0^6)(w^2+\rho^2) \\ &\quad +16(Q^6-r_0^6)(\tilde{w}^2-\tilde{\rho}^2)\Big)\,\mathrm{d}u^2\,, \end{aligned} \tag{7.25}$$

where

$$\tilde{w} = \sin\left(\frac{\omega_2}{\omega_1}u\right)\rho + \cos\left(\frac{\omega_2}{\omega_1}u\right)w\,, \qquad \tilde{\rho} = \cos\left(\frac{\omega_2}{\omega_1}u\right)\rho - \sin\left(\frac{\omega_2}{\omega_1}u\right)w\,. \tag{7.26}$$

Like in the previous case, each of the pairs $(y_1,\, \varphi_3)$ and $(y_2,\, \varphi_2)$ parametrise a Euclidean plane.

For the self-dual five-form we find

$$\begin{aligned} F_5 = \frac{8}{3}\frac{\sqrt{r_0^6+8Q^6}}{r_0^3\omega_1\omega_2}\Bigg(&\mathrm{d}u\wedge\mathrm{d}x_1\wedge\mathrm{d}x_2\wedge\mathrm{d}\rho\wedge\mathrm{d}w - \frac{\sqrt{r_0^6+8Q^6}}{6r_0^3}y_1\mathrm{d}u\wedge\mathrm{d}y_1\wedge\mathrm{d}\varphi_3\wedge\mathrm{d}\rho\wedge\mathrm{d}w \\ &- \frac{\sqrt{r_0^6+8Q^6}}{6r_0^3}y_2\mathrm{d}u\wedge\mathrm{d}y_2\wedge\mathrm{d}\varphi_2\wedge\mathrm{d}\rho\wedge\mathrm{d}w - \frac{\omega_2}{4}y_1\mathrm{d}u\wedge\mathrm{d}x_1\wedge\mathrm{d}x_2\wedge\mathrm{d}y_1\wedge\mathrm{d}\varphi_3 \\ &- \frac{\omega_2}{4}y_2\mathrm{d}u\wedge\mathrm{d}x_1\wedge\mathrm{d}x_2\wedge\mathrm{d}y_2\wedge\mathrm{d}\varphi_2 - \frac{3r_0^3\omega_2}{2\sqrt{r_0^6+8Q^6}}y_1y_2\mathrm{d}u\wedge\mathrm{d}y_1\wedge\mathrm{d}y_2\wedge\mathrm{d}\varphi_2\wedge\mathrm{d}\varphi_3\Bigg)\,. \end{aligned} \tag{7.27}$$

Notice that when $Q=0$, both pp-wave backgrounds that we discussed above reduce to flat spaces with vanishing RR fields.

7.2 Motion along $(t,\, \phi,\, \varphi_2)$

We will now consider the case where the motion of the particle is realised in the t, ϕ and φ_2 directions. Therefore, we will take x_1, x_2, r, θ, φ to be fixed and $\theta = \frac{\pi}{2}$, $\varphi = 0$. One can easily see from (7.1), that for this values of θ and φ, the terms of the line element involving

JHEP04(2026)184

$\mathrm{d}\varphi_1$ and $\mathrm{d}\varphi_3$ vanish. Therefore, the particle does not "feel" the presence of φ_2 and φ_3. From the geodesic equations of motion we find that

$$t = \mathcal{E}u\,, \qquad \phi = \left(\mathcal{J} + \frac{r_0^2}{Q^2 - r_0^2}\mathcal{J}_2\right)u\,, \qquad \varphi_2 = Q\mathcal{J}_2 u\,, \tag{7.28}$$

where r_0 is the fixed value of the r direction and $\mathcal{E}$, $\mathcal{J}$, $\mathcal{J}_2$ are integration constants. On top of that, the equation for the radial direction r reduces into the algebraic constraint

$$\mathcal{E}^2 = \left(1 + 2\frac{Q^4}{r_0^4}\right)\mathcal{J}^2 + \frac{2}{r_0^4}\frac{Q^6 + Q^4 r_0^2 + r_0^6}{Q^2 - r_0^2}\mathcal{J}\mathcal{J}_2 + \frac{2Q^6 + r_0^6}{\left(Q^2 - r_0^2\right)^2}\frac{\mathcal{J}_2^2}{r_0^2}\,. \tag{7.29}$$

The null condition relates $\mathcal{J}$ with $\mathcal{J}_2$ and it turns out that one has to consider the following two cases[35]

$$\begin{aligned} &\textbf{Case A:} \qquad \mathcal{E}^2 = \mathcal{J}_2^2\,, && \mathcal{J} = -\frac{Q^2}{Q^2 - r_0^2}\mathcal{J}_2\,, \\ &\textbf{Case B:} \qquad \mathcal{E}^2 = \frac{8Q^6 + r_0^6}{\left(4Q^2 - r_0^2\right)^2}\frac{\mathcal{J}_2^2}{r_0^2}\,, && \mathcal{J} = -\frac{3Q^2 r_0^2}{4Q^4 - 5Q^2 r_0^2 + r_0^4}\mathcal{J}_2\,. \end{aligned} \tag{7.30}$$

Like in the previous example, in order to take the Penrose limit we will adopt the rescalings

$$x_1 \to \frac{x_1}{L}\,, \qquad x_2 \to \frac{x_2}{L}\,, \qquad r \to r_0 + \frac{\rho}{L}\,, \qquad \theta \to \frac{\pi}{2} + \frac{y_1}{L}\,, \qquad \varphi \to \frac{y_2}{L} \tag{7.31}$$

together with

$$t \to \mathcal{E}u\,, \qquad \phi \to \left(\mathcal{J} + \frac{r_0^2}{Q^2 - r_0^2}\mathcal{J}_2\right)u + \frac{w}{L}\,, \qquad \varphi_2 \to Q\mathcal{J}_2 u + c\frac{w}{L} + \frac{v}{L^2}\,. \tag{7.32}$$

Here again c is a constant which must be fixed to the value (7.14) (**case A**) or (7.21) (**case B**), so that the Penrose limit makes sense.[36]

It turns out that if we compute the limit in the **case A**, one derives the pp-wave background (7.19) and (7.20) with $\varphi_2 \to \varphi_1$ and $\mathcal{J}_1 \to \mathcal{J}_2$. Similarly, in the **case B** one finds (7.25), (7.26) and (7.27), where again $\varphi_2 \to \varphi_1$ and $\mathcal{J}_1 \to \mathcal{J}_2$.

7.3 Motion along (t, ϕ, φ_3)

In the last example, we will consider the case where the particle moves in the t, ϕ and φ_3 directions. For this reason, we will fix x_1, x_2, r ,θ and set $\theta = 0$ while keeping φ arbitrary. As it can be confirmed from (7.1), the terms involving $\mathrm{d}\varphi_1$ and $\mathrm{d}\varphi_2$ shrink to zero, and therefore the particle does not "feel" these directions. The geodesic equations of motion now imply

$$t = \mathcal{E}u\,, \qquad \phi = \left(\mathcal{J} + \frac{r_0^2}{Q^2 - r_0^2}\mathcal{J}_3\right)u\,, \qquad \varphi_3 = Q\mathcal{J}_3 u\,, \tag{7.33}$$

[35] Again, one can also consider the case where $\mathcal{J} + \frac{r_0^2}{Q^2 - r_0^2}\mathcal{J}_2 = 0$, which corresponds to particle motion only along t and φ_2.

[36] These values ensure the vanishing of the term that is proportional to L in the expansion of the line element for large L.

JHEP04(2026)184

with r_0 being the fixed value of the r direction and $\mathcal{E}$, $\mathcal{J}$, $\mathcal{J}_3$ are integration constants. Like in the previous two examples, the equation of motion for the radial direction r is equivalent to an algebraic constraint, where now

$$\mathcal{E}^2 = \left(1 + 2\frac{Q^4}{r_0^4}\right)\mathcal{J}^2 + \frac{2}{r_0^4}\frac{Q^6 + Q^4 r_0^2 + r_0^6}{Q^2 - r_0^2}\mathcal{J}\mathcal{J}_3 + \frac{2Q^6 + r_0^6}{(Q^2 - r_0^2)^2}\frac{\mathcal{J}_3^2}{r_0^2}\,. \tag{7.34}$$

On top of that, we need to take into account the null condition of the geodesic which provides a relation between $\mathcal{J}$ and $\mathcal{J}_3$, namely

$$\mathcal{J} = -\frac{Q^2}{Q^2 - r_0^2}\mathcal{J}_3 \qquad \text{or} \qquad \mathcal{J} = -\frac{3Q^2 r_0^2}{4Q^4 - 5Q^2 r_0^2 + r_0^4}\mathcal{J}_3\,. \tag{7.35}$$

This suggests that we need to consider the following two cases

$$\begin{aligned} &\textbf{Case A:} \qquad \mathcal{E}^2 = \mathcal{J}_3^2\,, && \mathcal{J} = -\frac{Q^2}{Q^2 - r_0^2}\mathcal{J}_3\,, \\ &\textbf{Case B:} \qquad \mathcal{E}^2 = \frac{8Q^6 + r_0^6}{(4Q^2 - r_0^2)^2}\frac{\mathcal{J}_3^2}{r_0^2}\,, && \mathcal{J} = -\frac{3Q^2 r_0^2}{4Q^4 - 5Q^2 r_0^2 + r_0^4}\mathcal{J}_3\,. \end{aligned} \tag{7.36}$$

For the Penrose limit we will adopt the rescalings

$$x_1 \to \frac{x_1}{L}\,, \qquad x_2 \to \frac{x_2}{L}\,, \qquad r \to r_0 + \frac{\rho}{L}\,, \qquad \theta \to \frac{y}{L} \tag{7.37}$$

together with[37]

$$t \to \mathcal{E}u\,, \qquad \phi \to \left(\mathcal{J} + \frac{r_0^2}{Q^2 - r_0^2}\mathcal{J}_3\right)u + \frac{w}{L}\,, \qquad \varphi_3 \to Q\mathcal{J}_3 u + c\frac{w}{L} + \frac{v}{L^2}\,. \tag{7.38}$$

Like in the previous two examples, c is a constant which must be fixed to the value (7.14) (**case A**) or (7.21) (**case B**), to ensure the vanishing of the term that is linear in L when taking the Penrose limit.

At the end of the day, one obtains a pp-wave background for each of the two cases A and B. However, it turns out that both pp-wave backgrounds are equivalent to the ones found in the previous two examples. In particular, if we want to match the two solutions with the ones that correspond to motion along φ_1 all we have to do is to apply the following change of coordinates

$$y \to \sqrt{y_1^2 + y_2^2}\,, \qquad \varphi \to \tan^{-1}\frac{y_1}{y_2} \qquad \varphi_1 \to \varphi_3\,, \tag{7.39}$$

together with $\mathcal{J}_3 \to \mathcal{J}_1$.

We can make the following comment: as we are fibering the three U(1) isometries φ_i inside the $\mathbb{S}^5$ in an identical way, these directions are indistinguishable from each other which explains the same behaviour found for the three geodesic motions studied above (cases A and B respectively). Even though the embedding coordinates μ_i are different with respect to each other, one can chose any one of the expressions to correspond to μ_1 etc. In other words, there is a freedom to exchange μ_is among themselves. We conclude that the pp-wave analysis showcases an isotropy between the three U(1) coordinates, encoded in the coordinate change (7.39).

[37] Like before, one can also consider the case where $\mathcal{J} + \frac{r_0^2}{Q^2 - r_0^2}\mathcal{J}_3 = 0$, which corresponds to particle motion only along t and φ_3.

JHEP04(2026)184

8 Conclusions and discussion

In this work, we studied in detail the solutions presented in [1] which describe supersymmetric RG flows between various UV SCFTs in 4d and $(2+1)$ dimensional SQFTs in the IR. The construction of these systems was done by implementing SUSY preserving Coulomb branch deformations, realized as a twisted compactification in the dual supergravity backgrounds. More specifically,

- We have constructed smooth supersymmetric asymptotically AdS solutions in type II and eleven-dimensional supergravity, realizing holographic RG flows from four-dimensional SCFTs to three-dimensional SQFTs which have a mass gap and in some cases, confine external quarks. We extend and complement the results of [1], showing that distinct UV fixed points exhibit universal IR behaviour.

- For the uplifts we used the five-dimensional gauged supergravity soliton of [33] to construct new infinite families of solutions in type IIA, type IIB, and M-theory. In all cases, the geometries are smooth and free of conical singularities for appropriate parameter ranges, ensuring physical regularity of the dual theories.

- We computed a variety of holographic observables not included in [1], namely new embeddings for the Wilson loops, 't Hooft loops and entanglement entropy. These quantities display a universal factorization property: the dependence on the internal space is separated from the dynamics along the holographic radial direction. This universality points towards a deeper geometric structure underlying the supersymmetric confinement mechanism. The new results showcasing phase transitions in the 't Hooft loops and entanglement entropy, complementing the Wilson loop calculation performed in [1], further hint towards a confining behaviour for the dual. That confining behaviour is also reflected in the form of the D7-brane embeddings that avoid the central region of the geometry. The plot of the condensate with respect to the quark mass shows an interesting non monotonic behaviour, where the condensate flows to zero both for large and small quark mass.

- The holographic renormalization of the type IIB background revealed the operator VEVs driving the flow, offering a clear dictionary between the bulk deformation parameters and boundary field-theory operators. The boundary analysis confirmed the consistency of the UV and IR asymptotics and provided finite counterterms for the renormalized action.

- We investigated in detail the stability of the Wilson loop embedding used to study the type IIB background, under linear fluctuations of the coordinates. We found that the configuration is stable, however, when $\hat{\nu} \approx -1^+$ (or $Q \ll 1$) we see tachyonic modes appearing, further supporting our claims about this parametric region being untrustworthy, as discussed in [1].

- The study of Penrose limits for the Anabalon-Ross deformed $AdS_5 \times S^5$ solution offers insight into the spectrum of excitations and possible integrable subsectors in the dual theory, paving the way for future studies of string dynamics on these backgrounds.

JHEP04(2026)184

From a broader perspective, our results provide a unified and systematic framework for studying supersymmetric compactifications of $SCFT_4$s on a circle that flow to confining three-dimensional theories. Is is important to emphasize that the dual QFT*s* described by these systems are all strongly coupled. Our deformation procedure should be applicable to any four-dimensional superconformal theory with a known holographic dual, as long as the later admits a consistent truncation to five-dimensional gauged supergravity. The interplay between topological twisting, smooth IR geometries, and holographic universality could shed light on nonperturbative dynamics beyond the present models.

This work opens many interesting research directions for future exploration, some of which include:

- Extension of the holographic renormalization analysis to the 11d and type IIA uplifts, to extract the corresponding VEVs and compare the operator maps across dimensions.
- Investigation of the stability of the (non-SUSY) soliton configurations under perturbations and exploration of possible phase transitions associated with varying the compactification radius or the holonomy parameters.
- Study the supersymmetric defect and domain-wall configurations supported by these geometries, which could model interfaces between different confining phases.
- Analysis of the Penrose limits and pp-wave sectors in more detail to identify potential integrable subsectors and compute semiclassical string spectra.
- We should explore the inclusion of flavour branes and their impact on the universal structure of observables, particularly in the 11d embeddings with M5 flavour branes.
- It would be interesting if more elaborated solitons than the ones studied in [33] could cure the singularities of the flavoured backgrounds in [74], along the lines discussed in [30].

Finally, we wish to examine the effects of higher-curvature corrections near the large-curvature region ($\hat{\nu} \approx -1$) to assess their impact on the holographic predictions for IR observables. This will potentially provide information about the light modes appearing near the Coulomb branch VEV, which were not accounted for in the supergravity solutions presented here. There are two possible corrections one can include: corrections to the metric and corrections to the observable itself (in the case of the Wilson loop, which is able to detect the high curvature effects). We believe that if the needed corrections in next-to-leading order in α' are found and included in the calculation, the Wilson loop phase transition observed near the region where $\hat{\nu} = -1$ will potentially disappear. This will be a fascinating phenomenon to observe. We hope to address these interesting points and many others in future work.

Acknowledgments

The authors would like to thank the following colleagues for the useful discussions, their interesting comments and for sharing their knowledge and ideas with us: Andres Anabalón, Alexandre Mathieu Frederic Belin, Francesco Bigazzi, Nicoló Bragagnolo, Federico Castellani,

JHEP04(2026)184

Aldo Lorenzo Cotrone, Anton Faedo, Ali Fatemiabhari, Prem Kumar, Yolanda Lozano, Noppadol Mekareeya, René Meyer, Alfonso Ramallo, Ricardo Stuardo, Daniel C. Thompson, Alessandro Tomasiello. The research of D.C. has been supported by the STFC consolidated grand ST/Y509644-1. D.C. would also like to thank the universities of Santiago de Compostela, Oviedo, as well as the Galileo Galilei Institute for theoretical physics in Florence, Milano Bicocca and INFN for their hospitality while in the last stages of this work. M.H. has been supported by the STFC consolidated grant ST/Y509644/1. M.H. would like to thank Humboldt-Universität zu Berlin during the KMPB school. G.I. is supported by the Einstein Stiftung Berlin via the Einstein International Postdoctoral Fellowship program "Generalised dualities and their holographic applications to condensed matter physics" (project number IPF- 2020-604). C.N. is supported by STFC's grants ST/Y509644-1, ST/X000648/1 and ST/T000813/1. This paper has been financed by the funding programme "MEDICUS", of the University of Patras (D.Z. with grant number: 83800).

A Polyakov loop embedding

Here we explore two cases of embeddings of D1 branes in the type IIB solution of section 3.1, which will *not* give the same dynamics as the 't Hooft loop. The reason being that they are not extended enough to include time, a profile in $r(w)$, as well as the shrinking circle ϕ. The inclusion of the later in the various probes is responsible for the vanishing of the tension of the effective string at $r = r_\star$, as it conspires to the appearance of a multiplicative factor of $\sqrt{F(r)}$ in $\mathcal{F}_t$ through the determinant. This suggests to us that the minimal probe brane which is capable of capturing the 't Hooft loop in this background is a D3.

Case I. We first consider a D1 on $\Sigma_2 = [t, w]$ with $r = r(w)$ and all the other coordinates set to constant values. We have the induced metric on the D1:

$$\mathrm{d}s^2_{\mathrm{ind,D1}} = \frac{\zeta(r,\theta)}{L^2}\left[-r^2\mathrm{d}t^2 + \mathrm{d}w^2\left(r^2 + \frac{L^2 r'^2}{F(r)\lambda(r)^6 r^2}\right)\right], \tag{A.1}$$

and its action which reads:

$$\begin{aligned} S_{\mathrm{D1}} &= T_{\mathrm{D1}}\int_{\Sigma_2}\mathrm{d}^2\sigma\sqrt{-e^{-2\Phi}\det(g_{\mathrm{ind,D1}})} = T_{\mathrm{D1}}\mathcal{T}\int\mathrm{d}w\,\sqrt{\mathcal{F}^2_{\mathrm{D1}} + \mathcal{G}^2_{\mathrm{D1}}r'^2}, \\ \mathcal{F}_{\mathrm{D1}} &= \frac{\zeta(r,\theta_0)r^2}{L^2}, \quad \mathcal{G}_{\mathrm{D1}} = \frac{\zeta(r,\theta_0)}{L\sqrt{F(r)}\lambda^3(r)}. \end{aligned} \tag{A.2}$$

We notice that one does not get the same functions as is the case for the rest of the probes, furthermore, the function $\zeta(r,\theta_0)$ is strictly nonzero for all values of r and θ_0 from which it follows that the object we are calculating does not have a vanishing tension at the end of the space.

Case II. Another interesting embedding one can calculate is that of a Eucledian D1 that extends on $\Sigma_2 = [w, \phi]$, is localized in time and the rest of the coordinates are constant. The induced metric in this case is:

$$\begin{aligned} \mathrm{d}s^2_{\mathrm{ind,ED1}} = &\frac{1}{\zeta(r,\theta_0)}\left[\cos^2\theta_0 A_1^2 + \sin^2\theta_0\lambda^6(r)A_3^2 + r^2F(r)\zeta^2(r,\theta_0)\right]\mathrm{d}\phi^2 \\ &+ \zeta(r,\theta_0)\left[\frac{r^2}{L^2} + \frac{r'^2}{r^2F(r)\lambda^6(r)}\right]\mathrm{d}w^2, \end{aligned} \tag{A.3}$$

JHEP04(2026)184

and its action is given by:

$$
\begin{aligned}
S_{\rm ED1} &= T_{\rm ED1}\int_{\Sigma_2} {\rm d}^2\sigma\sqrt{e^{-2\Phi}{\rm det}(g_{\rm ind,ED1})} = {\rm T}_{\rm ED1}L_\phi\int {\rm d}w\sqrt{\mathcal{F}^2_{\rm ED1}+\mathcal{G}^2_{\rm ED1}r'^2},\\
\mathcal{F}^2_{\rm ED1} &= \frac{r^2}{L^2}\left[\cos^2\theta_0 A_1^2+\sin^2\theta_0\lambda^6(r)A_3^2+r^2F(r)\zeta^2(r,\theta_0)\right],\\
\mathcal{G}^2_{\rm ED1} &= \frac{\cos^2\theta_0 A_1^2+\sin^2\theta_0\lambda^6(r)A_3^2+r^2F(r)\zeta^2(r,\theta_0)}{r^2F(r)\lambda^6(r)}.
\end{aligned}
\tag{A.4}
$$

Again, the functions appearing in the dynamical part of this observable disagree with the ones in the 't Hooft loop.

B Gauge coupling

We calculate the gauge coupling for the effective (2+1)-dimensional theories dual to the type IIB and IIA backgrounds. The procedure is as written in [27, 75]. We begin by writing the DBI action for a probe Dp-brane and perform an expansion of the field strength

$$
{\rm S}_{{\rm D}p,{\rm DBI}} = T_{{\rm D}p}\int_{\Sigma_{p+1}} {\rm d}^{p+1}\hat{\sigma}\sqrt{-e^{2\Phi}{\rm det}(g_{\rm ind}+F)}. \tag{B.1}
$$

From the following we can read off the gauge coupling,

$$
S_{{\rm D}_p,{\rm DBI}} = T_{{\rm D}_p}\int_{\Sigma_{p+1}} {\rm d}^{p+1}\sigma\sqrt{-e^{-2\Phi}\,{\rm det}(g_{\rm ind})}\left(1+\frac{1}{4}F_{\mu\nu}F^{\mu\nu}+\mathcal{O}\left(F^4\right)\right). \tag{B.2}
$$

Gauge coupling for the Type IIB background. We consider a probe D3 that extends in $[t,w,z,\phi]$, with the shrinking circle ϕ being wrapped. The worldvolume field strength is turned on which we take without loss of generality to have only the F_{tw} component be non-zero. The rest of the coordinates are kept fixed. The induced metric on the D3 is

$$
\begin{aligned}
{\rm d}s^2_{\rm ind} = &\frac{r^2\zeta(r,\theta_0)}{L^2}(-{\rm d}t^2+{\rm d}w^2+{\rm d}z^2)\\
&+\left\{r^2F(r)\zeta(r,\theta_0)+\frac{1}{\zeta(r,\theta_0)}\left[\cos^2\theta_0 A_1^2+\sin^2\theta_0\lambda^6(r)A_3^2\right]\right\}{\rm d}\phi^2.
\end{aligned}
\tag{B.3}
$$

We will now compute the DBI action for the D3 over the manifold Σ_4 spanned by $[t,w,z,\phi]$, which takes the form[38]

$$
{\rm S}_{\rm D3} = T_{\rm D3}\int_{\Sigma_4}{\rm d}^4\hat{\sigma}\sqrt{-e^{2\Phi}{\rm det}(g_{\rm ind}+F)} = T_{\rm D3}\int_{\Sigma_4}{\rm d}^4\hat{\sigma}\sqrt{\alpha-\beta F_{tw}^2}, \tag{B.4}
$$

with the expressions:

$$
\begin{aligned}
\alpha &:= r^4\zeta^2(r,\theta_0)\left[\cos^2\theta_0 A_1^2+r^2F(r)\zeta^2(r,\theta_0)+\sin^2\theta\lambda^6(r)A_3^2\right],\\
\beta &:= L^4\left[\cos^2\theta_0 A_1^2+r^2F(r)\zeta^2(r,\theta)+\sin^2\theta_0\lambda^6(r)A_3^2\right].
\end{aligned}
\tag{B.5}
$$

We can now expand for small values of the field strength ($|F_{tw}|\ll 1$) up to $\mathcal{O}(F^2)$ to get

$$
{\rm S}_{\rm D3}\approx T_{\rm D3}\int_{\Sigma_4}{\rm d}^4\sigma\frac{2r^4\zeta^2(r,\theta)-L^4F_{tw}^2}{2L^3r\zeta(r,\theta)}\sqrt{\cos^2\theta_0 A_1^2+r^2F(r)\zeta^2(r,\theta_0)+\sin^2\theta_0\lambda^6(r)A_3^2}, \tag{B.6}
$$

[38] Notice that the dilaton factor in this case is trivial.

JHEP04(2026)184

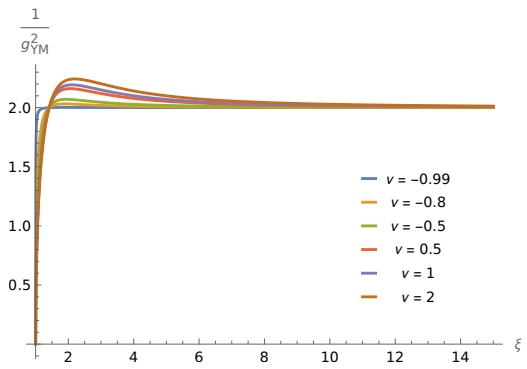

(a) Plot of the square of the inverse gauge coupling for $\theta_0 = 0$.

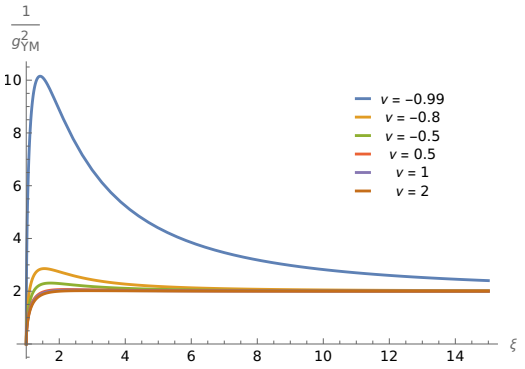

(b) Plot of the square of the inverse gauge coupling for $\theta_0 = \pi/2$.

Figure 13. Plots of the gauge coupling constant of the dual QFT with respect to the radial coordinate for the type IIB background.

By expanding the DBI action to quadratic order in F_{tw} and extracting the prefactor of the kinetic term, one obtains an expression for the gauge coupling. Its dependence on the radial coordinate r reflects how the effective coupling evolves across energy scales in the dual QFT. Hence we can study the gauge coupling's behaviour in strongly coupled regimes that are otherwise difficult to access.

$$\begin{aligned}\frac{1}{g^2_{\rm YM}} &= \frac{T_{\rm D3}LL_\phi}{r\zeta(r,\theta_0)}\sqrt{\cos^2\theta_0 A_1^2 + r^2F(r)\zeta^2(r,\theta_0) + \sin^2\theta_0\lambda^6(r)A_3^2} \\ &= \frac{2T_{\rm D3}LL_\phi}{\xi\sqrt{\nu+2\xi^2+\nu\cos(2\theta_0)}}\sqrt{\frac{(\xi^2-1)\left[4+5\nu+2\nu^2+2(1+\nu)\xi^2+\nu(3+2\nu)\cos(2\theta_0)\right]}{1+\nu}},\end{aligned} \tag{B.7}$$

where in the last line we expressed everything in terms of the dimensionless variable $\xi = r/r_\star$ for the case where $q_1 = q_2 = q$.

We can plot the above function for given values of θ_0. The result can be seen in figure 13. We see that as $r \to r_\star$ the gauge coupling constant diverges, reflecting the fact that the dual QFTs are strongly coupled in the deep IR. In the UV the coupling constant takes a fixed value, which is a consequence of the conformal symmetry that is present as $r \to \infty$.

Gauge coupling for Gaiotto-Maldacena background. We consider a probe D4 extending along $\Sigma_5 = [t, w, z, \phi, \eta]$ between η_i, η_{i+1} and has a field strength which we take to have only the F_{tz} component being non-zero. The other coordinates are kept fixed.

The induced metric is

$$\mathrm{d}s^2_{\rm ind} = (\tilde{f}_1^3\tilde{f}_5)^{\frac{1}{2}}\left\{4\tilde{f}\left[\frac{r^2\lambda(r)^2}{L^2}\left(-\mathrm{d}t^2+\mathrm{d}w^2+\mathrm{d}z^2+L^2F(r)\mathrm{d}\phi^2\right)\right]+\tilde{f}_4\mathrm{d}\eta^2\right\}. \tag{B.8}$$

We utilise the formula as given in [27, 75],

$$S_{\rm D4} = T_{\rm D4}\int_{\Sigma_5}\mathrm{d}^5\hat{\sigma}\sqrt{-e^{-2\Phi}\det(g_{\rm ind}+F)}. \tag{B.9}$$

JHEP04(2026)184

The expansion gives

$$\sqrt{-e^{-2\Phi}\det(g_{\rm ind}+F)} = 32\tilde{f}_1^3\tilde{f}_4^{\frac{1}{2}}\tilde{f}_5^{\frac{1}{2}}\tilde{f}^2\frac{r^4\lambda(r)^4\sqrt{F(r)}}{L^3}\left[1-\frac{L^4F_{tz}^2}{32\tilde{f}^2\tilde{f}_1^3\tilde{f}_5\, r^4\lambda(r)^4}\right]. \tag{B.10}$$

Hence we have

$$S_{\rm D4} = 32\, T_{\rm D4}L_\phi\int_{\eta_i}^{\eta_{i+1}}{\rm d}\eta\int{\rm d}t{\rm d}w{\rm d}z\tilde{f}_1^3\tilde{f}_4^{\frac{1}{2}}\tilde{f}_5^{\frac{1}{2}}\tilde{f}^2\frac{r^4\lambda(r)^4\sqrt{F(r)}}{L^3}\left[1-\frac{L^4F_{tz}^2}{32\tilde{f}^2\tilde{f}_1^3\tilde{f}_5\, r^4\lambda(r)^4}\right]. \tag{B.11}$$

We find the gauge coupling as

$$\frac{1}{4g_{\rm YM}^2} = T_{\rm D4}L_\phi L\sqrt{F(r)}\int_{\eta_i}^{\eta_{i+1}}{\rm d}\eta\ \tilde{f}_5^{-\frac{1}{2}}\tilde{f}_4^{\frac{1}{2}}. \tag{B.12}$$

C Details of the computations

In this appendix, we have gathered lengthy expressions and useful details of the calculations that are discussed in the main text.

The Hodge dual of G_5 can also be written in terms of a four-form $\tilde{C}_4$ as $\star G_5 = {\rm d}\tilde{C}_4$, where

$$\begin{aligned}
\tilde{C}_4 = {}& \frac{L^4q_1}{2}(\lambda^6-1)\sin(2\theta)\,{\rm d}\theta\wedge{\rm d}\phi\wedge\left(\sin^2\psi\,{\rm d}\phi_1+\cos^2\psi\,{\rm d}\phi_2\right)\wedge{\rm d}\phi_3\\
&+\frac{L^4q_2}{2}\frac{(\lambda^6-1)\zeta_\star^2}{\lambda_\star^6\zeta^2}\cos^4\theta\sin(2\psi)\,{\rm d}\phi\wedge{\rm d}\phi_1\wedge{\rm d}\phi_2\wedge{\rm d}\psi\\
&+\frac{L^4q_1}{8}\frac{(\lambda^6-1)\zeta_\star^2}{\zeta^2}\sin^2(2\theta)\sin(2\psi)\,{\rm d}\phi\wedge{\rm d}(\phi_1-\phi_2)\wedge{\rm d}\phi_3\wedge{\rm d}\psi\\
&-\frac{L^4}{8}\frac{\zeta^2-1}{\zeta^2}\sin^2(2\theta)\sin(2\psi)\,{\rm d}\phi_1\wedge{\rm d}\phi_2\wedge{\rm d}\phi_3\wedge{\rm d}\psi\\
&-\frac{L^4q_2}{\lambda_\star^6}(\zeta_\star^2-1)\sin(2\theta)\cos^2\psi\,{\rm d}\theta\wedge{\rm d}\phi\wedge{\rm d}\phi_1\wedge{\rm d}\phi_2\\
&+L^4q_1(\zeta_\star^2-1)\sin(2\theta)\cos^2\psi\,{\rm d}\theta\wedge{\rm d}\phi\wedge{\rm d}(\phi_1-\phi_2)\wedge{\rm d}\phi_3\\
&-L^4\sin(2\theta)\cos^2\theta\cos^2\psi\,{\rm d}\theta\wedge{\rm d}\phi_1\wedge{\rm d}\phi_2\wedge{\rm d}\phi_3\,.
\end{aligned} \tag{C.1}$$

The expressions for the length and the energy in the case of the 't Hooft loops read:

$$\begin{aligned}
L_{\rm MM}(\xi_0) = {}& \frac{\sqrt{2}L^2}{r_\star}\sqrt{-(1+\hat{\nu})+\xi_0^4(\xi_0^2+\hat{\nu})}\\
&\times\int_{\xi_0}^\infty{\rm d}\xi\sqrt{\frac{\xi}{\left[-(1+\hat{\nu})+\xi^4(\xi^2+\hat{\nu})\right]\left[\xi^6-\xi_0^6+\hat{\nu}(\xi^4-\xi_0^4)\right]}},
\end{aligned} \tag{C.2}$$

$$\begin{aligned}
E_{\rm MM}(\xi_0) = {}& \frac{r_\star^3}{L}\sqrt{-(1+\hat{\nu})+\xi_0^4(\xi_0^2+\hat{\nu})}L_{{\rm MM}(\xi_0)}\\
&+2Lr_\star^2\int_{\xi_0}^\infty\frac{{\rm d}\xi\,\xi\sqrt{\left[\xi^6-\xi_0^6+\hat{\nu}(\xi^4-\xi_0^4)\right]}}{\sqrt{-(1+\hat{\nu})+\xi_0^4(\xi_0^2+\hat{\nu})}}-2Lr_\star^2\int_1^\infty{\rm d}\xi\,\xi,
\end{aligned} \tag{C.3}$$

$$\begin{aligned}
L_{\rm MM,app}(\xi_0) = {}& \frac{L^2\pi\sqrt{-(1+\hat{\nu})+\xi_0^4(\xi_0^2+\hat{\nu})}}{r_\star^2\xi^2(2\hat{\nu}+3\xi_0)},\\
E_{\rm MM,app}(\xi_0) = {}& Lr_\star\pi\int^{\xi_0}{\rm d}s\,\frac{3\hat{\nu}(1+\hat{\nu})+12(1+\hat{\nu})s^2-4\hat{\nu}s^6-3s^8}{s^3(2\hat{\nu}+3s^3)^2},
\end{aligned} \tag{C.4}$$

JHEP04(2026)184

Now moving to the calculations for the stability analysis of the Wilson loop, to write the equations of the fluctuations in a compact form, we introduce the following functions

$$\begin{aligned} f_z(r,\theta) &= -\,G_{tt}G_{zz}\,, & f_\theta(r,\theta) &= -\,G_{tt}G_{\theta\theta}\,, & f_\phi(r,\theta) &= -\,G_{tt}G_{\phi\phi} \\ f_{\varphi_1}(r,\theta,\psi) &= -\,G_{tt}G_{\varphi_1\varphi_1}\,, & f_{\varphi_2}(r,\theta,\psi) &= -\,G_{tt}G_{\varphi_2\varphi_2} & & \\ f_\psi(r,\theta) &= -\,G_{tt}G_{\psi\psi}\,, & f_{\varphi_3}(r,\theta) &= -\,G_{tt}G_{\varphi_3\varphi_3}\,, & h(r,\theta) &= G_{rr}G_{yy}\,. \end{aligned} \tag{C.5}$$

Introducing a time dependence in the fluctuations of the form $e^{-\mathrm{i}\,\omega\,\tau}$, we have

$$\begin{aligned} \delta z(\tau,\sigma) &= \delta z(\sigma)\,e^{-\mathrm{i}\,\omega\,\tau}\,, & \delta y(\tau,\sigma) &= \delta y(\sigma)\,e^{-\mathrm{i}\,\omega\,\tau}\,, & \delta\theta(\tau,\sigma) &= \delta\theta(\sigma)\,e^{-\mathrm{i}\,\omega\,\tau} \\ \delta\phi(\tau,\sigma) &= \delta\phi(\sigma)\,e^{-\mathrm{i}\,\omega\,\tau}\,, & \delta\varphi_1(\tau,\sigma) &= \delta\varphi_2(\tau,\sigma) = \delta\varphi_{12}(\sigma)\,e^{-\mathrm{i}\,\omega\,\tau} & & \\ \delta\varphi_3(\tau,\sigma) &= \delta\varphi_3(\sigma)\,e^{-\mathrm{i}\,\omega\,\tau}\,, & \delta\psi(\tau,\sigma) &= \delta\psi(\sigma)\,e^{-\mathrm{i}\,\omega\,\tau}\,. & & \end{aligned} \tag{C.6}$$

Notice that we have used the same function for the σ dependence of the modes of $\delta\varphi_1$ and $\delta\varphi_2$, something that is consistent with the equations of motion for the corresponding fluctuations.

The equations for the fluctuations δz, $\delta\psi$, δy and $\delta\theta$ are

$$\left[\frac{\mathrm{d}}{\mathrm{d}\sigma}\left(\frac{f_z}{F^{1/2}}\frac{\mathrm{d}}{\mathrm{d}\sigma}\right)+\omega^2\,\frac{h\,f_z\,F^{1/2}}{g\,f_y}\right]\delta z=0 \tag{C.7}$$

$$\left[\frac{\mathrm{d}}{\mathrm{d}\sigma}\left(\frac{f_\psi}{F^{1/2}}\frac{\mathrm{d}}{\mathrm{d}\sigma}\right)+\omega^2\,\frac{h f_\psi\,F^{1/2}}{g\,f_y}\right]\delta\psi=0\,,\quad \left[\frac{\mathrm{d}}{\mathrm{d}\sigma}\left(\frac{g\,f_y}{F^{3/2}}\frac{\mathrm{d}}{\mathrm{d}\sigma}\right)+\omega^2\,\frac{h}{F^{1/2}}\right]\delta y=0$$

$$\left[\frac{\mathrm{d}}{\mathrm{d}u}\left(\frac{f_\theta}{F^{1/2}}\frac{\mathrm{d}}{\mathrm{d}\sigma}\right)+\omega^2\,\frac{h f_\theta F^{1/2}}{g\,f_y}-\frac{1}{2\,F^{1/2}}\,\partial_\theta^2 g-\frac{f_y^0\,F^{1/2}}{2\,f_y^2}\,\partial_\theta^2 f_y\right]\delta\theta=0$$

while the equations for the modes $\delta\phi$, $\delta\varphi_{12}$ and $\delta\varphi_3$ are

$$\begin{aligned} &\frac{\mathrm{d}}{\mathrm{d}\sigma}\left[\frac{f_\phi}{F^{1/2}}\,\delta\phi'+f_{12}\,\frac{f_{\varphi_1}+f_{\varphi_2}}{F^{1/2}}\,\delta\varphi_{12}'+f_3\,\frac{f_{\varphi_3}}{F^{1/2}}\,\delta\varphi_3'\right] \\ &+\omega^2\,\frac{h\,F^{1/2}}{g\,f_y}\left[f_\phi\,\delta\phi+f_{12}\,\left(f_{\varphi_1}+f_{\varphi_2}\right)\,\delta\varphi_{12}+f_3\,f_{\varphi_3}\,\delta\varphi_3\right]=0 \end{aligned} \tag{C.8}$$

$$\frac{\mathrm{d}}{\mathrm{d}\sigma}\left[\frac{f_{\varphi_1}+f_{\varphi_2}}{F^{1/2}}\,\left(\delta\varphi_{12}'+f_{12}\,\delta\phi'\right)\right]+\omega^2\,\frac{h\,F^{1/2}}{g\,f_y}\,\left(f_{\varphi_1}+f_{\varphi_2}\right)\left[\delta\varphi_{12}+f_{12}\,\delta\phi\right]=0$$

$$\frac{\mathrm{d}}{\mathrm{d}\sigma}\left[\frac{f_{\varphi_3}}{F^{1/2}}\,\left(\delta\varphi_3'+f_3\,\delta\phi'\right)\right]+\omega^2\,\frac{h\,F^{1/2}}{g\,f_y}\,f_{\varphi_3}\left[\delta\varphi_3+f_3\,\delta\phi\right]=0\,. \tag{C.9}$$

The expressions for the Schrödinger potentials in each fluctuation mode, in the $Q=0$ case, are

$$\begin{aligned} V_{\delta z}(\sigma,r_0) &= V_{\delta\phi}(\sigma,r_0)=\frac{\left[2r_0^2\left(r_0^2-1\right)-1\right]\sigma^2+r_0^2\left(r_0^2-1\right)+8\sigma^8-18\sigma^6+11\sigma^4}{4\sigma^2\left(\sigma^2-1\right)^2} \\ V_{\delta y}(\sigma,r_0) &= \frac{-\left[8r_0^2\left(r_0^2-1\right)-11\right]\sigma^4+\left[6r_0^2\left(r_0^2-1\right)-1\right]\sigma^2-3r_0^2\left(r_0^2-1\right)+8\sigma^8-18\sigma^6}{4\sigma^2\left(\sigma^2-1\right)^2} \\ V_{\delta\theta}(\sigma,r_0) &= \frac{\left[6r_0^2\left(r_0^2-1\right)-1\right]\sigma^2-3r_0^2\left(r_0^2-1\right)+2\sigma^6-\sigma^4}{4\sigma^2\left(\sigma^2-1\right)^2} \\ V_{\delta\psi}(\sigma,r_0) &= V_{\delta\varphi_{12}}(\sigma,r_0)=\frac{-\left[\left(r_0^2-1\right)r_0^2+1\right]\sigma^2+r_0^2\left(r_0^2-1\right)+2\sigma^6-\sigma^4}{4\sigma^2\left(\sigma^2-1\right)^2}\,. \end{aligned} \tag{C.10}$$

JHEP04(2026)184

The expressions for the Schrödinger potentials of the decoupled modes in the case of finite Q, when expanded around the $Q = 0$ value, are

$$\begin{aligned}
V_{\delta z} &= V_{\delta z}^{Q=0} + \frac{r_0^4\left(-12\sigma^4+12\sigma^2-5\right)+r_0^2\left(12\sigma^4-12\sigma^2+5\right)+4\sigma^8-8\sigma^6+7\sigma^4-3\sigma^2}{4\sigma^6\left(\sigma^2-1\right)^3}Q^2 \\
&\quad +\mathcal{O}(Q^4) \\
V_{\delta y} &= V_{\delta y}^{Q=0} + \frac{r_0^4\left(20\sigma^4-20\sigma^2+7\right)+r_0^2\left(-20\sigma^4+20\sigma^2-7\right)+4\sigma^8-8\sigma^6+7\sigma^4-3\sigma^2}{4\sigma^6\left(\sigma^2-1\right)^3}Q^2 \\
&\quad +\mathcal{O}(Q^4) \\
V_{\delta\theta} &= V_{\delta\theta}^{Q=0} + \frac{\left(-12r_0^4+12r_0^2+5\right)\sigma^2+7r_0^2\left(r_0^2-1\right)+8\sigma^6-13\sigma^4}{4\sigma^6\left(\sigma^2-1\right)^3}Q^2+\mathcal{O}(Q^4) \\
V_{\delta\psi} &= V_{\delta\psi}^{Q=0} + \frac{3\left(4r_0^4-4r_0^2-1\right)\sigma^2-5r_0^2\left(r_0^2-1\right)-8\sigma^6+11\sigma^4}{4\sigma^6\left(\sigma^2-1\right)^3}Q^2+\mathcal{O}(Q^4)\,.
\end{aligned} \tag{C.11}$$

From the transformation of the coupled system of $\delta\phi$ and $\delta\varphi_{12}$ to a Schrödinger form, the expressions of the functions Ω_i, with $i = 1, \cdots, 4$ are

$$\begin{aligned}
&\Omega_1 = \frac{1}{\sqrt{\sigma}\sqrt[4]{\sigma^2-1}}+\mathcal{O}(Q^2)\,,\quad \Omega_3 = \frac{Q}{2\,\sigma^{5/2}\sqrt[4]{\sigma^2-1}}\left[\sqrt{\sigma^2-1}+\sigma^2\arctan\left(\sqrt{\sigma^2-1}\right)\right]+\mathcal{O}(Q^3) \\
&\Omega_3 = Q\,\frac{\sqrt[4]{\sigma^2-1}}{2\,\sigma^{5/2}}\left[\sqrt{\sigma^2-1}-\sigma^2\arctan\left(\sqrt{\sigma^2-1}\right)\right]+\mathcal{O}(Q^3)\,,\quad \Omega_4 = \frac{\sqrt[4]{\sigma^2-1}}{\sqrt{\sigma}}+\mathcal{O}(Q^2)\,.
\end{aligned} \tag{C.12}$$

while the insertions of the matrix potential V from (6.22) are

$$\begin{aligned}
V_{11} &= V_{\delta z}^{Q=0}\,, \\
V_{12} = V_{21} &= \frac{Q}{2}\left\{\frac{\left(2r_0^4-2r_0^2+2\sigma^6-5\sigma^4+3\sigma^2\right)\arctan\left(\sqrt{\sigma^2-1}\right)}{\left(\sigma^2-1\right)^2}\right. \\
&\quad \left.+\frac{r_0^4\left(4-6\sigma^2\right)+r_0^2\left(6\sigma^2-4\right)+(\sigma-1)\sigma^2(\sigma+1)\left(2\sigma^4+\sigma^2-2\right)}{\sigma^4\left(\sigma^2-1\right)^{3/2}}\right\}, \\
V_{22} &= V_{\delta\psi}^{Q=0}\,.
\end{aligned} \tag{C.13}$$

Data Availability Statement. This article has no associated data or the data will not be deposited.

Code Availability Statement. This article has no associated code or the code will not be deposited.

JHEP04(2026)184

References

[1] D. Chatzis et al., *Universal observables, SUSY RG-flows and holography*, *JHEP* **08** (2025) 134 [arXiv:2506.10062] [INSPIRE].

[2] J.M. Maldacena, *The Large N limit of superconformal field theories and supergravity*, *Adv. Theor. Math. Phys.* **2** (1998) 231 [hep-th/9711200] [INSPIRE].

[3] I.R. Klebanov and E. Witten, *Superconformal field theory on three-branes at a Calabi-Yau singularity*, *Nucl. Phys. B* **536** (1998) 199 [hep-th/9807080] [INSPIRE].

[4] L. Girardello, M. Petrini, M. Porrati and A. Zaffaroni, *Confinement and condensates without fine tuning in supergravity duals of gauge theories*, *JHEP* **05** (1999) 026 [hep-th/9903026] [INSPIRE].

[5] J. Polchinski and M.J. Strassler, *The String dual of a confining four-dimensional gauge theory*, hep-th/0003136 [INSPIRE].

[6] I.R. Klebanov and M.J. Strassler, *Supergravity and a confining gauge theory: Duality cascades and chi SB resolution of naked singularities*, *JHEP* **08** (2000) 052 [hep-th/0007191] [INSPIRE].

[7] J.M. Maldacena and C. Nunez, *Towards the large N limit of pure $N = 1$ superYang-Mills*, *Phys. Rev. Lett.* **86** (2001) 588 [hep-th/0008001] [INSPIRE].

[8] M. Atiyah, J.M. Maldacena and C. Vafa, *An M theory flop as a large N duality*, *J. Math. Phys.* **42** (2001) 3209 [hep-th/0011256] [INSPIRE].

[9] J.D. Edelstein and C. Nunez, *D6-branes and M theory geometrical transitions from gauged supergravity*, *JHEP* **04** (2001) 028 [hep-th/0103167] [INSPIRE].

[10] C. Nunez, I.Y. Park, M. Schvellinger and T.A. Tran, *Supergravity duals of gauge theories from $F(4)$ gauged supergravity in six-dimensions*, *JHEP* **04** (2001) 025 [hep-th/0103080] [INSPIRE].

[11] I.R. Klebanov and A.A. Tseytlin, *Gravity duals of supersymmetric $SU(N) \times SU(N+M)$ gauge theories*, *Nucl. Phys. B* **578** (2000) 123 [hep-th/0002159] [INSPIRE].

[12] J.P. Gauntlett, N. Kim, D. Martelli and D. Waldram, *Wrapped five-branes and $N = 2$ superYang-Mills theory*, *Phys. Rev. D* **64** (2001) 106008 [hep-th/0106117] [INSPIRE].

[13] F. Bigazzi, A.L. Cotrone and A. Zaffaroni, *$N = 2$ gauge theories from wrapped five-branes*, *Phys. Lett. B* **519** (2001) 269 [hep-th/0106160] [INSPIRE].

[14] F. Bigazzi, A.L. Cotrone, M. Petrini and A. Zaffaroni, *Supergravity duals of supersymmetric four-dimensional gauge theories*, *Riv. Nuovo Cim.* **25N12** (2002) 1 [hep-th/0303191] [INSPIRE].

[15] M. Bertolini, *Four lectures on the gauge/gravity correspondence*, *Int. J. Mod. Phys. A* **18** (2003) 5647 [hep-th/0303160] [INSPIRE].

[16] S. de Haro, S.N. Solodukhin and K. Skenderis, *Holographic reconstruction of space-time and renormalization in the AdS/CFT correspondence*, *Commun. Math. Phys.* **217** (2001) 595 [hep-th/0002230] [INSPIRE].

[17] M. Bianchi, D.Z. Freedman and K. Skenderis, *How to go with an RG flow*, *JHEP* **08** (2001) 041 [hep-th/0105276] [INSPIRE].

[18] I. Papadimitriou and K. Skenderis, *AdS/CFT correspondence and geometry*, *IRMA Lect. Math. Theor. Phys.* **8** (2005) 73 [hep-th/0404176] [INSPIRE].

[19] F. Aramini et al., *Gravity, finite duality cascades and confinement*, *JHEP* **09** (2025) 054 [arXiv:2506.18988] [INSPIRE].

[20] E. Witten, *Anti-de Sitter space, thermal phase transition, and confinement in gauge theories*, *Adv. Theor. Math. Phys.* **2** (1998) 505 [hep-th/9803131] [INSPIRE].

JHEP04(2026)184

[21] G.T. Horowitz and R.C. Myers, *The AdS/CFT correspondence and a new positive energy conjecture for general relativity*, *Phys. Rev. D* **59** (1998) 026005 [hep-th/9808079] [INSPIRE].

[22] D. Cassani and Z. Komargodski, *EFT and the SUSY Index on the 2nd Sheet*, *SciPost Phys.* **11** (2021) 004 [arXiv:2104.01464] [INSPIRE].

[23] S.P. Kumar and R. Stuardo, *Twisted circle compactification of $\mathcal{N} = 4$ SYM and its holographic dual*, *JHEP* **08** (2024) 089 [arXiv:2405.03739] [INSPIRE].

[24] A. Anabalon and S.F. Ross, *Supersymmetric solitons and a degeneracy of solutions in AdS/CFT*, *JHEP* **07** (2021) 015 [arXiv:2104.14572] [INSPIRE].

[25] A. Fatemiabhari and C. Nunez, *From conformal to confining field theories using holography*, *JHEP* **03** (2024) 160 [arXiv:2401.04158] [INSPIRE].

[26] D. Chatzis, A. Fatemiabhari, C. Nunez and P. Weck, *Conformal to confining SQFTs from holography*, *JHEP* **08** (2024) 041 [arXiv:2405.05563] [INSPIRE].

[27] D. Chatzis, A. Fatemiabhari, C. Nunez and P. Weck, *SCFT deformations via uplifted solitons*, *Nucl. Phys. B* **1006** (2024) 116659 [arXiv:2406.01685] [INSPIRE].

[28] F. Castellani and C. Nunez, *Holography for confined and deformed theories: TsT-generated solutions in type IIB supergravity*, *JHEP* **12** (2024) 155 [arXiv:2410.00094] [INSPIRE].

[29] N.T. Macpherson, P. Merrikin and R. Stuardo, *Circle compactifications of Minkowski$_D$ solutions, flux vacua and solitonic branes*, *JHEP* **08** (2025) 143 [arXiv:2412.15102] [INSPIRE].

[30] N.T. Macpherson, P. Merrikin, C. Nunez and R. Stuardo, *Twisted-circle compactifications of SQCD-like theories and holography*, *JHEP* **08** (2025) 146 [arXiv:2506.15778] [INSPIRE].

[31] M. Barbosa, H. Nastase, C. Nunez and R. Stuardo, *Penrose limits of I-branes, twist-compactified D5-branes, and spin chains*, *Phys. Rev. D* **110** (2024) 046015 [arXiv:2405.08767] [INSPIRE].

[32] A. Fatemiabhari, C. Nunez, M. Piai and J. Rucinski, *Stability of holographic confinement with magnetic fluxes*, *Phys. Rev. D* **111** (2025) 066009 [arXiv:2411.16854] [INSPIRE].

[33] A. Anabalón, H. Nastase and M. Oyarzo, *Supersymmetric AdS solitons and the interconnection of different vacua of $\mathcal{N} = 4$ Super Yang-Mills*, *JHEP* **05** (2024) 217 [arXiv:2402.18482] [INSPIRE].

[34] D.Z. Freedman, S.S. Gubser, K. Pilch and N.P. Warner, *Continuous distributions of D3-branes and gauged supergravity*, *JHEP* **07** (2000) 038 [hep-th/9906194] [INSPIRE].

[35] S.S. Gubser, *Curvature singularities: The Good, the bad, and the naked*, *Adv. Theor. Math. Phys.* **4** (2000) 679 [hep-th/0002160] [INSPIRE].

[36] M. Cvetic et al., *Embedding AdS black holes in ten-dimensions and eleven-dimensions*, *Nucl. Phys. B* **558** (1999) 96 [hep-th/9903214] [INSPIRE].

[37] T. Canneti, F. Castellani and W. Mück, *Vacuum configuration of winding superstrings from non-standard semiclassical quantization*, *JHEP* **06** (2025) 172 [arXiv:2501.14532] [INSPIRE].

[38] A. Kehagias and K. Sfetsos, *On asymptotic freedom and confinement from type IIB supergravity*, *Phys. Lett. B* **456** (1999) 22 [hep-th/9903109] [INSPIRE].

[39] A. Brandhuber and K. Sfetsos, *Wilson loops from multicenter and rotating branes, mass gaps and phase structure in gauge theories*, *Adv. Theor. Math. Phys.* **3** (1999) 851 [hep-th/9906201] [INSPIRE].

[40] L.J. Romans, *Gauged $N = 4$ Supergravities in Five-dimensions and Their Magnetovac Backgrounds*, *Nucl. Phys. B* **267** (1986) 433 [INSPIRE].

JHEP04(2026)184

[41] H. Lin, O. Lunin and J.M. Maldacena, *Bubbling AdS space and 1/2 BPS geometries*, *JHEP* **10** (2004) 025 [hep-th/0409174] [INSPIRE].

[42] J.P. Gauntlett and O. Varela, *$D = 5$ $SU(2) \times U(1)$ Gauged Supergravity from D=11 Supergravity*, *JHEP* **02** (2008) 083 [arXiv:0712.3560] [INSPIRE].

[43] J.P. Gauntlett, O.A.P. Mac Conamhna, T. Mateos and D. Waldram, *AdS spacetimes from wrapped M5 branes*, *JHEP* **11** (2006) 053 [hep-th/0605146] [INSPIRE].

[44] D. Gaiotto and J. Maldacena, *The Gravity duals of $N = 2$ superconformal field theories*, *JHEP* **10** (2012) 189 [arXiv:0904.4466] [INSPIRE].

[45] N.T. Macpherson, P. Merrikin and C. Nunez, *Marginally deformed AdS_5/CFT_4 and spindle-like orbifolds*, *JHEP* **07** (2024) 042 [arXiv:2403.02380] [INSPIRE].

[46] A. Legramandi and C. Nunez, *Electrostatic description of five-dimensional SCFTs*, *Nucl. Phys. B* **974** (2022) 115630 [arXiv:2104.11240] [INSPIRE].

[47] C. Núñez, D. Roychowdhury, S. Speziali and S. Zacarías, *Holographic aspects of four dimensional $\mathcal{N} = 2$ SCFTs and their marginal deformations*, *Nucl. Phys. B* **943** (2019) 114617 [arXiv:1901.02888] [INSPIRE].

[48] J.P. Gauntlett and O. Varela, *Consistent Kaluza-Klein reductions for general supersymmetric AdS solutions*, *Phys. Rev. D* **76** (2007) 126007 [arXiv:0707.2315] [INSPIRE].

[49] D. Cassani, G. Josse, M. Petrini and D. Waldram, *Systematics of consistent truncations from generalised geometry*, *JHEP* **11** (2019) 017 [arXiv:1907.06730] [INSPIRE].

[50] J.M. Maldacena, *Wilson loops in large N field theories*, *Phys. Rev. Lett.* **80** (1998) 4859 [hep-th/9803002] [INSPIRE].

[51] C. Nunez, M. Piai and A. Rago, *Wilson Loops in string duals of Walking and Flavored Systems*, *Phys. Rev. D* **81** (2010) 086001 [arXiv:0909.0748] [INSPIRE].

[52] U. Kol et al., *Confinement, Phase Transitions and non-Locality in the Entanglement Entropy*, *JHEP* **06** (2014) 005 [arXiv:1403.2721] [INSPIRE].

[53] C. Nunez and D. Roychowdhury, *Timelike entanglement entropy: A top-down approach*, *Phys. Rev. D* **112** (2025) 026030 [arXiv:2505.20388] [INSPIRE].

[54] C. Nunez and D. Roychowdhury, *Holographic timelike entanglement across dimensions*, *JHEP* **11** (2025) 100 [arXiv:2508.13266] [INSPIRE].

[55] M. Giliberti, A. Fatemiabhari and C. Nunez, *Confinement and screening via holographic Wilson loops*, *JHEP* **11** (2024) 068 [arXiv:2409.04539] [INSPIRE].

[56] G. 't Hooft, *On the Phase Transition Towards Permanent Quark Confinement*, *Nucl. Phys. B* **138** (1978) 1 [INSPIRE].

[57] S. Ryu and T. Takayanagi, *Holographic derivation of entanglement entropy from AdS/CFT*, *Phys. Rev. Lett.* **96** (2006) 181602 [hep-th/0603001] [INSPIRE].

[58] I.R. Klebanov, D. Kutasov and A. Murugan, *Entanglement as a probe of confinement*, *Nucl. Phys. B* **796** (2008) 274 [arXiv:0709.2140] [INSPIRE].

[59] G. Georgiou and D. Zoakos, *Entanglement entropy of the Klebanov-Strassler model with dynamical flavors*, *JHEP* **07** (2015) 003 [arXiv:1505.01453] [INSPIRE].

[60] Y. Bea et al., *Compactifications of the Klebanov-Witten CFT and new AdS_3 backgrounds*, *JHEP* **05** (2015) 062 [arXiv:1503.07527] [INSPIRE].

JHEP04(2026)184

[61] P. Merrikin, C. Nunez and R. Stuardo, *Compactification of 6d $N = (1,0)$ quivers, 4d SCFTs and their holographic dual Massive IIA backgrounds*, *Nucl. Phys. B* **996** (2023) 116356 [arXiv:2210.02458] [INSPIRE].

[62] N.T. Macpherson et al., *Type IIB supergravity solutions with AdS_5 from Abelian and non-Abelian T dualities*, *JHEP* **02** (2015) 040 [arXiv:1410.2650] [INSPIRE].

[63] N. Jokela et al., *On entanglement c-functions in confining gauge field theories*, *JHEP* **11** (2025) 101 [arXiv:2505.14397] [INSPIRE].

[64] M. Kruczenski, D. Mateos, R.C. Myers and D.J. Winters, *Meson spectroscopy in AdS/CFT with flavor*, *JHEP* **07** (2003) 049 [hep-th/0304032] [INSPIRE].

[65] D. Mateos, R.C. Myers and R.M. Thomson, *Thermodynamics of the brane*, *JHEP* **05** (2007) 067 [hep-th/0701132] [INSPIRE].

[66] N. Jokela, J. Mas, A.V. Ramallo and D. Zoakos, *Thermodynamics of the brane in Chern-Simons matter theories with flavor*, *JHEP* **02** (2013) 144 [arXiv:1211.0630] [INSPIRE].

[67] Y. Seo, J.P. Shock, S.-J. Sin and D. Zoakos, *Holographic Hadrons in a Confining Finite Density Medium*, *JHEP* **03** (2010) 115 [arXiv:0912.4013] [INSPIRE].

[68] S.S. Gubser, *Dilaton driven confinement*, hep-th/9902155 [INSPIRE].

[69] M. Henningson and K. Skenderis, *The Holographic Weyl anomaly*, *JHEP* **07** (1998) 023 [hep-th/9806087] [INSPIRE].

[70] V. Balasubramanian and P. Kraus, *A Stress tensor for Anti-de Sitter gravity*, *Commun. Math. Phys.* **208** (1999) 413 [hep-th/9902121] [INSPIRE].

[71] S.D. Avramis, K. Sfetsos and K. Siampos, *Stability of strings dual to flux tubes between static quarks in $N = 4$ SYM*, *Nucl. Phys. B* **769** (2007) 44 [hep-th/0612139] [INSPIRE].

[72] S. Kuperstein and J. Sonnenschein, *A New Holographic Model of Chiral Symmetry Breaking*, *JHEP* **09** (2008) 012 [arXiv:0807.2897] [INSPIRE].

[73] V.G. Filev, M. Ihl and D. Zoakos, *Holographic Bilayer/Monolayer Phase Transitions*, *JHEP* **07** (2014) 043 [arXiv:1404.3159] [INSPIRE].

[74] R. Casero, C. Nunez and A. Paredes, *Towards the string dual of $N = 1$ SQCD-like theories*, *Phys. Rev. D* **73** (2006) 086005 [hep-th/0602027] [INSPIRE].

[75] C. Nunez, M. Oyarzo and R. Stuardo, *Confinement in $(1+1)$ dimensions: a holographic perspective from I-branes*, *JHEP* **09** (2023) 201 [arXiv:2307.04783] [INSPIRE].

JHEP04(2026)184